Reactions of Nitrogen Oxides and Oxygen with Hydrocarbons over Manganese and Related Oxides

Abstract

The catalytic reactions of nitric oxide, nitrous oxide or oxygen with either ethane or 1-butene were studied. Manganese (III) oxide was evaluated as a catalyst for these reactions in a differential-reactor flow system operated at atmospheric pressure. This system allowed the kinetics of reaction to be calculated and kinetic modelling studies were used as an aid in determining reaction mechanisms.

Nitric oxide reacted in a complex sequence of steps beginning with an irreversible bimolecular reaction between adsorbed species on the catalyst surface. In the case of the reactions with ethane, each reactant was adsorbed on one surface site, while in reactions with 1-butene each was adsorbed on two sites. Nitrous oxide was one of the products of reaction when nitric oxide was a reactant. In reactions with nitrous oxide or oxygen, similar mechanisms operated and only the products of complete hydrocarbon oxidation were observed.

In all reactions, the manganese (III) oxide went through a phase change from the alpha to the gamma phase. A nitro or nitrate species appeared on the catalyst surface after reactions involving nitric oxide.

The effects of a series of oxide catalysts were observed on the nitrous oxide / 1-butene reaction. Reactivity decreased down the series:

CuO, Fe_2O_3, NiO, Mn_2O_3, Cr_2O_3, TiO_2,
Sc_2O_3, SnO, ZnO, V_2O_5, Al_2O_3.

The use of carbon fibres as catalyst supports or co-catalysts was assessed, and the kinetics of the oxygen / ethane and oxygen / 1-butene reactions over manganese oxide / carbon fibre were determined.

REACTIONS OF NITROGEN OXIDES AND OXYGEN WITH HYDROCARBONS OVER MANGANESE AND RELATED OXIDES

A thesis
presented for the degree of
DOCTOR OF PHILOSOPHY
in the Faculty of Science of the
University of St. Andrews
by

CRAIG WILLIAM FAIRBRIDGE, M.Sc.

October 1981

United College of St. Salvator
and St. Leonard, St. Andrews.

To my wife

SHELLEY

and my parents

DECLARATION

I declare that this thesis is my own composition, that the work of which it is a record has been carried out by myself, and that it has not been submitted in any previous application for a Higher Degree.

This thesis describes the results of research carried out at the Chemistry Department, United College of St. Salvator and St. Leonard, University of St. Andrews and the Chemistry Department, Lakehead University, Thunder Bay, Ontario, Canada under the supervision of Dr. J. R. MacCallum and Professor R. A. Ross since the 1st of October, 1977.

Craig Fairbridge

CERTIFICATE

I hereby certify that Craig W. Fairbridge has spent 12 terms of research under my supervision, has fulfilled the conditions of Ordinance No. 12 (St. Andrews) and is qualified to submit the accompanying thesis in application for the degree of Doctor of Philosophy.

J. R. MacCallum
Director of Research
Department of Chemistry
University of St. Andrews.

ACKNOWLEDGEMENTS

The author wishes to thank his supervisor Professor R. A. Ross, DSc(Strath), PhD,BSc(Glas), ARCST, CEng, FInstE, FCIC, CChem, FRSC(UK), for his constant advice and direction throughout this programme. Thanks are also due to the technical staff of the Faculty of Science, Lakehead University.

The author also appreciates the facilities provided by the University of St. Andrews during studies there in the period 1978 through 1979. Special thanks go to Dr. J. R. MacCallum for his interest and encouragement in this work.

The financial support received from the National Science and Engineering Research Council of Canada and Imperial Oil Enterprises (Toronto) is gratefully acknowledged.

TABLE OF CONTENTS

LIST OF FIGURES

LIST OF TABLES

SUMMARY

The reduction of oxides of nitrogen and the complete oxidation of hydrocarbons are important reactions because of the impact of these species on the urban environment. The major source of these compounds is the automobile exhaust.

In this thesis, the catalytic reactions of nitric oxide, nitrous oxide or oxygen with either ethane or 1-butene were studied. Manganese (III) oxide was evaluated as a catalyst for these reactions in a differential-reactor flow system operated at atmospheric pressure. This system allowed the kinetics of reaction to be calculated and kinetic modeling studies were used as an aid in determining reaction mechanisms.

Nitric oxide reacted in a complex sequence of steps beginning with an irreversible bimolecular reaction between adsorbed species on the catalyst surface. In the case of the reactions with ethane, each reactant was adsorbed on one surface site, while in reactions with 1-butene each was adsorbed on two sites. Nitrous oxide was one of the products of reaction when nitric oxide was one of the reactants. In reactions with nitrous oxide or oxygen, similar mechanisms operated and only the products of complete hydrocarbon oxidation were observed.

In all reactions, the manganese (III) oxide went through a phase change from the alpha to the gamma phase. A nitro or nitrate species appeared on the catalyst surface after reactions involving nitric oxide.

The effects of a series of oxide catalysts, including the transition metal oxides, were observed on the nitrous oxide/1-butene reaction.

The use of carbon fibres as catalyst supports or co-catalysts in the oxidation of ethane and 1-butene by oxygen was assessed.

CHAPTER I

LITERATURE SURVEY

1.1 *Introduction*

In previous related studies, the kinetics of several catalytic reactions of industrial significance have been determined over manganese and related transition metal oxides (1-8). Mechanisms were proposed and, wherever possible, conclusions based upon kinetic data were tested by surface chemical and physical analyses based on established techniques - electron microscopy, infrared spectroscopy, surface area and pore characterization by adsorption and by X-ray diffraction. Those features of the surface chemical properties of manganese oxides, specifically, which appeared to contribute to catalysis were investigated most recently in studies of the water-gas shift reaction (7), the decomposition of formic acid (8), and the redox reactions of nitrous oxide with carbon monoxide (9-13).

Thus, the present work was intended to extend and test some of the concepts generated by previous colleagues involved in this particular area of heterogeneous catalysis where oxidation/reduction reactions of environmental or industrial prominence have been examined over "practical" oxide surfaces. In this light, the oxidation of ethane and 1-butene by oxygen, nitric oxide and nitrous oxide has been observed over a manganese (III) oxide catalyst. Oxides of nitrogen, NO_x, and unburned hydrocarbons are the principal noxious contaminants arising from combustion reactions. The removal of these pollutants by catalytic processes has received, and continues to receive considerable attention with the ultimate aim of reducing the amounts discharged into the atmosphere to acceptable levels. The present work has been mainly concerned with contributing to knowledge

of automobile exhaust emission conversion and control systems based on the application of solid catalysts.

This study considers the interaction of light hydrocarbons with nitric and nitrous oxides as well as with oxygen for comparison. It was hoped that an increased understanding of the surface reactions would evolve. Although the emphasis is placed on manganese oxides, a number of other transition metal oxides will be evaluated as possible catalysts and the feasibility of using activated carbon fibres as a novel support or catalytic material will also be assessed.

1.2 *Nitric oxide*

Nitric oxide is formed from nitrogen and oxygen as a result of endothermic changes and its formation is favoured by an increase in temperature (14). This gas, together with other oxides of nitrogen, is one of the major urban atmospheric pollutants. In practice, they normally occur as nitric oxide with small quantities of nitrogen dioxide, and are together referred to as NO_x.

Nitric oxide is the primary product formed during high temperature combustion processes when atmospheric oxygen and nitrogen combine. As the gas mixture cools, nitric oxide is oxidized to nitrogen dioxide (15) by the mechanism:

$$NO + O_2 \rightleftharpoons NO_3 \qquad [1.2.1]$$

$$NO_3 + NO \longrightarrow 2NO_2 \qquad [1.2.2]$$

which invokes an unstable nitrogen trioxide intermediate. Higher temperatures would be expected to decrease the NO_3 equilibrium concentration and therefore the rate of nitrogen dioxide formation. Normally, exhaust gases from combustion reactions are cooled and diluted in a matter of seconds so that some nitrogen dioxide is produced, however, the oxidation of nitric oxide ceases when its concentration is less than 1 ppm (16).

1.2.1 *Catalytic decomposition*

The heterogeneous decomposition of nitric oxide has been studied over a number of catalysts and the following reactivity series established (17):

$$Pt > CuO > Fe_2O_3 > NiO > Al_2O_3.$$

The extreme kinetic stability of nitric oxide with regard to its catalytic removal from exhaust gases has been demonstrated (18) and the catalytic decomposition of nitric oxide shown to be a very slow reaction (19). It would seem that the catalytic removal of nitric oxide might then be promoted by suitable choice of surfaces with the potential to enhance reduction pathways.

1.2.2 *Catalytic reduction*

It has been suggested that an efficient catalyst for the reduction of nitric oxide should possess a number of key physical and chemical properties (20). The catalyst should have a low thermal capacity coupled with high strength and thermal shock resistance in order to operate over a wide range of temperatures. The surface should be resistant to sulphur and to oxidation corrosion.

A number of gas-phase reducing agents - carbon monoxide, hydrogen and hydrocarbons - augment the heterogeneous reaction rates such that many catalysts, most notably supported precious metals (21), catalyse the reduction of nitric oxide. Generally, the presence of excess oxygen inhibits nitric oxide reduction (22) by altering the catalyst oxidation state (23) and preferentially reacting with the reducing agent on the catalyst surface (21,24). Iron (III) and chromium (III) oxide supported on silica-alumina were found to be more active catalysts at lower temperatures for the nitric oxide/carbon monoxide reaction than the oxygen/carbon monoxide reaction (22). In a competitive reaction with both nitric oxide and oxygen present, the catalytic reaction of carbon monoxide with oxygen

predominated.

The nitric oxide/carbon monoxide reaction mechanism was initially interpreted using a Hougen-Watson approach (25,26) as a surface reaction between adsorbed species (27,28). This proposal, however, could not explain either the formation of intermediate nitrous oxide (21,22,29-32) or the presence of an isocyanate complex (30,33). A number of mechanisms have since been postulated to describe the nitric oxide/carbon monoxide reaction on various catalysts (29,30,34,35). The reaction mechanism has been interpreted by Shelef and co-workers (21,22,29) as proceeding via a redox process in which surface oxidation by nitric oxide was thought to be the rate-controlling step and the following reactivity series was proposed:

$$Fe_2O_3 > CuCr_2O_4 > Cu_2O > Cr_2O_3 > NiO > Pt$$

$$> Co_3O_4 > Al_2O_3\ (5\%\ SiO_2) > MnO > V_2O_5.$$

A somewhat different specific reactivity series as proposed by Alkhazov et al. (23) corresponds more closely with other more recent investigations of the nitric oxide/carbon monoxide reaction (36) and the nitric oxide decomposition reaction (17):

$$CuO > Co_3O_4 > Mn_3O_4 > Fe_2O_3 > NiO > Cr_2O_3 > ZnO$$

$$>> V_2O_5 = TiO_2.$$

The formation of a nitrous oxide intermediate in the nitric oxide/carbon monoxide reaction was thought to involve adsorption of nitric oxide via the oxygen end of the molecule (37). However, isotopic exchange studies of nitric oxide on iron oxides (38) and nickel (II) oxide (29) failed to support this model. Surface intermediates such as nitrite (39,40) or nitro complexes (30,41) have since been proposed in mechanistic descriptions of the catalytic nitric oxide/carbon monoxide reaction.

In connection with NO_x reduction catalysts, Andrew (20) proposed the following reactivity series:

Pt, Pd, Rh > other group VIII metals > CoO = MnO

> CuO > NiO > Fe_2O_3.

The reduction of nitric oxide by methane has been studied over a deposited platinum catalyst at 573 K (42). The reduction of nitric oxide was thought to be described by a three-centre, four-parameter Langmuir-Hinshelwood equation. The initial reaction involved disproportionation between two nitric oxide molecules to produce nitrous oxide in a manner analogous to the nitric oxide/carbon monoxide mechanism proposed by Sazanova et al. (35):

$$2NO + 2\varepsilon \rightleftharpoons 2NO^-_{(ads)} \qquad [1.2.3]$$

$$2NO^-_{(ads)} \longrightarrow N_2O^-_{(ads)} + O^-_{(ads)} \qquad [1.2.4]$$

$$N_2O^-_{(ads)} \rightleftharpoons N_2O + \varepsilon \qquad [1.2.5]$$

where ε represents an electron.

The oxidizing species in the nitric oxide/methane reaction would presumably be an adsorbed oxygen ion produced by step [1.2.4] and the rupture of a C-H bond was believed to be the rate-limiting step (42) in the redox reaction. In this static system, when all of the nitric oxide was consumed, the methane was then oxidized on the surface by the intermediate nitrous oxide.

The reaction rate for the reduction of nitric oxide by propane was 0.5 order in each reactant with an activation energy of 37.5 kJ mol^{-1} (43). The activation energy for nitrogen formation in the nitric oxide/propane reaction over a bismuth phosphomolybdate catalyst was 92 kJ mol^{-1} while that for nitrous oxide formation was 55 kJ mol^{-1} (44). The reaction of nitric oxide with propylene over a copper-silica (3:7 w/w) catalyst from 573 to 773 K (45) produced carbon dioxide, water and nitrogen according to the overall reaction:

$$C_3H_6 + 9NO \longrightarrow 3CO_2 + 3H_2O + \tfrac{9}{2}N_2. \qquad [1.2.6]$$

The reaction rate was shown to be 0.5 order with respect to both nitric oxide and propylene with an activation energy of 25 kJ mol^{-1}.

The catalytic reduction of nitric oxide by hydrocarbons over co-precipitated binary metal oxides was studied in a flow reactor from 543 to 823 K (46) and the following activity series for the reaction of nitric oxide with benzene was proposed:

$$CuO - Al_2O_3 > Fe_2O_3 - Cr_2O_3 > CuO - Cr_2O_3$$

$$> Co_3O_4 - Al_2O_3 > Fe_2O_3 - Al_2O_3.$$

Over the copper (II) oxide-alumina catalyst, a hydrocarbon activity sequence for reaction was given as:

alkylbenzene > benzene > ethylene > octane

> isooctane > hexane > methane.

The adsorption of oxides of nitrogen on various surfaces has frequently been studied by infrared absorption (47-50). Initially, it was thought (47) that nitric oxide was adsorbed on a nickel catalyst as the linear, neutral NiNO molecule. Recent evidence (50), however, suggests that undissociated nitric oxide exists on nickel surfaces as $Ni(NO)_2$. It has been proposed that nitrogen dioxide may be adsorbed as a nitrate species while nitric oxide may be adsorbed as a nitro species (48).

1.3 *Nitrous oxide*

The observation that the catalytic reduction of nitric oxide often occurs through a nitrous oxide intermediate (29,42) makes studies of the reactions of nitrous oxide important to current activities concerned with the removal of NO_x from the urban environment.

1.3.1 *Catalytic decomposition*

A number of good reviews of the catalytic decomposition of nitrous oxide are available (51-54). In these reviews it is generally agreed that the following mechanism may be applicable:

$$N_2O_{(ads)} + \varepsilon \rightleftharpoons N_2 + O^-_{(ads)} \qquad [1.3.1]$$

$$2O^-_{(ads)} \longrightarrow O_2 + 2\varepsilon \qquad [1.3.2]$$

$$O^-_{(ads)} + N_2O \longrightarrow N_2 + O_2 . \qquad [1.3.3]$$

The rate-controlling step has been associated with either oxygen desorption or nitrous oxide adsorption.

The decomposition below 670 K proceeded favourably on p-type semiconductor oxides (Cu_2O, CoO, Mn_2O_3, NiO) while n-type oxides were less active (ZnO, CdO, TiO_2, Fe_2O_3, Ga_2O_3). In the reactivity series noted by Winter (55):

$$CaO > CuO > Fe_2O_3 > NiO > MnO_2 > MgO > Cr_2O_3$$
$$> ZnO > Al_2O_3 > TiO_2,$$

the catalytic activity was associated with the oxygen desorption reaction and was related to the crystal structure and lattice parameters of the oxide. It is interesting to note that the reactivity series obtained for the heterogeneous decomposition of nitric oxide (17) and the nitric oxide/carbon monoxide reaction (23) follow the same pattern. The rate-controlling step in the nitrous oxide reaction (55) involved the decomposition of adsorbed nitrous oxide while the overall reaction rate was explained by the number of nitrous oxide decomposition sites which were determined by the oxygen desorption reaction. Elsewhere, it was noted that several oxides - CaO, ZnO, TiO_2, Al_2O_3 - did not exhibit poisoning by oxygen (56). The decomposition of nitrous oxide was thought to occur only on specific surface sites.

The dissociative adsorption of nitrous oxide on titanium dioxide has been shown to be proportional to the number of lattice anionic vacancies while the electrical conductivity of the catalyst was reduced (57). Cimino and Indovina (58) drew a parallel between catalyst activity towards nitrous oxide decomposition and the strength of the oxygen-surface bond. Samples of α-Mn_2O_3 prepared at 873 and 1073 K gave different values for activation energy, 118 and 92 kJ mol^{-1}, respectively, from 550 to 700 K for the nitrous oxide decomposition reaction. The value found by Tanaka

and Ozaki (59) for reaction over manganese (III) oxide was 71 kJ mol^{-1}, while a detailed kinetic study on the same catalyst by Rheaume and Parravano (60) gave a higher value, 146 kJ mol^{-1}, from 559 to 619 K.

Cimino and Indovina (58) proposed the presence of two types of adsorbed oxygen, one weakly bound and one strongly bound to the surface of manganese(III) oxide. The release of oxygen was thought to be facilitated by the formation of a peroxide radical:

$$N_2O_{(ads)} + [\ ]_A + [O^{2-}]_B \longrightarrow N_2 + [O]_A + [O^{2-}]_B \qquad [1.3.4]$$

$$[O]_A + [O^{2-}]_B \longrightarrow [\ ]_A + [O_2^{2-}]_B \qquad [1.3.5]$$

$$N_2O + [\ ]_A + [O_2^{2-}]_B \longrightarrow N_2 + [O^-]_A + [\varepsilon]_B + O_2 \qquad [1.3.6]$$

$$[O^-]_A + [\varepsilon]_B \longrightarrow [\ ]_A + [O^{2-}]_B . \qquad [1.3.7]$$

A similar peroxide mechanism had earlier been presented by Bickley and Stone (61). The stability of an $[O^-]$ species on magnesium oxide in the presence of nitrous oxide was shown to involve an $N_2O_2^-$ surface complex (62).

1.3.2 *Catalytic reduction*

Most of the studies in the literature which concern the catalytic reduction of nitrous oxide involve reaction with carbon monoxide. The reaction between nitrous oxide and carbon monoxide on copper(I) oxide (63,64) has been interpreted as a two-stage redox process. The rate of nitrous oxide reduction was not appreciably influenced by carbon monoxide, however, the slight increase in rate noted was associated with the formation of anionic lattice vacancies, [ ], as shown in the equation:

$$CO + 2O^{2-} \rightleftharpoons CO_{3(ads)}^{2-} + [\ ] + 2\varepsilon . \qquad [1.3.8]$$

The nitrous oxide/carbon monoxide reaction on zinc(II) oxide was first

order in carbon monoxide concentration and independent of nitrous oxide concentration (65). The surface oxygen species involved in the oxidation of carbon monoxide was the same whether it arose from nitrous oxide or oxygen:

$$N_2O + [\ ] \longrightarrow [O^*] + N_2 \qquad [1.3.9]$$

or

$$O_2 + [\ ] \longrightarrow 2[O^*] \qquad [1.3.10]$$

$$CO + [O^*] \longrightarrow CO_2 + [\ ]\ . \qquad [1.3.11]$$

In competitive experiments with oxygen and nitrous oxide, the surface sites were preferentially occupied by oxygen atoms from the molecular oxygen. The photocatalytic oxygen/carbon monoxide reaction was 0.5 order with respect to oxygen concentration and zero order in carbon monoxide (65) with the following reaction scheme proposed:

$$O_2 \rightleftharpoons 2\ O_{(ads)} \qquad [1.3.12]$$

$$O_{(ads)} + \varepsilon \longrightarrow O^-_{(ads)} \qquad [1.3.13]$$

$$O^-_{(ads)} + CO \longrightarrow CO_2 + \varepsilon\ . \qquad [1.3.14]$$

A surface reaction scheme involving chemisorbed nitrous oxide and carbon monoxide species was described for catalysis on chromium-promoted iron(III) oxide (66). The results of a study of the nitrous oxide/carbon monoxide reaction on p- and n-type cobalt ferrite were explained by a mechanism invoking initial dissociative chemisorption of nitrous oxide to produce active surface oxygen (67) and a redox mechanism was proposed for the same reaction over tin(IV) oxide (68). The chemisorption of carbon monoxide was followed by lattice oxygen abstraction and the desorption of carbon dioxide. The rate-determining step was felt to be re-oxidation of the catalyst by nitrous oxide.

Recent work by Krupay and Ross (10-13) on the nitrous oxide/carbon

monoxide reaction on several transition metal oxides indicated that a carbonate intermediate probably formed during catalysis over magnesium oxide, scandium(III) oxide, vanadium(V) oxide, chromium(III) oxide and cobalt(II,III) oxide. The reaction over manganese(II) oxide (11) and nickel(II) oxide (9) was thought to involve interaction of adsorbed species as the rate-limiting step followed by carbon dioxide desorption:

$$N_2O_{(ads)} + CO_{(ads)} \longrightarrow N_2 + CO_{2(ads)} \cdot \qquad [1.3.15]$$

On the other oxides, reaction was thought to proceed further:

$$N_2O + CO_{2(ads)} \longrightarrow CO_{3(ads)} + N_2 \qquad [1.3.16]$$

$$CO + CO_{3(ads)} \longrightarrow CO_2 + CO_{2(ads)} \qquad [1.3.17]$$

$$CO_{2(ads)} \longrightarrow CO_2 + 2\ S \qquad [1.3.18]$$

where S represents a surface site, while the mechanism proposed for reaction over vanadium(V) oxide (10) involved a concerted redox scheme:

$$CO_{(ads)} + [O]_A + [O]_B \rightleftharpoons CO_{3(ads)} \qquad [1.3.19]$$

$$CO_{3(ads)} \longrightarrow CO_2 + [\ ]_A + [O]_B \qquad [1.3.20]$$

$$N_2O_{(ads)} + [\ ]_A \longrightarrow N_2 + [O]_A \cdot \qquad [1.3.21]$$

Generally, then, the catalytic reactions of nitric or nitrous oxide involve a reduction/oxidation cycle. On this basis, the catalytic decomposition and reduction of these oxides has been reviewed and, the inclusion of a brief summary of the kinetics of the complete oxidation of hydrocarbons seems appropriate.

1.4 Hydrocarbon oxidation

The catalytic conversion of hydrocarbons to CO_2 and H_2O is particu-

larly important in the control of air pollution as a method of reducing noxious organic impurities by catalytic combustion. The chief problem in finding a suitable catalyst, according to Kemball and Patterson (69), is in obtaining high activity for oxidation at low temperatures combined with high stability.

The differences in the nature of the interactions of hydrocarbon and oxidant on the catalyst surface determines whether partial or complete oxidation of the hydrocarbon occurs (70). The two alternatives were described as occurring by parallel, not consecutive, reactions (71).

Various models have been proposed to describe hydrocarbon oxidation reactions. A Hinshelwood mechanism (72) would involve the interaction of adsorbed oxygen with a weakly adsorbed or gas phase hydrocarbon molecule. At the steady state, the rate of removal of adsorbed oxygen by reaction would equal the rate of oxygen adsorption. A Mars and van Krevelen mechanism (73) would require the assumption of a steady state between two steps:

$$\text{hydrocarbon} + \text{catalyst} \longrightarrow \text{product} + \text{reduced catalyst} \qquad [1.4.1]$$

$$\text{reduced catalyst} + O_2 \longrightarrow \text{catalyst} . \qquad [1.4.2]$$

Lyubarskii (74) proposed that oxidation occurred through the initial interaction of a chemisorbed hydrocarbon species with either gaseous or chemisorbed oxygen. This would be followed by a complex series of steps involving surface radical reactions. The Knox theory for saturated hydrocarbon oxidation (75) assumes the sequence:

$$\text{alkane} \longrightarrow \text{alkene} \longrightarrow \text{aldehydes, alcohols.}$$

A number of reviews of the catalytic oxidation of hydrocarbons are available in the literature (76-80). Generally, the reaction rate for complete oxidation has been described as proportional to the first power of the hydrocarbon concentration in the presence of excess oxygen (76). The activation energy and pre-exponential factor increase with the number of

carbon atoms and the rate-limiting step has been related to the nature of the adsorbed hydrocarbon radical or to the chemisorption of oxygen. In spite of all of the studies attempted on the subject, the mechanism of the action of catalysts in hydrocarbon oxidation often remains unclear.

1.4.1 Saturated hydrocarbons

The most active oxide catalysts in hydrocarbon oxidation reactions (81) were found to be those of cobalt(II,III), chromium(III), manganese(III), nickel(II) and cerium(IV). Later, the same investigators (82) defined an activity series for methane oxidation:

$$Cr_2O_3 > Mn_2O_3 > CuO > Co_3O_4 > Fe_2O_3 > ZnO .$$

Slow ethane oxidation at 576 K produced CH_2O, CO, CO_2, HCOOH and peroxides (83). It has been suggested (84) that the partial oxidation of methane and ethane involved a radical chain mechanism. The gas phase oxidation of ethane by oxygen at 313 to 523 K was thought to involve two reactions - the stripping of hydrogen atoms (C-H bond cleavage) and the cleavage of a carbon-carbon bond (85). The overall rate constant (J) was given by:

$$k_{C_2H_6} = 0.9\times10^{-11} \exp(-21{,}758/RT)$$

and the following reactions were proposed:

$$O + C_2H_6 \longrightarrow CH_2O + H_2 + CH_2 \qquad [1.4.3]$$

$$k = 2.05\times10^{-12} \exp(-17{,}992/RT)$$

$$CH_2 + O_2 \longrightarrow CO + OH + H + 126 \text{ kJ mol}^{-1} \qquad [1.4.4]$$

$$O + C_2H_6 \longrightarrow \dot{O}H + \dot{C}_2H_5 \qquad [1.4.5]$$

$$k = 3.8\times10^{-11} \exp(-31{,}381/RT)$$

$$\dot{C}_2H_5 + O_2 \longrightarrow [C_2H_5O_2]^* \longrightarrow C_2H_4O + \dot{O}H . \qquad [1.4.6]$$

Reaction [*1.4.5*] was predominant at high temperatures. The main route in the gas phase oxidation of ethane from 573 to 673 K consists of the reactions of peroxide radicals (86) and recently (87) a number of reactions were described:

$$C_2H_6 + O_2 \longrightarrow C_2H_5 + HO_2 \qquad [1.4.7]$$

$$C_2H_5 + O_2 \longrightarrow C_2H_4 + HO_2 \qquad [1.4.8]$$

$$C_2H_5 + O_2 \rightleftharpoons C_2H_5O_2 \qquad [1.4.9]$$

$$C_2H_5O_2 \longrightarrow CH_3O + CH_2O \qquad [1.4.10]$$

$$C_2H_5O_2 \longrightarrow C_2H_4 + HO_2 \qquad [1.4.11]$$

$$C_2H_5O_2 + C_2H_4 \longrightarrow C_2H_4O + C_2H_5O \qquad [1.4.12]$$

$$C_2H_5O + C_2H_6 \longrightarrow C_2H_5OH + C_2H_5 \qquad [1.4.13]$$

$$CH_3O + O_2 \longrightarrow CH_2O + HO_2 \qquad [1.4.14]$$

$$C_2H_5O_2 + O_2 \longrightarrow C_2H_5O_4 \longrightarrow CH_3O + CH_2O + O_2 \qquad [1.4.15]$$

$$C_2H_5O_2 \longrightarrow \text{termination at wall.} \qquad [1.4.16]$$

A negative temperature coefficient for the reaction rate of ethane oxidation was observed around 623 K (87) and it has been reported that in the partial oxidation of light hydrocarbons some oxidation steps apparently occur on the surfaces of all reactors (88).

The chemisorption of ethane on iron(III) and nickel(II) oxides has been shown to involve C-H bond rupture (89) while studies of ethane oxidation (90) on nickel(II) oxide indicated that the hydrocarbon was adsorbed prior to any surface reaction with preadsorbed oxygen. The formation of a $C_2H_{5(ads)}$ species was proposed.

The ethane/water reaction was studied from 573 to 633 K over a nickel-chromium catalyst (91) and the rate equation evaluated:

$$r = \frac{k\, P_{C_2H_6}}{1 + A\, \frac{P_{H_2O}}{P_{H_2}}} \qquad [1.4.17]$$

where A = 0.644. The following sequence of surface reactions was postulated:

$$C_2H_6 + S \rightleftharpoons SC_2H_4 + H_2 \qquad [1.4.18]$$

$$SC_2H_4 + S \rightleftharpoons 2SCH_2 \qquad [1.4.19]$$

$$SCH_2 + H_2 \rightleftharpoons S + CH_4 \qquad [1.4.20]$$

$$SCH_2 + 2H_2O \longrightarrow S + CO_2 + 3H_2 \qquad [1.4.21]$$

$$H_2O + S \longrightarrow SO + H_2 \qquad [1.4.22]$$

where S represents a surface site.

The oxidation of methanol over vanadium(V) oxide at 519 to 554 K was described by the rate expression (92):

$$r = \frac{2k_1k_2P_{CH_3OH}P_{O_2}}{k_1P_{CH_3OH} + 2k_2P_{O_2}} \; . \qquad [1.4.23]$$

The authors favoured a Mars and van Krevelen mechanism where the activation energies for catalyst reduction and oxidation were 32 and 38 kJ mol^{-1}, respectively.

The kinetics of oxidation over palladium oxide of several C_1 to C_4 alkanes and cycloalkanes has been observed (93) from 588 to 873 K. Reaction appeared to involve the interaction of hydrocarbon from the gas phase with palladium oxide, followed by the rapid desorption of carbon dioxide and the slower desorption of water. The activation energy for ethane oxidation was 84 kJ mol^{-1} from 671 to 719 K.

The complete oxidation of isobutane, isobutene and n-butane was studied from 473 to 673 K over a supported barium chromate catalyst (94). The proposed mechanism involved the formation of lattice defects in hydrocarbon oxidation followed by re-oxidation of the catalyst with oxygen. The same catalyst was also very active in the complete oxidation of aromatic hydrocarbons.

The oxidation of methane by nitrous oxide has been observed at 873 K in a static system (95). The products were nitrogen, ethane, carbon monoxide and water. The dehydrogenation of butane in nitrous oxide with water present gave butene, 19%, and butadiene, 7.5% (96).

The complete oxidation of propane has been studied over hydrated manganese(IV) oxide (97) and supported copper(II) oxide, chromium(III) oxide and palladium (98). The activation energy for this first order, irreversible reaction was 90 kJ mol^{-1} in both cases and the products, carbon dioxide and water, had no effect on the reaction rate (97). A recent study of the complete oxidation of propane over nickel(II) oxide at 553 to 763 K (99) gave the rate of CO_2 formation as:

$$r = \frac{k p_{O_2}^{m} p_{HC}^{n}}{p_{H_2O}^{\ell}} . \qquad [1.4.24]$$

Values for ℓ, 0.35, m, 0.25 to 0.43, n, 0.50 to 0.37, and the activation energy, 107 kJ mol^{-1}, were in reasonable agreement with similar studies (100,101). At low temperatures, the rate-limiting step was thought to involve the interaction of adsorbed propane with an adsorbed oxygen species.

The complete oxidation of ethylene, ethane, propane and carbon monoxide was observed on a nickel(II) oxide catalyst at temperatures from 473 to 673 K (101). It was found that water inhibited oxidation reversibly. The rate of carbon dioxide production was given by equation [1.4.24] and the values for ℓ, m, and n for ethane oxidation were 0.35, 0.44 and 0.50 at 623 K; and 0.35, 0.07 and 0.95 at 513 K. The activation energy for

ethane oxidation was 29 kJ mol^{-1} below 543 K and 71 kJ mol^{-1} above. The change in activation energy was ascribed to a change in the rate-determining step. Evidence obtained from the kinetic isotope effect indicated that the rate-determining step from 573 to 673 K was either the adsorption of ethane as C_2H_5, if the chemisorption of ethane was rate-limiting, or the interaction between adsorbed oxygen and adsorbed ethane through attack at the C-H bond to produce a C_2H_5 species.

1.4.2 *Unsaturated hydrocarbons*

Generally, unsaturated hydrocarbons are more reactive towards oxygen than are saturated hydrocarbons and therefore they react over "milder" catalysts with better selectivity. The rates and selectivities vary with the position of the double bond and the nature of substituent groups (77).

The complete oxidation of ethylene over a palladium film was first order in ethylene and zero order in oxygen (69). The mechanism was believed to occur through the interaction of adsorbed species on the surface with the slow step, C-H bond rupture. The same authors studied olefin oxidation over precious metals (102) and produced the activity series:

$$Pt > Pd > Rb > Au.$$

The complete oxidation of ethylene over supported transition metal oxides (103) gave the following activity sequence at 535 K:

$$Co_3O_4 > Cr_2O_3 > Ag_2O > Mn_2O_3 > CuO > NiO > V_2O_5 =$$

$$CdO > Fe_2O_3 > MoO_3 > WO_3 > TiO_2 > ZnO.$$

The activation energy for ethylene oxidation over manganese(III) oxide supported on silica or alumina-silica from 535 to 617 K was 57 kJ mol^{-1}. The same value was obtained for the oxidation of benzene over a similar catalyst (103). The rate of ethylene oxidation over copper(II) oxide from 490 to 613 K was 0.6 order in ethylene with activation energy between 84 and 113 kJ mol^{-1} (104).

The catalytic properties of a number of oxides were studied in the

complete oxidation of isobutene, acetylene, ethylene and propane (100) and propylene (105). The authors determined a relationship between catalytic activity in terms of reaction order and ΔH_0, where ΔH_0 is the heat of formation of the oxide divided by the number of oxygen atoms in the oxide molecule. The sequence of hydrocarbon adsorption strength was:

isobutene > acetylene > propylene > ethylene > propane

which was the reverse of the activity sequence in terms of reaction order. The reaction order with respect to each hydrocarbon concentration over manganese(IV) oxide, for example, increased from -0.25 for isobutene to 1.0 for propane while the order with respect to oxygen concentration decreased from 0.54 to 0.0. In the oxidation of isobutene, the reaction order with respect to isobutene concentration increased along the catalyst series:

$$Pt < MnO_2 < Pd < Co_3O_4 < NiO < Fe_2O_3 < Cr_2O_3 < CeO_2.$$

In studies of the oxidation of a number of hydrocarbons, Yu Yao and Kummer (101) determined that the rate order with respect to oxygen concentration was usually 0.5. The inhibiting effect of water was described by orders of 0.25 to 0.35, representing values of ℓ in equation [*1.4.24*].

The oxidation of propylene over cobalt-manganese oxide spinels at 473 to 623 K was first order in oxygen and zero order in hydrocarbon (106, 107). It was suggested that the rate of the oxidation reaction was determined by the rate of oxygen chemisorption. Further studies on the complete oxidation of propylene over transition metal oxides (108) produced the activity series:

$$Mn_2O_3 > CuO > Cr_2O_3 > Co_3O_4 > Fe_2O_3 .$$

Using a static system, Anderson and Swanson (109) studied the complete oxidation of propylene, isobutene and benzene over lead(II) oxide at 503 to 583 K. The reaction was first order oxygen and zero order in hydrocarbon concentration with activation energies from 109 to 126 kJ mol^{-1}. It was believed that the oxygen which takes part in the reaction at the

steady state is van der Waals adsorbed molecular oxygen at low surface coverages. The hydrocarbons were strongly adsorbed on the catalyst surface. In the complete oxidation of propylene, it was felt that a negatively charged complex participated in the rate-limiting step (70) and that the active form initiating oxidation should be propylene.

The catalytic activity of various manganese oxides for the complete oxidation of propylene has been studied (110) in the presence of excess oxygen. It was observed that the derived activation energies were close to the bond energies of surface oxygen, and suggested the rate-limiting steps could involve cleavage of the metal-oxygen bond on the catalyst surface.

The catalytic oxidation of 1-butene over bismuth molybdate (111,112) was found to involve a surface reduction reaction followed by catalyst re-oxidation with gaseous oxygen. A number of reaction steps were given:

$$C_4H_8 + [\ ] + O^{2-} \rightleftharpoons \bar{C}_4H_7 + \bar{O}H \qquad [1.4.25]$$

$$Mo^{6+} + \bar{C}_4H_7 \longrightarrow [Mo = C_4H_7]^{5+} \qquad [1.4.26]$$

$$[Mo = C_4H_7]^{5+} + O^{2-} \longrightarrow Mo^{4+} + [\ ] + \bar{O}H + C_4H_6 \qquad [1.4.27]$$

$$2\bar{O}H \rightleftharpoons O^{2-} + [\ ] + H_2O \qquad [1.4.28]$$

$$O_2 + 2[\ ] + 2Mo^{4+} \longrightarrow 2O^{2-} + 2Mo^{6+}\ . \qquad [1.4.29]$$

The principal products of oxidation were butadiene, carbon monoxide and carbon dioxide with some cis and trans-butene formed.

The following activity series was determined in the complete oxidation of benzene (113) over transition metal oxides:

$$Co_3O_4 > CuO > MnO_2 > Cr_2O_3 > NiO > V_2O_5 > TiO_2 > Fe_2O_3 > ZnO\ .$$

Rate orders with respect to benzene ranged from 0.5 to 1.0 and water had an inhibiting effect. A correlation was found between catalytic activity and the bond energy of the oxygen on the oxide surface.

The catalytic reactivity series presented in the literature for transition metal oxides (82,100,103,108,113) in the complete oxidation of

hydrocarbons show little agreement. However, some general features do arise. Those oxides with poor reactivity-vanadium(V), iron(III), titanium(IV) and zinc(II) - consist of metal atoms with empty, half-filled, or completely filled d orbitals. Nickel(II) oxide, d^8, is usually in the middle of the series. The most active oxides - cobalt(II,III), chromium(III), manganese(III) and copper(II) - however, exhibit no apparent regularity. As evidenced by the preceding review, the catalytic oxidation of even the simplest of hydrocarbons is not fully understood at the molecular level.

1.5 *Carbon fibres*

In the present study, the use of carbon fibres as catalyst supports was evaluated. It is necessary at this point, then, to review some of the general physical and chemical properties of these polymers.

Carbon fibres are usually prepared by the controlled pyrolysis of synthetic organic polymer fibres under stress. There are essentially two types of fibres:

Type I, high modulus, formed by pyrolysis at ∿3000 K and,

Type II, high strength, formed by pyrolysis at ∿1500 K.

There are a number of basic reviews of the structure and physical properties of carbon fibres available in the literature (114-119). A complete description is outside the scope of this thesis. Those used in the present study were based on polyacrylonitrile (PAN) and a detailed account of their structure may be obtained elsewhere (120,121).

Generally, the basic structural unit of the fibre consists of undulating ribbons of sp^2 carbon which form microfibrils and fibrils orientated along the fibre axis. The fibres consist of a circumferentially-aligned outer shell connected to a central core by a honeycombed radial continuum. The structure contains internal voids, flaws and cracks as well as surface flaws (121).

Other general properties of carbon fibres (122) include a physical density of approximately 1.8 g cm^{-3}, an approximate crystal density of

2.2 g cm^{-3}, an expected porosity of 17% and a fibre diameter of 8 μ.

The surface characteristics of various carbon fibres have been examined by nitrogen (123,124) and krypton adsorption (125,126). Carbon fibres and surface-treated fibres (with nitric acid) have a low specific surface area, < 1 m^2 g^{-1}, with no significant hysteresis evident in nitrogen adsorption/desorption isotherms. However, a desorption phenomenon related to light exposure has been observed.

The activation of carbon fibres by controlled pyrolysis and steam activation has been studied in order to prepare fibres with controlled adsorption and structural properties (128-132). Fibres with specific surface areas of up to 2000 to 3000 m^2 g^{-1} have been prepared (128,133). Most of this work has been directed towards refining selective adsorption properties of the fibres and a general review of their pore structures and properties has been written by Bohra (134).

The use of carbon fibres as catalyst supports, however, has received relatively little attention. And yet, because of their mechanical strength, thermal stability, flame and chemical resistance, carbon fibres could prove to be applicable as supports with long service life (135), particularly in the hydrocarbon conversion field (136).

Carbon filaments alloyed with transition metals (nickel, cobalt, chromium, manganese) have been used as catalysts in the dehydration of secondary alcohols (137). An investigation into the use of a platinum/carbon fibre catalyst (136) indicated that the catalyst had to be thermally activated. A palladium/carbon fibre catalyst was prepared by first activating the fibre in air at 673 K for 2 h before immersing it into a palladium(II) chloride solution (135).

The patent literature describes a number of catalysts for NO_x reduction which consist of transition metals on activated carbon supports (138,139). In the oxidation of olefins by oxygen and steam on a palladium/carbon catalyst (140), the carbon was thought to act as a co-catalyst. The following order of reactivity was obtained for partial oxidation:

ethylene > propylene > butene > cyclohexene > butadiene

Another related series of catalysts would include graphite intercalation compounds. The scope of these catalysts, however, is severely limited by their sensitivity to oxygen and water vapour. A recent review of the catalytic properties of these compounds has been published (141).

CHAPTER II

EXPERIMENTAL PROCEDURE

2.1 *Introduction*

The investigation of reaction rate and factors affecting reaction rate is of importance to research in heterogeneous catalysis. Kinetic data are used to develop rate equations which are consistent with observations of the reaction mechanism. Although it is not usually possible to obtain a complete description of a catalytic reaction from kinetic studies alone, the method has substantial significance to both laboratory and plant scale investigations.

There are essentially three different types of laboratory reactors which have been used in basic kinetic studies - the constant volume "static" reactor and the steady and non-steady-type flow reactors. "Static" reactors were the earliest used to study catalytic reactions (142,143), however, they are seldom employed today because of the experimental uncertainties involved with the technique.

Of the non-steady flow reactors, the pulsed microcatalytic reactor is commonly used. In this technique, a fixed bed of catalyst is exposed to a small quantity of reactants (a pulse) injected into the carrier gas stream (144). It provides a convenient and rapid method for studying the process of catalyst "conditioning" by pretreating with reactants under non-steady state conditions. A major disadvantage is that rates are not usually extractible from the data obtained from such reactors, so comparison with other work is not always possible unless a number of assumptions are made (145).

Weisz and Prater (146) used a modified Schwab reactor (147) which has been developed into the continuous-flow technique (148). In this system a mixture of reactants, diluted by carrier gas, is passed continuously

through a reaction vessel containing the catalyst. Reaction rates and activities may then be determined when the reactor system operates under steady-state conditions. The system can then be treated by the Damköhler equation (149) or by equations such as that developed by Menold (150). Reaching steady-state activity, however, creates an inherent problem regarding the exact chemical and physical nature of the catalyst after conditioning. Complimentary data may be obtained with the steady and non-steady type flow reactors.

2.2 *Flow system*

High purity helium (>99.99%) was passed through a drying column, containing Davison Grade 564 molecular sieve, which also acted as a pressure stablizer, into a common junction, Figure 2.2.1. Flow rates were established using Matheson Flowmeters fitted with Matheson Millimite fine-control needle valves and calibrated for each gas used with a soap bubble flow meter.

The helium carrier gas was channeled into a common manifold where it mixed with the other reactant gases in quantities related to the experimental requirements. All reactant gases were maintained at an equivalent backing pressure. The temperature of the manifold was maintained at 423 K by heating tape. The reaction mixture then entered a preheater, which raised the temperature of the gas stream close to that of the reaction conditions, and then was fed into the reactor where it contacted the catalyst. The effluent was conducted to the gas chromatograph by heated flow lines. Product gases were periodically analyzed via a gas sampling valve. The reaction products were otherwise vented to a fume hood.

Flow line (b), Figure 2.2.1, was used for the addition of pure helium carrier gas to maintanin a constant total flow of 350 dm^3 min^{-1}(NTP) in the system. Lines (c) and (d) were used for the addition of hydrocarbon and oxidant, respectively. In reaction rate studies, line (a) was used to

introduce reaction products, such as nitrogen, carbon dioxide and water vapour.

To introduce water vapour to the reactor, helium was passed through an all-glass, double-pass water saturator, maintained at a constant temperature by a water bath equipped with a Braun Thermomix II circulatory heater which maintained the temperature at 323.0 ±0.1 K. This corresponds to a water vapour pressure of 12.3 kPa. A thin layer of silicone oil on the top of the bath prevented the loss of bath water. Water used in the saturator was deionized, double distilled and degased prior to use by purging with helium for 30 min. The saturator efficiency with respect to saturation by water vapour was examined using helium flow rates of 10, 50, and 100 $dm^3\ min^{-1}$ and found to be 97.2, 97.7 and 97.6%, respectively (appendix A1).

The vertical catalytic reaction chamber was constructed from 20 mm i.d. quartz tubing and, with B24/40 ground joints at each end to facilitate the loading and removal of catalyst samples, had an overall length of 58 cm. The catalysts were sandwiched between quartz wool plugs supported on three dimples in the reactor wall 32 cm from the entry port.

The tubular furnace consisted of 5.14 m of chromel A resistance wire (5.45 ohms m^{-1}) uniformly and non-inductively wound in parallel grooves on the quartz tube. The tube was then covered with asbestos string (6.35 mm d) and asbestos tape to give an outside diameter of 6 cm. The reactor was finally wrapped tightly with two layers of aluminum foil.

Reactor temperature was controlled by a Thermo Electric 400 indicating controller with a chromel/alumel thermocouple positioned in a thermometer well touching the catalyst bed. A ballast variable resistance was connected in series to the furnace windings and adjusted with temperature to eliminate slow temperature cycling. Careful adjustments to the proportional and reset controls of the Thermo Electric 400 and the ballast resistor were required to maintain the reactor temperature to within ±0.2°C of the setpoint.

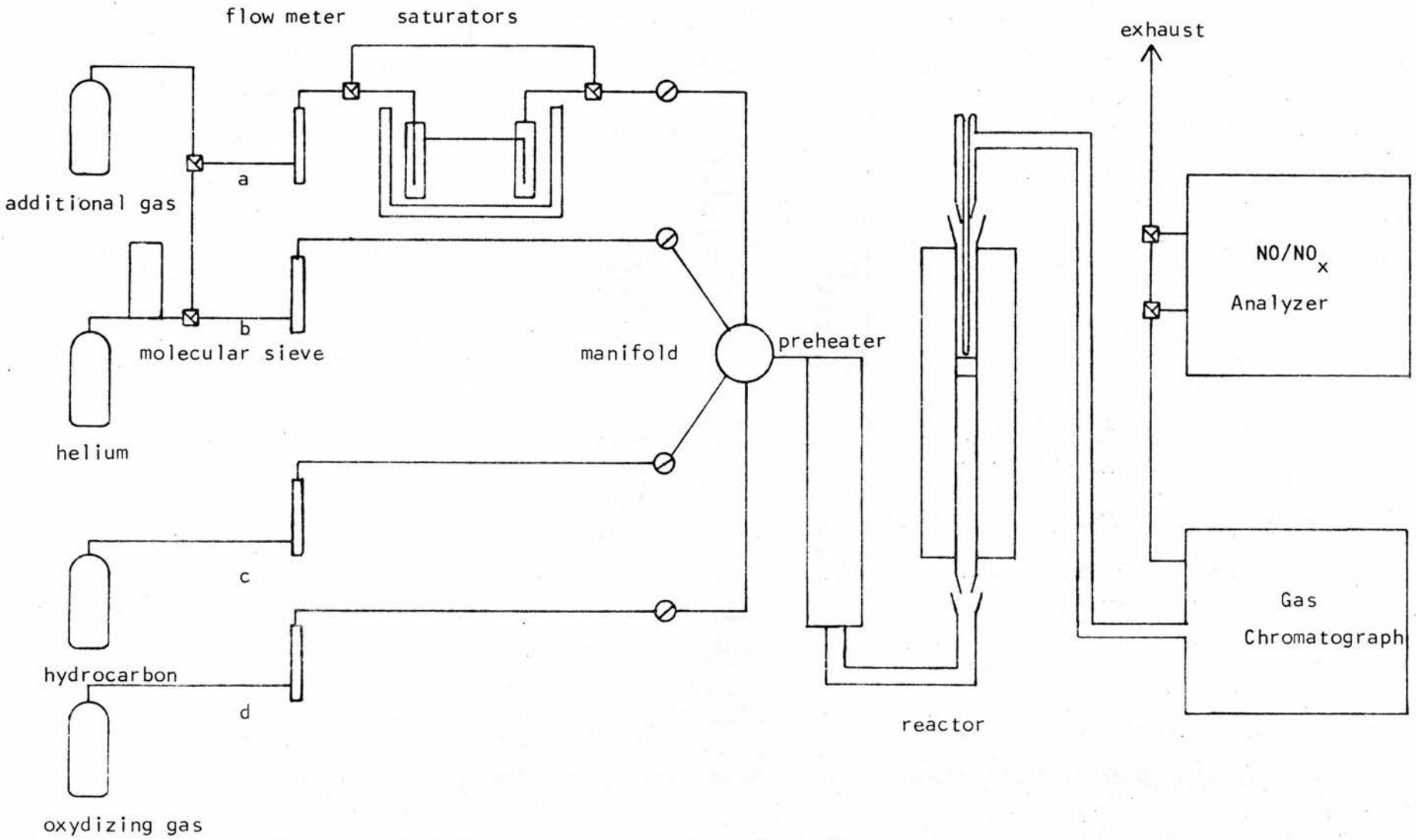

Figure 2.2.1 Schematic representation of the flow system.

The temperature distribution within the reactor was recorded by incorporating eight chromel/alumel thermocouples at 2 cm intervals on the outside of the quartz tubing in the asbestos string. At a helium flow of 350 dm^3 min^{-1} (NTP), the catalyst bed was well within the region of homogeneous temperature and at the temperature indicated by the controller setpoint, ±0.1°C, from 373 to 773 K.

The ground glass joints on the reactor were fitted with B24/40 teflon sleeves. The integrity of these joints was checked by mixing nitric oxide with the helium carrier gas and checking for leaks using a Beckman Model 951 NO/NO_x Analyzer on its most sensitive range of 10 ppm fullscale.

2.3 *Analysis*

2.3.1 *Gas chromatograph*

The gas stream containing reaction products was analysed using a Hewlett Packard Research Chromatograph Model 5754B with both flame ionization and thermal conductivity detectors. Samples were injected by a dual-loop gas sampling valve maintained at 468 K.

Two different analytical columns were used throughout the study. The first was constructed from stainless steel tubing, 305x0.32 cm o.d., packed with Poropak Q (120-150 mesh). Prior to each injection, the column oven was maintained at 333 K and this temperature was held for a post-injection interval of 3 min which allowed nitrogen, oxygen, nitric oxide, carbon dioxide and nitrous oxide to be eluted. The column oven was then heated by linear-temperature programming at 60 K min^{-1} to a maximum of of 408 K where it was maintained for 8 min to allow water, ethane and 1-butene to be eluted. The column oven was then recycled to 333 K. The gas stream could be sampled every 20 min in this manner.

The second column was constructed from 244x0.32 cm o.d. stainless steel tubing packed with 61 cm Carbosieve B and 183 cm Poropak T. The column oven was temperature programmed with a two-minute post-injection interval at 333 K followed by a 60 K min^{-1} temperature rise to 443 K where

the temperature was maintained for five minutes to allow ethane to be eluted prior to recycling. When operated at low temperatures (i.e. 293 K) this column allowed the separation of nitrogen, nitric oxide and carbon monoxide.

Helium was passed continuously through the columns at 30 dm^3 min^{-1}. Compressed air, 300 dm^3 min^{-1}, and hydrogen, 30 dm^3 min^{-1}, were used as a source for the jet flame of the ionization detector. In addition, an auxillary stream of helium, 40 dm^3 min^{-1}, was passed through the flame detector which was maintained at 448 K. This detector was used to determine the presence of any partial oxidation products.

The flame detector oven was maintained at 453 K. The thermal conductivity detector oven was maintained at 473 K with a current of 235 mA passing through the filaments. Detector amplifiers were adjusted to ensure that individual component peaks remained on scale. Chromatograms were recorded on a Servogor S potentiometric flatbed recorder with integrator, Brinkman Instruments model 2542.

For each experiment, samples of the first gases eluted through the columns were analysed on an Hitachi-Perkin Elmer RMU-7 mass spectrometer. This check was necessary to ensure that the first chromatogram peak was identified accurately. With this method, nitrogen, oxygen and carbon monoxide could easily be recognized.

2.3.2 *NO/NO_x analyser*

The gas effluent stream could also be passed through a Beckman Model 951 NO/NO_x Analyser. On its most sensitive range, 10 ppm fullscale, the analyser was used to check for leaks in the apparatus and to monitor the atmosphere in the laboratory when nitric oxide was used. It was also used to calibrate the gas chromatograph for nitric oxide. The analyser converts nitric oxide to nitrogen dioxide by gas-phase oxidation with ozone. A characteristic of this reaction is the elevation of approximately 10% of the nitrogen dioxide molecules to an electronically-excited state. These

immediately revert to the non-excited state accompanied by the emission of photons which impinge on a photomultiplier detector generating a current which is amplified to drive a front-panel meter. For NO_x determination, the sample first passes through a converter which dissociates any nitrogen dioxide to nitric oxide and the total nitric oxide in the converted sample is measured.

2.4 *Gas chromatograph calibration*

Detectors were calibrated for concentrations of gaseous components by the exponential dilution method (151). The SKC Exponential Dilution Flask consisted of a glass flask of known volume containing a magnetically-driven stainless steel mixer and fitted with a septum injection port. A constant flow of helium was passed through the flask and into the sample loop of the gas chromatograph. A known volume of gas was injected into the dilution flask at time =0 and by the use of equation [*2.4.1*] the partial pressure of gas at time = t, pt, could be calculated.

$$pt = po \exp - \frac{f}{v} t \qquad [2.4.1]$$

where po is the partial pressure of the gas at t=0, f, the flow rate, and v, the flask volume. At timed intervals the gas stream was sampled by the gas chromatograph and a calibration curve of peak area against partial pressure was constructed. All such plots were linear.

2.5 *Surface area measurements*

It is well established that the surface area, SA ($m^2\ g^{-1}$), of non-porous solids may be estimated from the physical adsorption of gases by deriving a value for the monolayer capacity at NTP, X_m, and using the equation:

$$SA = \frac{X_m}{22414} \cdot 6.023 \times 10^{23} \cdot A_m \times 10^{-20} \qquad [2.5.1]$$

where A_m is the area in square Ångstrom units occupied per molecule of adsorbate. The technique has been used extensively and gives reliable results for relative surface area values (152).

The kinetic approach of Brunauer, Emmett and Teller (153) and the statistical mechanical approach of Hill (154) both lead to the BET multilayer equation relating the monolayer volume, V_m ($dm^3\ g^{-1}$), at the saturation pressure of the adsorbate gas, po, to the total volume of gas adsorbed, V, at a measured pressure, p, thus:

$$\frac{p}{V(po-p)} = \frac{1}{V_m C} + \frac{(c-1)p}{V_m C po} \qquad [2.5.2]$$

where C is a constant related to the heats of adsorption and liquifaction of the gas.

Although the BET treatment may have little theoretical validity, it still provides a useful mathematical description of physical adsorption processes at low temperatures. A plot of p/V(po-p) against p/po gives a straight line of slope $(C-1)/V_m C$ and intercept $1/V_m C$ for a usual range of relative pressures (p/po) from 0.05 to 0.35. The monolayer volume can then be determined from the simple relationship:

$$V_m = 1/(\text{slope} + \text{intercept}). \qquad [2.5.3]$$

2.5.1 *Krypton surface areas*

For the measurement of small values of surface area, $<20\ m^2\ g^{-1}$, it is necessary to use an adsorbate such as krypton which has a low saturation pressure at the temperature of the experiment so that the number of adsorbed molecules is approximately equal to the number remaining in the gas phase (155). The cross-sectional area of the adsorbed krypton molecule was assumed to be 19.5 Å (156) and hence, specific surface area was given by:

$$SA = 5.24\ V_m. \qquad [2.5.4]$$

The apparatus for the determination of specific surface area by

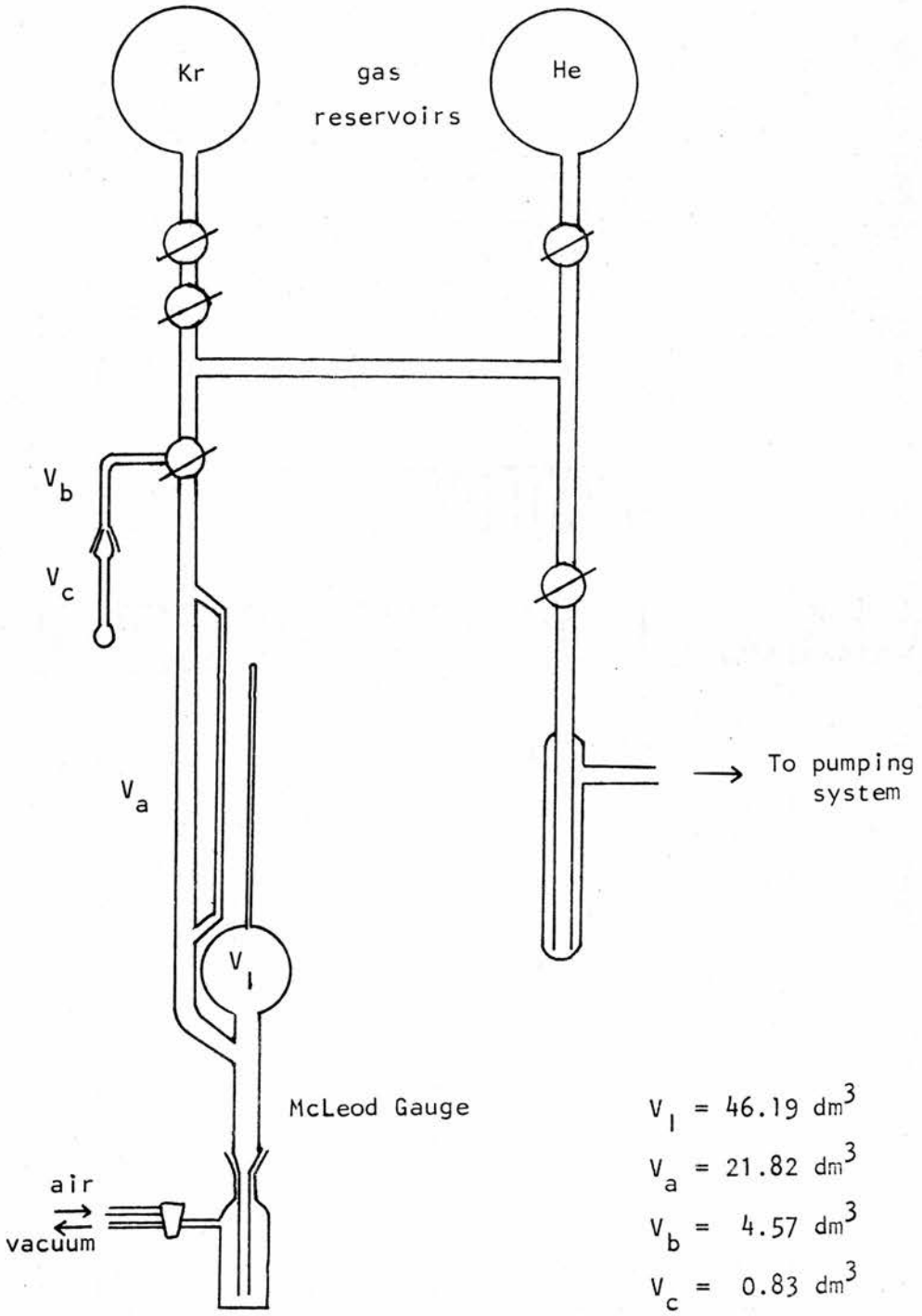

Figure 2.5.2 Apparatus for the determination of surface area using krypton gas as adsorbate at 77 K.

krypton adsorption is shown in Figure 2.5.1. Equilibrium pressures were corrected for thermal transpiration (156) which occurs at low pressures (10^{-4} kPa) when the mean free path of the gas molecules is of the same order of magnitude as the diameter of the adsorbent vessel. The corrected pressure, pe, was given from the empirical equation (157):

$$pe = pm \left[1 - \frac{0.490}{37.2\ (dpm)^2 + 14.45\ dpm + 1} \right] \qquad [2.5.5]$$

where pm is the McLeod gauge pressure, and d, the vessel diameter.

2.6 *X-ray analysis*

The oxides were analysed by X-ray powder diffraction techniques before and after catalysis using a 114.83 mm Debye-Scherrer camera and nickel-filtered copper Kα radiation from a Philips PW/1130/00/60 X-ray Generator. Interplanar spacings were calculated from the photographic film and compared to standard data (158).

2.7 *Scanning electron microscopy*

Samples were characterized by scanning electron microscopy (SEM) using a Cambridge Stereoscan 600. A standard flash evaporation technique at 10^{-5} kPa was used to coat samples with a thin layer of gold. Pictures were taken with a 35 mm camera attached to the CRT screen.

2.8 *Infrared analysis*

Specimens were prepared by grinding a mixture of the oxide sample with dry potassium bromide (0.5% w/w) in an agate mortor. Pellets were prepared in a 1.27 cm die on a hydraulic press. Infrared spectra were recorded on a Beckman IR12 Spectrophotometer operated in the double-beam mode with a pellet of pure potassium bromide positioned in the reference beam. Calibration of the instrument was checked against a standard polystyrene film.

2.9 *Thermal analysis*

Carbon fibres, 40 mg, were examined on a Stanton-Redcroft Thermobalance, Model HT-5F. The sample temperature was monitored on a Leeds and Northrup recorder from a platinum/platinum-rhodium (13%) thermocouple positioned within the sample support, in contact with the platinum crucible. A silica sheath allowed control of the atmosphere surrounding the sample. The 37.5 mm bore platinum/rhodium wound furnace was heated linearly at 7 K min^{-1}. A flowing atmosphere of 230 dm^3 min^{-1} (NTP) air or nitrogen was maintained and weight changes of 0.1 mg could be detected.

2.10 *ESCA analysis*

X-ray photoelectron spectra were obtained on a Vacuum Generator Limited ESCA-3 spectrometer using aluminum K α radiation. A 50 eV electron analyser pass energy was used. Samples were run as powders, mounted on double-sided tape, and the spectra were corrected for charging by reference to the C(1s) line at 284.0 eV. Spectra were recorded and analysed by Mr. R. Lazier and Dr. D. K. Creber of Alcan International Limited, Kingston Laboratories, Kingston, Ontario.

2.11 *Materials*

2.11.1 *Manganese(III) oxide*

Manganese metal (Alfa Inorganics, 99.999% w/w) was dissolved in nitric acid to give a 4 M solution at pH6. This was maintained at 333 K while a 4 M solution of ammonium oxalate was added with vigorous stirring to precipitate $MnC_2O_4 \cdot 2H_2O$. The manganese oxalate was washed free of nitrate ions with de-ionized water and dried at 378 K for 16 h. Manganese (III) oxide was produced by calcining the oxalate at 573 K for 5 h, followed by 16 h at 673 K and 16 h at 873 K (159-161). X-ray powder diffraction confirmed the α-manganese(III) oxide phase, Table 3.3.3, and chemical analysis (162) indicated 69.7% manganese (theory 69.59%).

2.11.2 *Other oxides*

Scandium(III) oxide (99.9% w/w), zinc(II) oxide (99.99%), chromium (III) oxide (99%), iron(III) oxide (99.99%), vanadium(V) oxide (99.9%) and tin(II) oxide (99.99%) were obtained from Alfa Inorganics Limited along with manganese(II) (99.99%) and manganese(III) oxide (99.9%). Copper(II) oxide (99%), manganese(IV) oxide (99.9%) and nickel(II) oxide (99.99%) were obtained from BDH Chemicals Limited. Aluminum(III) oxide (99.9%) and titanium(IV) oxide (99%) were purchased from Baker Chemical Company. All oxides were heated in air at 773 K for 10 h and stored in desiccators prior to use.

2.11.3 *Carbon fibres*

Two types of PAN-based carbon fibres were studied. The first was Modmor high modulus reinforcing carbon, Type III S (surface treated) supplied by Morganite Modmor Limited and the second, Grafil carbon reinforcement Type HTV from Courtaulds, Coventry.

In order to activate or increase the surface area of these fibres, a number of techniques were evaluated. The first involved the effect of a microwave discharge on the fibres using a Microton 200 Microwave Power Generator MK2. Incorporated into a simple vacuum line was a plug-flow-type reactor which had two inlet lines used to leak in the gases required to strike a discharge. The carbon fibre plug was evacuated to 10^{-5} kPa, then the gases - argon, argon/water vapour or oxygen - were allowed to leak into the vacuum line. A discharge was struck with a Tesla coil at pressure ranging from 10^{-3} to 5×10^{-2} kPa and the effects upon fibre weight and surface area were recorded.

More conventional treatment studies involved the effects of air oxidation or steam activation at high temperatures up to 1200 K. A tube furnace was fitted with a silica sheath to hold the carbon fibres and allow a flowing atmosphere to be maintained. The effect of water vapour was observed by passing nitrogen through a double-pass water saturator thermo-

statted at 323 K and then over the fibre.

Samples of fibres were impregnated with transition metal nitrates - manganese(II), cobalt(II), nickel(II), copper(II) - by immersing 1 g of fibre (10 cm lengths) in 100 ml of a 10 % w/w solution of the nitrate for 24 h with constant stirring. Fibres were filtered, washed with distilled water and dried at 378 K for 24 h and 773 K for 2 h followed by steam activation at 773 K for 30 min. This method gave less than 1% w/w of metal on the fibre (162).

In a second method, Modmor fibres were sprayed with a 50% w/w aqueous solution of manganese(II) nitrate and then dried with a hot air gun at temperatures up to 573 K. The fibres were sprayed and dried in 10 cycles and chemical analysis (162) indicated 9.5% w/w manganese on the carbon after treatment in nitrogen at 773 K for 2 h.

2.11.4 Reagents

Ethane (99.0%), 1-butene (99.0%), nitric oxide (99.0%) and oxygen (99.99%) were supplied from Matheson of Canada Limited. Carbon dioxide (99.5%), nitrogen (99.99%) and helium (99.995%) were obtained from Canadian Liquid Air Limited and nitrous oxide (99.9%) from Liquid Carbonic Limited.

Water in the gas saturators was double-distilled and deionized prior to use. Transition metal nitrates were Fisons Laboratory Reagent grade while a 50% w/w manganese(II) nitrate solution was obtained from BDH Chemicals Limited.

The nitric oxide contained a 2.5% nitrous oxide impurity as determined by gas chromatography. A simple cold trap of liquid nitrogen and technical pentane (150 K) was demonstrated to be sufficient to remove this impurity to within the limits of detection, <0.002 kPa.

CHAPTER III

RESULTS

3.1 *Introduction*

Investigations of the mechanisms of heterogeneous catalytic reactions provide an important fundamental contribution to the development of industrial catalysts. The reaction mechanism is composed of the nature and sequence of the individual steps involved.

The evaluation of the kinetics of heterogeneous catalytic reactions under steady state conditions has evolved into a refined system of concepts and methods (163). This provides the basis of chemical reactor modeling, and a useful method for gaining knowledge of mechanisms.

The kinetic steps in a heterogeneous catalytic reaction are also related to the characteristics of the catalyst surface and the interaction between that surface and the reaction medium. The reaction rate as measured experimentally may therefore be controlled by transport phenomena such as flow, diffusion or convection gradients (164-167). Before kinetic modeling studies can lead to a meaningful mechanistic description, it is necessary to remove any contribution from transport processes.

It is generally accepted that there are five major steps involved in a heterogeneous catalytic reaction:

(1) transport of reactants to the catalyst

(2) adsorption of reactants on the surface

(3) interaction of adsorbed reactants

(4) desorption of products from the surface

(5) transport of products away from the catalyst.

Steps (1) and (5) may be rate-limiting, especially in highly porous catalyst systems, although they do not involve a chemical reaction.

If one of steps (2), (3) or (4) is rate-controlling, the catalytic

reaction may be interpreted using the Arrhenius equation:

$$k = A \exp(-E_a/RT) \qquad [3.1.1]$$

where k is the rate constant, A, the pre-exponential factor, and E_a, the apparent activation energy. For chemically-controlled reactions, the activation energy is generally greater than 40 kJ mol^{-1} while that for reactions which are entirely diffusion-controlled normally ranges from 8 to 16 kJ mol^{-1} (168). An intermediate contribution by diffusion factors would yield experimental activation energies somewhere between 8 kJ mol^{-1} and the true value. The evaluation of transport effects, then, is very important in any catalytic investigation.

The catalytic reaction rate is influenced by temperature and concentration gradients within the catalyst as a result of diffusion phenomena. To test for heat and mass transfer to the external surface of a fixed bed of catalyst, variations in the fluid diffusion coefficients are observed with changes in the linear velocity of the fluid (167,169). The reaction rate will be expected to increase with increase in flow rate in a catalytic reaction with film diffusion limitations.

Chambers and Boudart (170) noted that the usual test of examining the effect of total flow rate on the reaction may fail due to a lack of sensitivity under certain conditions of heat and mass transfer. The usual tests of examining the isothermal effects of flow rate (167) and particle size (167,171) were therefore extended by determining the experimental activation energy of the catalytic reaction under different conditions (172).

3.2 *Diffusion effects*

Preliminary investigations of the catalytic oxidation of a number of hydrocarbons - ethane, propane, butane, ethylene, propylene, 1-butene - by nitric oxide, nitrous oxide and oxygen over manganese(III) oxide indicated that complete oxidation occurred. It was decided to use the nitric oxide/ethane and nitrous oxide/ethane reactions as standards for in-depth

diffusion studies.

In order to determine the chemical kinetic parameters accurately, it was necessary to alter the experimental conditions of reaction to identify the true kinetic regime. Initial studies indicated that reactant partial pressures of approximately 2.6 kPa from 573 to 673 K gave less than 15% ethane conversion at total flow rates from 300 to 400 dm^3 min^{-1} (NTP). No reaction was observed when each reactant was passed individually over the catalyst in this temprature range. Similarly, no reaction was observed when mixtures of nitric oxide/ethane or nitrous oxide/ethane were passed through the reactor containing only quartz wool plugs at <723 K.

3.2.1 *The effect of flow rate: nitric oxide/ethane reaction*

With the partial pressures of both reactants held at 2.66 kPa, the total flow rate through the catalytic reactor was altered from 200 to 450 dm^3 min^{-1} (NTP). The experimental rate of product formation was examined at 573, 623 and 673 K.

Prior to use, the catalyst (1 g) was pretreated at 673 K for 180 min at the highest flow rate to ensure steady catalytic activity which was attained after 180 min. For each flow rate, three successive samples were analysed. The results are presented in Figure 3.2.1 as the rate of carbon dioxide formation expressed in mol m^{-2} s^{-1} versus total flow rate.

Generally, the rate of catalysis varied linearly with total flow rate from 200 to 300 dm^3 min^{-1} (NTP). From 300 to 400 dm^3 min^{-1} (NTP), the rate remained constant and increased again at higher flow velocities. The rate of nitrous oxide formation followed essentially the same curve for all temperatures similar to that for carbon dioxide formation at 573 K. The effect of temperature on the experimental activation energy for carbon dioxide formation was examined by plotting the logarithm of the reaction rate against the reciprocal temperature for each flow rate, Figure 3.2.2. The three points did not lie on a straight line so that two values for apparent activation energy were estimated, one from 673 to 623 K and

the other from 623 to 573 K. The values did not vary systematically with flow rate, Table 3.2.1, and the averages were 62 kJ mol^{-1} for the high temperature region and 34 for the low region. A similar two-stage Arrhenius plot was obtained using reaction rate constants, section 3.3.2.

3.2.2 *The effect of flow rate: nitrous oxide/ethane reaction*

Variations in the total gas flow rate on the catalytic rate were examined at 573, 623 and 675 K from 200 to 450 dm^3 min^{-1} (NTP). The partial pressures of nitrous oxide and ethane were both maintained at 2.66 kPa.

The manganese(III) oxide catalyst was pretreated with the reactant mixture at 673 K for 180 min to ensure steady catalytic activity. The results are presented in Figure 3.2.3 as the rate of nitrogen or carbon dioxide formation versus total flow rate. At 573 K, the catalytic rates were relatively unaffected by total gas flow rate. At 623 and 673 K, the rate increased with total flow rate, exhibiting a plateau in the 300 to 400 dm^3 min^{-1} (NTP) range. The effect of total gas flow rate upon the apparent activation energy was estimated from an Arrhenius-type plot. The results, Table 3.2.2, indicated that the apparent activation energy did not vary systematically with flow rate. The average value for the apparent activation energy for nitrogen formation was 96 kJ mol^{-1} and for carbon dioxide formation, 116 kJ mol^{-1}.

In all subsequent studies, a total gas flow rate of 350 dm^3 min^{-1} (NTP) was used since these experiments provided evidence that gas phase diffusion effects were then minimal.

3.2.3 *Particle size effects: nitric oxide/ethane reaction*

The effect of particle size on the catalytic rate of the nitric oxide/ethane reaction was examined by sieving the manganese(III) oxide through screens of dimensions: 0.149, 0.105, 0.074 , 0.054 and 0.037 mm. The experimental rate was measured at 623 and 673 K for each sieved sample

TABLE 3.2.1 The effect of total gas flow rate on the NO/C_2H_6 reaction over Mn_2O_3

Flow Rate $dm^3\ min^{-1}$	$r_2 \times 10^{-8}$ (mol $m^{-2}\ s^{-1}$)			$r_3 \times 10^{-8}$ (mol $m^{-2}\ s^{-1}$)			Experimental Ea (kJ mol^{-1})	
	573K	623K	673K	573K	623K	673K	673K-623K	623K-573K
200	1.97	3.49	8.89	1.69	2.34	2.15	65	34
250	2.54	4.15	10.50	2.05	2.76	2.39	65	29
300	2.85	5.10	12.35	2.34	3.36	3.26	62	35
350	2.88	5.41	12.76	2.77	3.73	3.43	60	37
400	2.90	5.39	12.92	2.80	3.83	4.07	61	37
450	3.85	6.61	15.83	3.60	4.69	4.82	61	32

TABLE 3.2.2 The effect of total gas flow rate on the N_2O/C_2H_6 reaction over Mn_2O_3

Flow Rate ($dm^3\ min^{-1}$)	$r_1 \times 10^{-8}$ (mol. $m^{-2}\ s^{-1}$)			$r_2 \times 10^{-8}$ (mol $m^{-2}\ s^{-1}$)			Experimental Ea	
	573K	623K	673K	573K	623K	673K	From r_1	From r_2
200	1.69	14.9	41.6	0.27	4.04	12.6	104	124
250	1.97	17.1	50.2	0.31	4.50	14.1	105	124
300	3.39	19.5	53.7	0.63	4.71	16.5	89	105
350	3.45	19.7	53.2	0.63	5.24	16.4	88	105
400	3.47	19.6	70.5	0.68	4.95	21.7	97	112
450	4.32	20.6	79.4	0.51	5.37	23.4	93	124

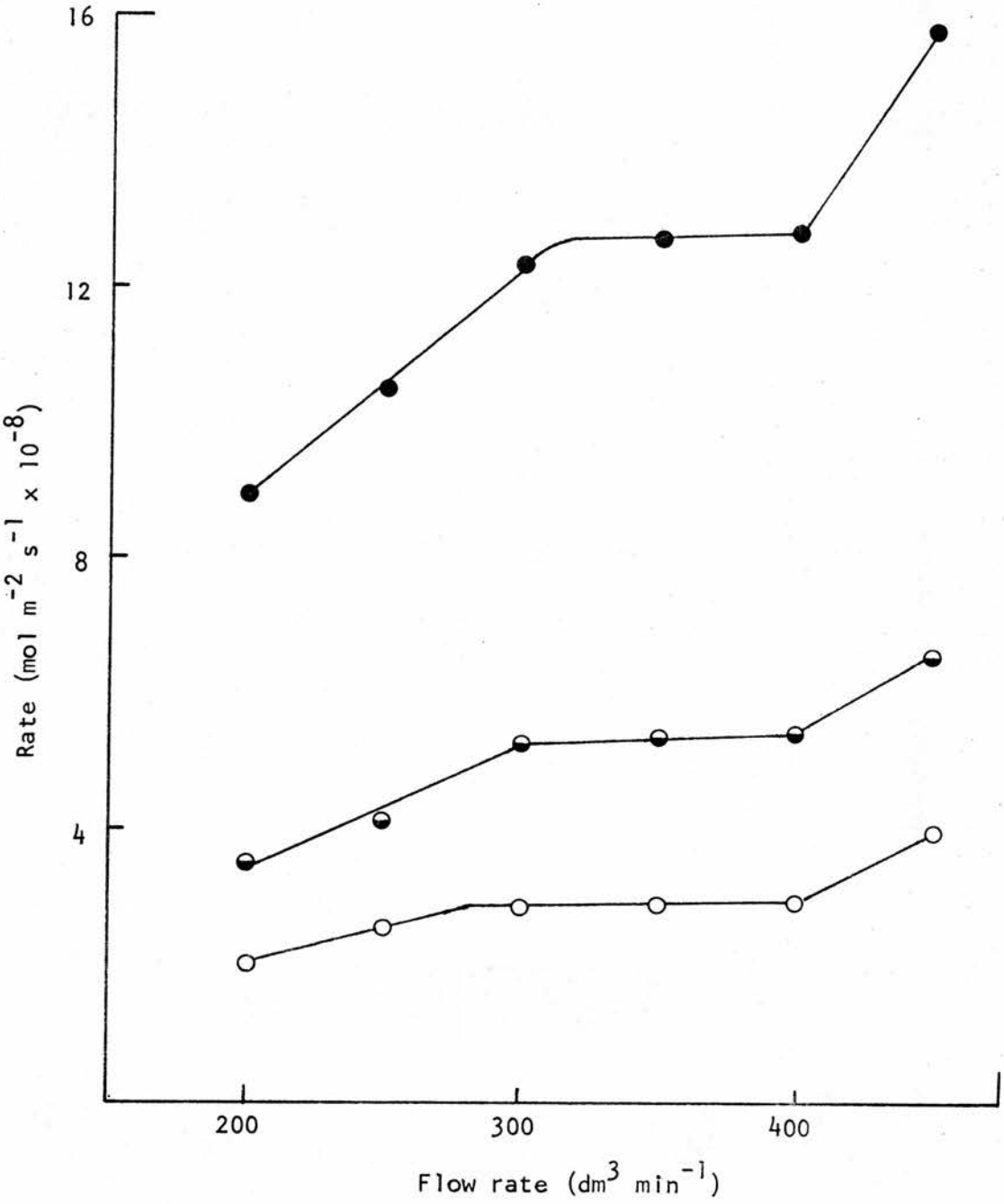

Figure 3.2.1 The effects of total gas flow rate on the NO/C_2H_6 reaction over Mn_2O_3;

○ 573 K ◒ 623 K ● 673 K.

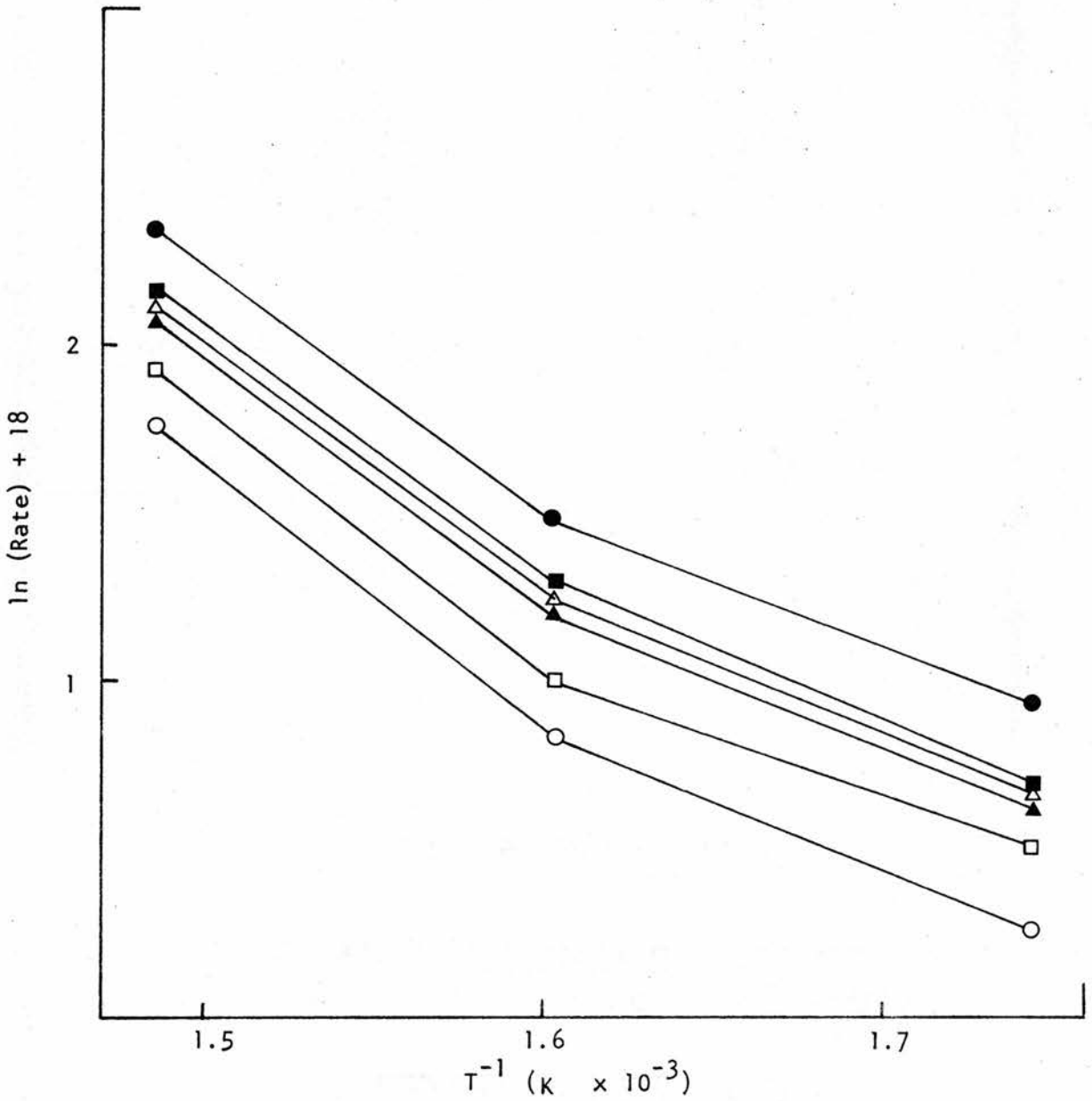

Figure 3.2.2 Arrhenius-type plot of the effects of total gas flow rate on the NO/C_2H_6 reaction over Mn_2O_3;
○ 200 dm^3 min^{-1} □ 250 dm^3 min^{-1} △ 300 dm^3 min^{-1}
▲ 350 dm^3 min^{-1} ■ 400 dm^3 min^{-1} ● 450 dm^3 min^{-1}.

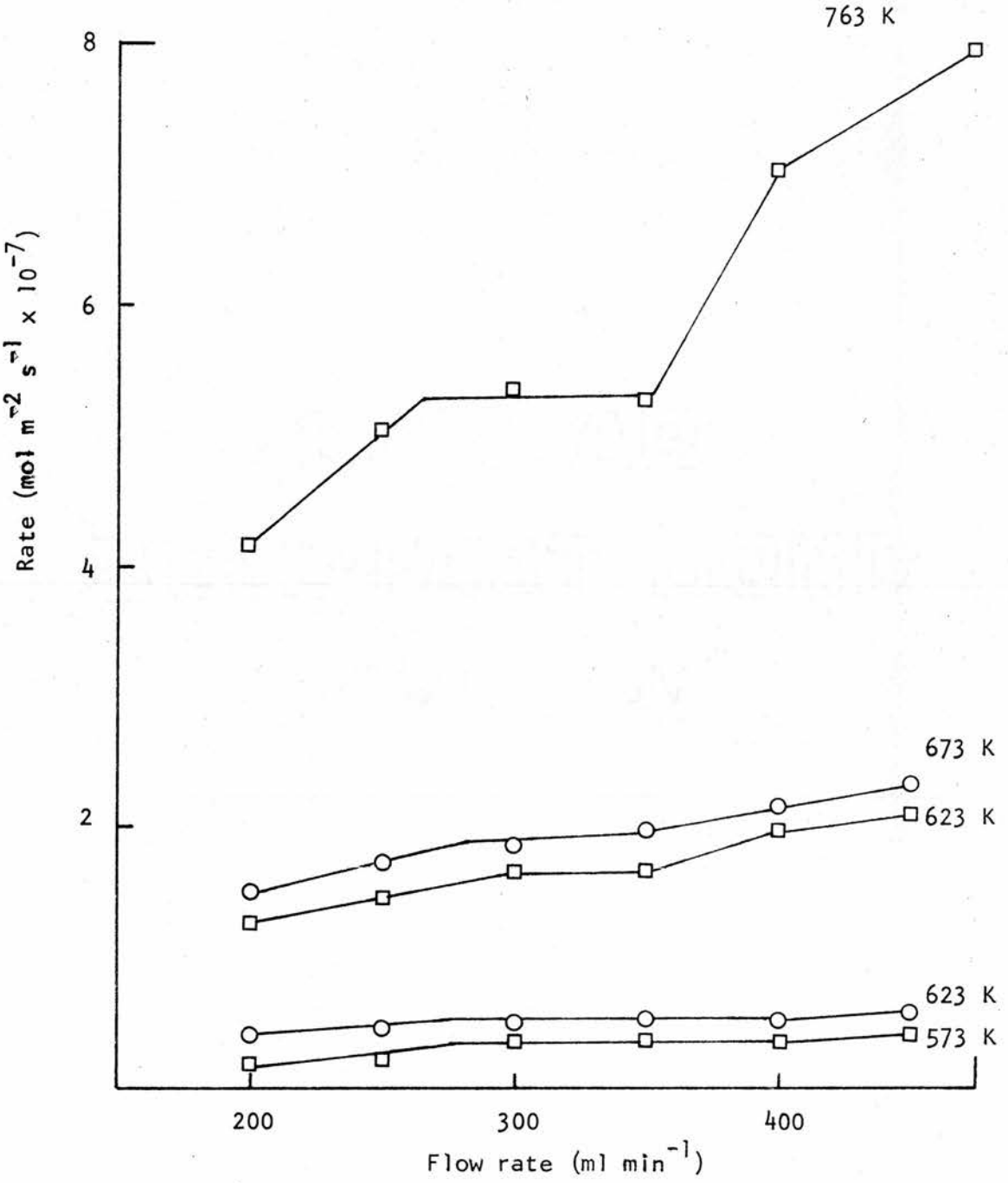

Figure 3.2.3 The effect of total gas flow rate on the rate of the NO/C_2H_6 reaction over Mn_2O_3; □ r_{N_2}, ○ r_{CO_2}.

TABLE 3.2.3 Mn_2O_3 particle size effects on the NO/C_2H_6 reaction

Sample Size (mm)	Weight Percent	Surface Area ($m^2\ g^{-1}$)	Rates at 623K (mol $m^{-2}\ s^{-1}$) $r_2 \times 10^{-2}$	$r_3 \times 10^{-8}$	Rates at 673K (mol $m^{-2}\ s^{-1}$) $r_3 \times 10^{-8}$	$r_3 \times 10^{-8}$	Experimental Ea (kJ mol^{-1})
<0.037	56	15.5	5.55	3.40	10.8	3.50	46
0.037-0.053	18	15.8	5.65	3.48	11.5	3.60	45
0.054-0.073	9	17.8	5.52	3.54	10.5	3.44	45
0.074-0.104	7	17.7	5.62	3.21	12.2	3.53	65
0.105-0.149	5	16.5	5.33	3.20	10.1	3.48	45
>0.149	5	14.8	5.10	3.31	9.8	3.40	46

TABLE 3.2.4 Mn_2O_3 particle size effects on the N_2O/C_2H_6 reaction

Sample Size (mm)	Rates at 623K (mol $m^{-2}\ s^{-1}$) $r_1 \times 10^{-7}$	$r_2 \times 10^{-8}$	Rates at 673K (mol $m^{-2}\ s^{-1}$) $r_1 \times 10^{-7}$	$r_2 \times 10^{-7}$	Experimental Ea (kJ mol^{-1}) From r_1	From r_2
<0.037	1.97	5.24	4.92	1.52	64	74
0.037-0.053	1.96	5.26	4.78	1.38	62	67
0.054-0.073	1.89	5.20	5.28	1.57	72	77
0.074-0.104	1.83	4.92	5.45	1.55	76	80
0.105-0.149	1.52	3.96	4.55	1.31	77	84
>0.149	1.55	3.96	5.03	1.44	82	90

after steady catalytic activity was attained.

The results are presented in Table 3.2.3 along with the weight percent obtained for each sieved sample and its surface area as measured by krypton adsorption. An approximate experimental activation energy value could be obtained from a two-point Arrhenius plot for each sample. These values were generally lower than those found in the flow rate studies, however, no systematic variation was noted in the experimental activation energy or in the reaction rates with particle size. Since the ratio of grain volumes between the largest and smallest particles differed by a factor of 65, the catalytic rate was regarded as independent of particle size and therefore pore diffusion influences were minimal (173).

3.2.4 *Particle size effects: nitrous oxide/ethane reaction*

The effect of variations in the catalyst particle size on the nitrous oxide/ethane reaction were examined in the manner described in the previous section. As indicated in Table 3.2.4, neither the catalytic rate of reaction nor the experimental activation energy altered systematically with particle size.

Further studies using manganese(III) oxide as catalyst were then performed on the sample with particle size <0.037 mm diameter since this fraction contained the greatest weight of sample (56%).

3.3 *The nitric oxide/ethane reaction over manganese(III) oxide*

Manganese(III) oxide was exposed to nitric oxide and ethane at partial pressures of 2.7 kPa each in helium at 673 K. The rate of product-nitrogen, carbon dioxide and nitrous oxide-formation increased slightly in the first 30 min and remained constant for at least 24 h. The percentage conversion of ethane was 6.5% at this temperature and no partial oxidation products were observed.

3.3.1 *Reaction rate orders*

Rate orders for the nitric oxide/ethane reaction were measured at 623 K for nitrogen (r_1), carbon dioxide (r_2) and nitrous oxide (r_3) formation.

Nitric oxide

With the partial pressure of ethane held constant at 2.71 kPa, the effect of nitric oxide on reaction rates was observed by varying its partial pressure from 0.83 to 11.75 kPa. Plots of ln (rate) versus ln (partial pressure) used to determine rate orders exhibited linear relationships in the range studied, Figure 3.3.1. The reaction rate orders with respect to nitric oxide partial pressure were described by:

$$r_1 \propto p_{NO}^{0.5} \; ; \quad r_2 \propto p_{NO}^{0.3} \; ; \quad \text{and } r_3 \propto p_{NO}^{1.2} \; .$$

Ethane

The dependence of reaction rates on variations in ethane partial pressure from 0.73 to 6.59 kPa was examined with nitric oxide maintained constant at 3.0 kPa. Again, linear relationships were observed, Figure 3.3.1, and the slopes gave the rate orders with respect to ethane as:

$$r_1 \propto p_{C_2H_6}^{0.5}; \qquad r_2 \propto p_{C_2H_6}^{0.7}; \qquad \text{and } r_3 \propto p_{C_2H_6}^{0.5}.$$

Nitrous oxide

The partial pressure of nitric oxide was maintained at 2.82 kPa and ethane at 2.41 kPa while the partial pressure of nitrous oxide was varied from 0.23 to 6.06 kPa. Over this range, nitrous oxide had no effect on the rate of nitrogen formation, $r_1 \propto p_{N_2O}^{0}$; while a linear logarithmic plot was observed for carbon dioxide formation, $r_2 \propto p_{N_2O}^{0.3}$, Figure 3.3.1. The rate order data are summarized in Table 3.3.1.

Nitrogen

The effect of nitrogen on the reaction rates r_2 and r_3 was observed

by maintaining the partial pressures of ethane and nitric oxide constant at 2.52 and 2.61 kPa, respectively, and altering the partial pressure of nitrogen from 0.09 to 9.21 kPa. The rate orders with respect to nitrogen were zero throughout the range investigated.

Carbon dioxide

Carbon dioxide partial pressure was altered from 0.15 to 5.87 kPa with the partial pressures of ethane, 2.57 kPa, and nitric oxide, 2.93 kPa, held constant in order to observe the effects of carbon dioxide on reaction rates. The relationships were: r_1 and $r_3 \propto P^0_{CO_2}$.

Water vapour

With the partial pressures of ethane and nitric oxide maintained at 2.47 and 2.88 kPa, respectively, from 0.04 to 1.4 kPa of water vapour was added to the system and shown to have no effect on the reaction rates.

On the basis of these rate order determinations, the rate of reaction of nitric oxide with ethane, r (mol m^{-2} s^{-1}), can be expressed as:

$$r_1 = k_1 P^{0.5}_{NO} P^{0.5}_{C_2H_6} \qquad [3.3.1]$$

$$r_2 = k_2 P^{0.3}_{NO} P^{0.7}_{C_2H_6} P^{0.3}_{N_2O} \qquad [3.3.2]$$

$$r_3 = k_3 P^{1.2}_{NO} P^{0.5}_{C_2H_6} . \qquad [3.3.3]$$

3.3.2 *The effect of temperature*

The catalytic reaction rates were determined from 673 to 573 K in decreasing 10 K intervals after catalyst pretreatment at 673 K for 2 h with nitric oxide and ethane at 2.74 and 2.71 kPa, respectively. Rate constants were calculated by integration of equations [3.3.1, 2, 3] as a function of concentration and the values obtained were plotted in the Arrhenius fashion, Figure 3.3.2. The rate of nitrous oxide formation was constant over this temperature range and hence the specific rate constant did not change with temperature. Two distinct temperature regions were observed in the linear

TABLE 3.3.1 The effect of component partial pressures on the rate of the NO/C_2H_6 reaction over Mn_2O_3 at 623 K

$P_{C_2H_6}$ (kPa)	$r_1 \times 10^{-8}$ (mol m^{-2} s^{-1})	$r_2 \times 10^{-8}$ (mol m^{-2} s^{-1})	$r_3 \times 10^{-8}$ (mol m^{-2} s^{-1})
0.73	2.06	2.44	1.37
1.05	2.49	3.17	1.46
1.42	3.09	3.69	1.97
2.08	3.60	5.02	2.23
2.83	4.25	6.30	2.53
3.47	4.72	6.86	2.66
4.62	5.53	8.84	3.30
5.45	6.00	9.86	3.60
6.59	6.65	10.98	4.16
P_{NO} (kPa)			
0.83	2.02	4.20	0.52
1.38	2.83	4.80	1.12
1.70	3.73	6.26	1.50
3.05	4.76	7.12	2.70
3.28	5.10	7.12	2.53
3.59	4.72	6.78	3.35
3.73	4.89	6.09	3.22
5.14	5.32	7.55	4.63
7.29	6.91	8.96	7.12
9.53	6.78	9.78	10.12
11.75	7.38	10.21	16.13
P_{N_2O} (kPa)			
0.59	9.99	8.15	-
0.70	9.26	8.11	-
1.02	9.52	8.84	-
1.56	9.82	9.95	-
3.30	9.74	12.35	-
5.04	11.32	13.81	-
6.06	10.38	14.50	-

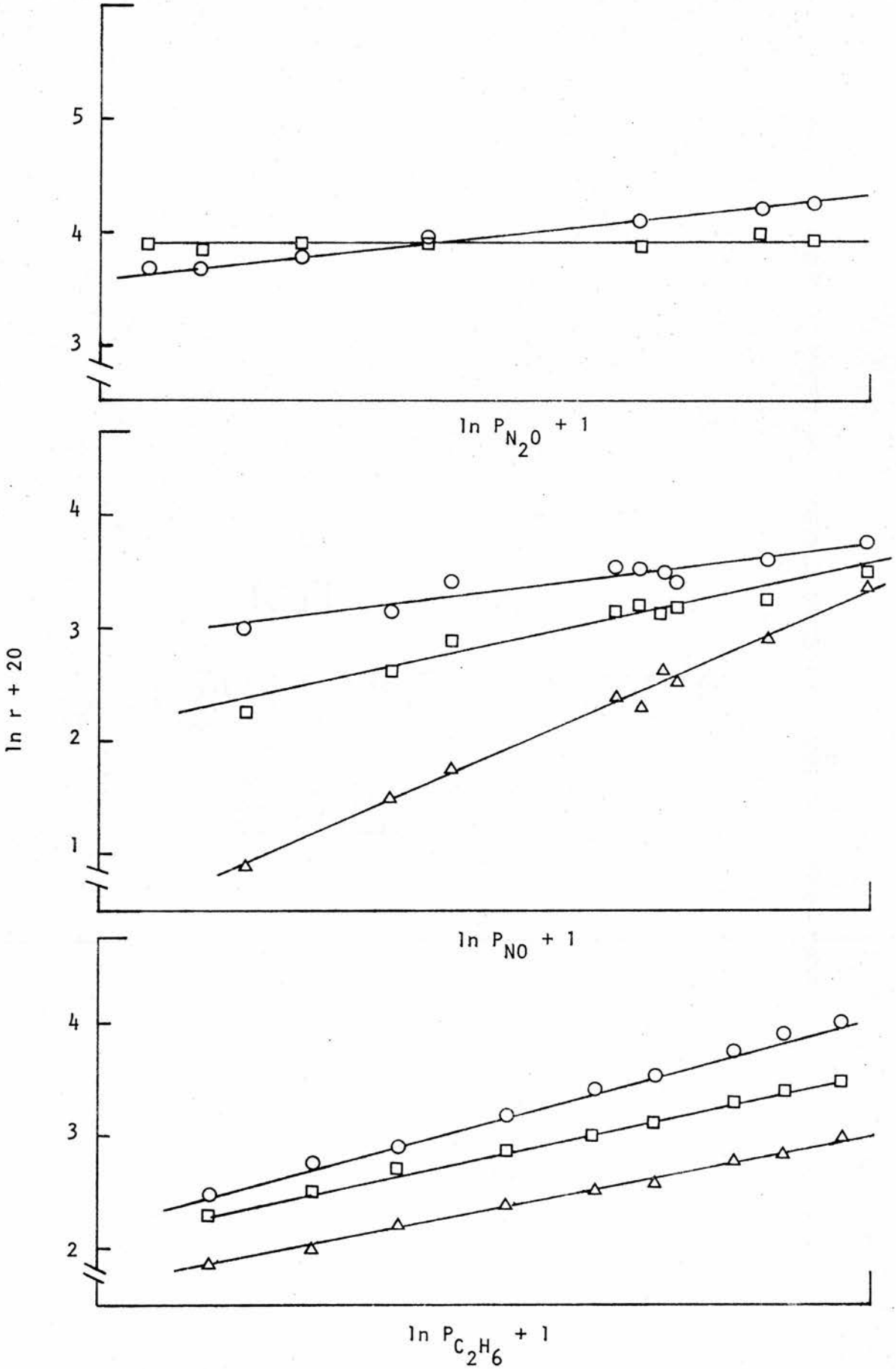

Figure 3.3.1 The effects of component partial pressures on the rate of the NO/C_2H_6 reaction over Mn_2O_3; □ r_1, ○ r_2, △ r_3.

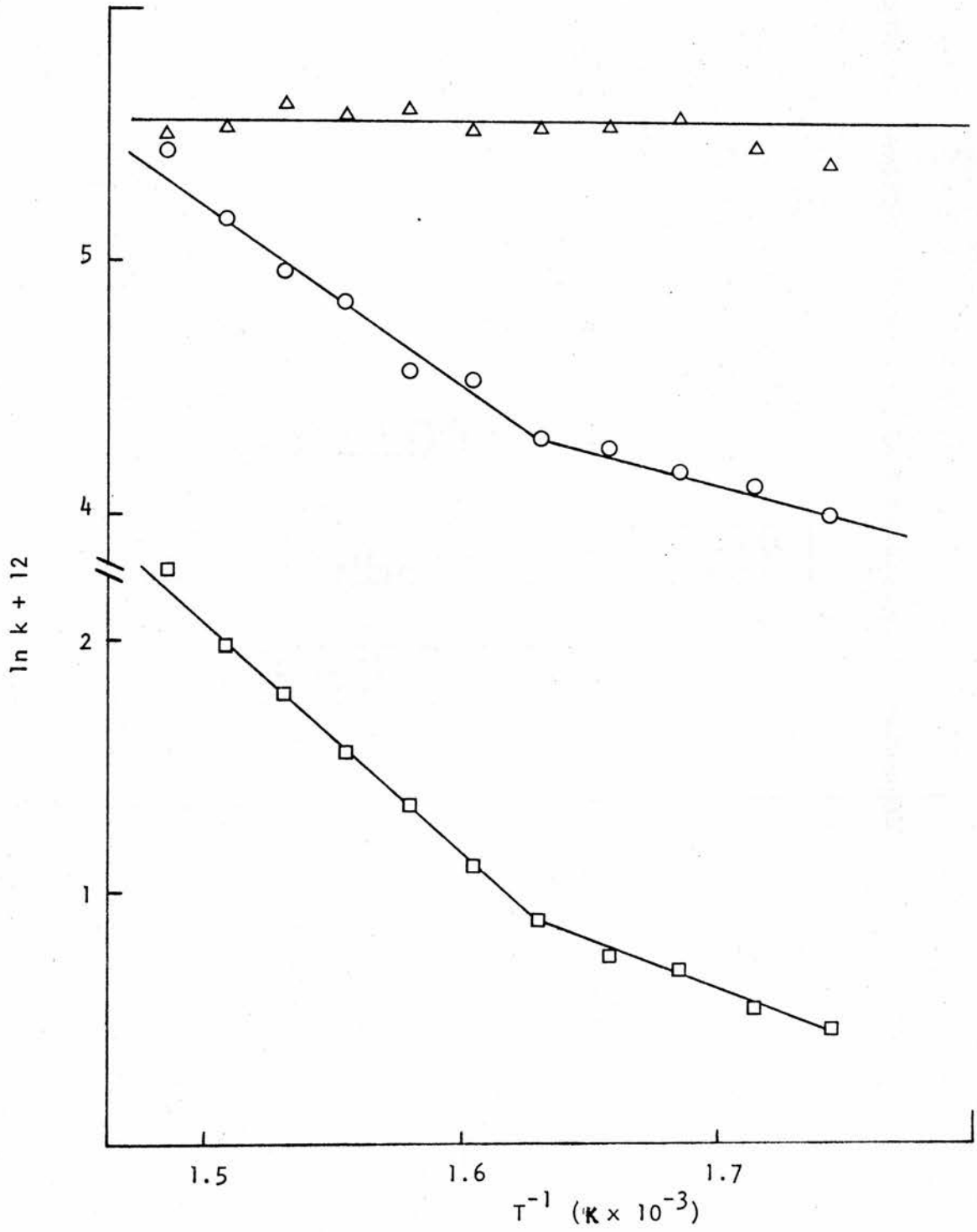

Figure 3.3.2 Arrhenius plots for the nitric oxide/ethane reaction over Mn_2O_3; □ k_1, ○ k_2, △ k_3.

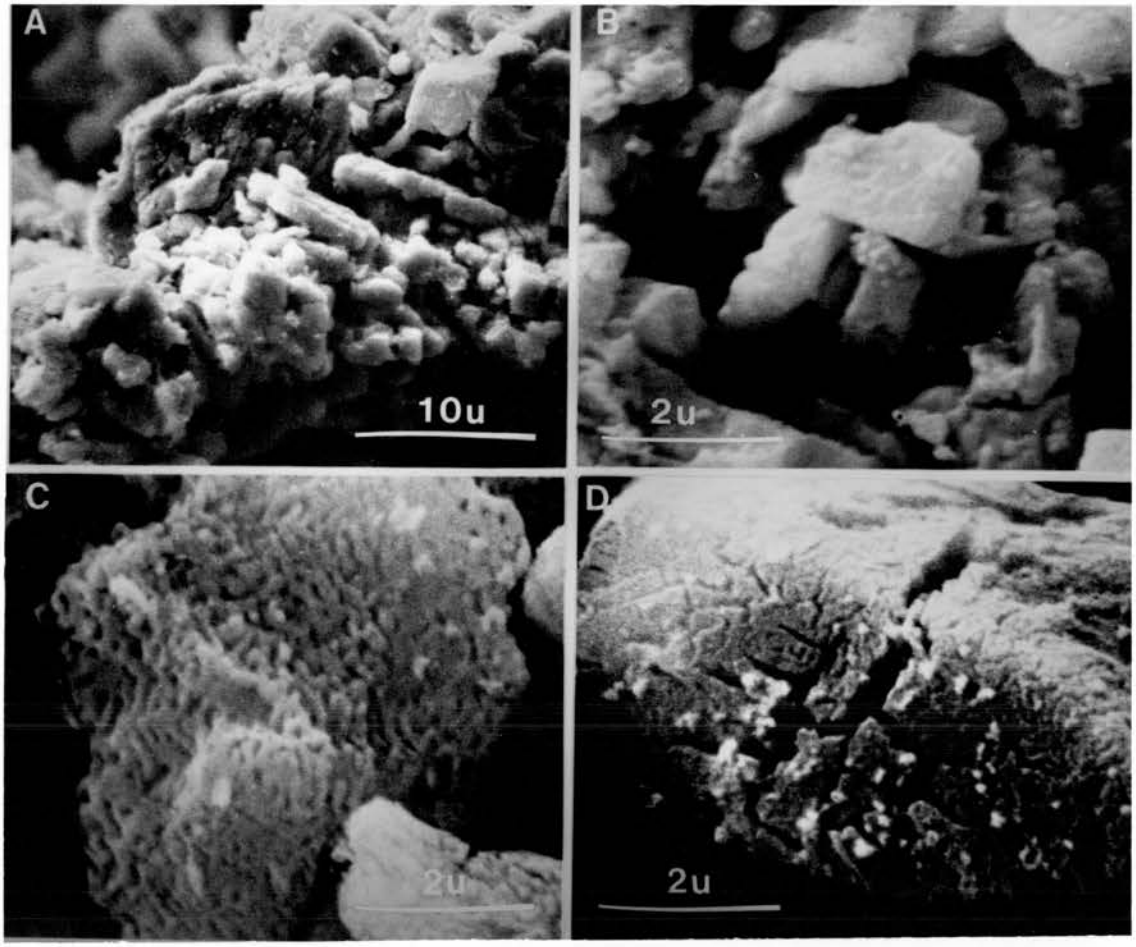

Figure 3.3.3 Scanning electron micrographs of Mn_2O_3 after the catalytic NO/C_2H_6 reaction; at 673 K, A, B and C; and at 873 K, D.

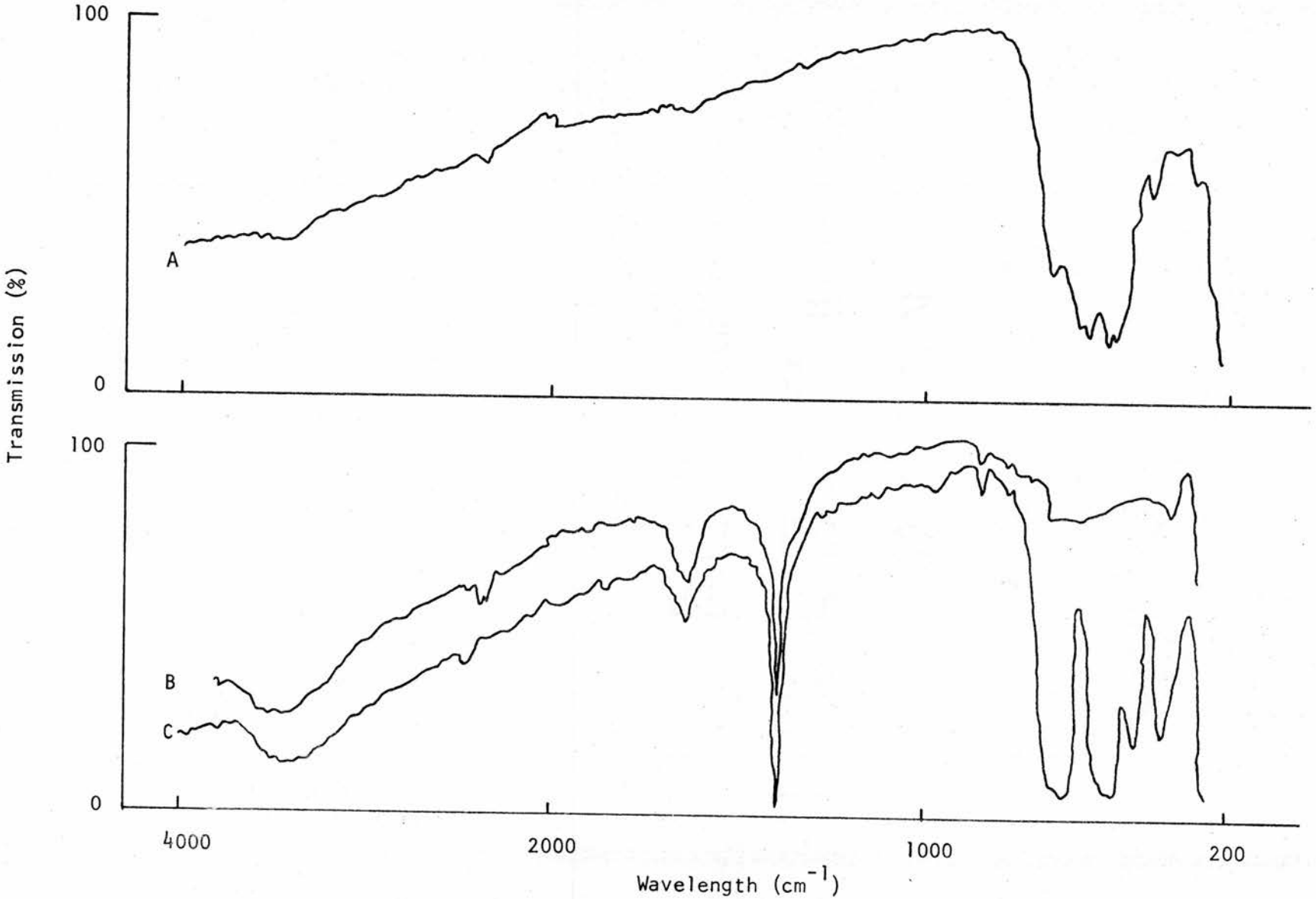

Figure 3.3.4 The infrared spectra of unreacted manganese (III) oxide catalyst, A;manganese (II)nitrate, B; and catalyst after the NO/C_2H_6 reaction, C.

plots obtained for both nitrogen and carbon dioxide rate constants, namely, from 673 to 613 K and from 613 to 573 K as shown in Table 3.3.2.

TABLE 3.3.2 Kinetic parameters for the NO/C_2H_6 reaction over Mn_2O_3

	673 - 613 K	613 - 573 K
E_a (from k_1) (kJ mol^{-1})	78 ±4	32 ±4
A ($mol^{-0}\ell^{0}m^{2}g^{-1}$)	53.1	9.96×10^{-2}
E_a (from k_2) (kJ mol^{-1})	63 ±4	22 ±4
A ($mol^{-0.3}\ell^{0.3}m^{2}g^{-1}$)	86.2	4.12×10^{-2}

3.3.3 *The effects of reaction conditions on catalyst properties*

The surface area of a freshly-prepared catalyst, 15.5 $m^2\ g^{-1}$, decreased slightly to 15.0 $m^2\ g^{-1}$ after 24 h exposure to nitric oxide, 2.7 kPa, and ethane, 2.7 kPa, at 673 K. Since surface areas as measured on the krypton BET apparatus could be reproduced to within ±0.3 $m^2\ g^{-1}$, the slight decrease in surface area was deemed insignificant.

Scanning electron micrographs, Figure 3.3.3, appeared to show a separate crystalline phase on parts of the oxide surface after catalysis at 673 K. The presence of smaller, more ordered particles may be observed in A and B of Figure 3.3.3, while the condition of the remainder of the surface of the particles, C, indicates rounded edges and a high degree of surface roughness. This surface appears identical to that noted for manganese(III) oxide prior to catalysis. Samples which were further heated under reaction conditions to 873 K exhibited surface sintering and crack formation, D.

The infrared spectrum of unreacted manganese(III) oxide, Figure 3.3.4 A, consisted of peaks at 670 (m), 600 (sh), 525 (s), 495 (sh) and 400 (w) cm^{-1} and was similar to that found for pure manganese(III) oxide (Alfa Inorganics, Ventron) with the exception that no peak was apparent at 400 cm^{-1}. After catalysis of the nitric oxide/ethane reaction, 573 to 673 K, the spectrum was altered to yield absorption at 1630 (m), 1390 (s) and

TABLE 3.3.3 Manganese oxide powder diffraction patterns. d-spacings are given in Ångstrom units

Unreacted	ASTM Index α-Mn_2O_3	I/I_o	Mn_2O_3 after catalysis (NO/C_2H_6)	ASTM Index γ-Mn_2O_3	I/I_o	ASTM Index Mn_3O_4	I/I_o
2.72	2.72	100	2.48	2.48	100	2.48	100
1.666	1.649	30	2.74	2.74	70	2.75	63
3.849	3.84	25	3.08	3.08	60	3.08	31
1.420	1.421	14	1.543	1.55	60	1.54	50
2.356	2.35	12	1.558	1.59	30	1.57	50
2.009	2.015	14	1.80	1.83	30	1.79	18
1.846	1.835	14	2.08	2.03	20	2.03	15
1.453	1.445	10		4.93	40	4.92	20
				2.39	40		

TABLE 3.3.4 X-ray photoelectron spectroscopy results

Catalyst	O 1 s (eV)	Mn 2p 3/2 (eV)	N 1 s (eV)
unreacted Mn_2O_3	528.7	640.7	-
Mn_2O_3 at 673 K for 24 h (NO/C_2H_6)	529.5	641.0	406.5
Mn_2O_3 at 673 to 573 K (NO/C_2H_6)	529.7	641.0	406.4
Mn_2O_3 at 673 K for 48 h (N_2O/C_2H_6)	529.3	641.0	-
Mn_2O_3 at 673 to 573 K (N_2O/C_2H_6)	529.0	641.0	-
Mn_2O_3 at 593 to 523 K (O_2/C_2H_6)	529.5	641.0	-

845 (w) cm^{-1}, which, along with the peak at 350 (m) cm^{-1}, Figure 3.3.4 C, is consistent with the spectrum of manganese(II) nitrate, Figure 3.3.4 B. Other peaks appeared at 615 (s), 490 (s) and 425 (m) cm^{-1}. The spectrum observed for pure manganese(II) oxide (Alfa Inorganics, Ventron) indicated a single peak at 340 cm^{-1} while that for manganese(IV) oxide (Alfa Inorganics, Ventron) showed absorption bands at 615, 400 and 335 cm^{-1}.

Chemical analysis of unreacted manganese(III) oxide indicated 69.7% w/w manganese (theory 69.59%). Analysis of the oxide after catalysis gave 68.56% w/w manganese. Exposure of the catalyst to the reaction mixture produced a brown surface colouration after the steady state was achieved.

The X-ray powder diffraction pattern of unreacted catalyst indicated that the sample was alpha-manganese sesquioxide (α - Mn_2O_3) which occurs naturally as partridgeite. After reaction at 623 K, the diffraction pattern was altered, Table 3.3.3, and this most closely corresponded to the pattern for gamma-manganese sesquioxide (γ-Mn_2O_3) which is nearly identical to that for manganese(II,III) oxide and, indeed, a close relationship between the two has been observed (159).

X-ray photoelectron spectroscopy results for unreacted manganese (III) oxide gave O (1s) and Mn (2p 3/2) values of 528.7 and 640.7 eV, respectively. These values were not altered appreciably after catalysis at 673 K or 623 K, Table 3.3.4. However, binding energy values of 406.5 and 406.4 eV were measured in the N (1s) spectra after catalysis.

3.4 *The nitrous oxide/ethane reaction over manganese(III) oxide*

The rate of nitrogen and carbon dioxide formation in the reaction of nitrous oxide with ethane over manganese(III) oxide at 673 K decreased slightly over the first 15 min of reaction. The partial pressures of both reactants were 2.66 kPa. The rates were constant for a minimum of 48 h at an ethane conversion of 15% at this temperature. The only products observed were nitrogen, carbon dioxide and water.

3.4.1 *Reaction rate orders*

Rate orders were determined at 623 K using nitrogen (r_1) and carbon dioxide (r_2) rates after catalyst pretreatment under standard conditons for 3 h.

Nitric oxide

Ethane partial pressure was maintained at 2.66 kPa while nitric oxide was varied from 0.67 to 5.32 kPa to observe the effects on r_1 and r_2. A reaction rate order of 0.8 was obtained with respect to nitric oxide partial pressure in the logarithmic plots for both rates, Figure 3.4.1.

Ethane

The effects of variations in ethane partial pressure were observed with the partial pressure of nitrous oxide held at 2.66 kPa. A reaction rate order of 0.7 was determined for ethane partial pressures from 0.67 to 3.33 kPa and, as indicated in Figure 3.4.1, a rate order of 0.2 was observed from 3.33 to 5.32 kPa. The data are summarized in Table 3.4.1

Nitrogen

With both nitrous oxide and ethane partial pressures held constant at 2.66 kPa, the effect of nitrogen partial pressure on r_2 was observed. The rate order with respect to nitrogen was zero in the range of partial pressures from 0.33 to 5.32 kPa.

Carbon dioxide

Variations in the carbon dioxide partial pressure from 0.33 to 5.32 kPa had no effect upon the rate of nitrogen formation, $r_1 \propto P^0_{CO_2}$. Nitrous oxide and ethane partial pressures were each held constant at 2.60 kPa.

TABLE 3.4.1.A The effects of component partial pressures on the rate of the N_2O/C_2H_6 reaction at 623 K over Mn_2O_3.

$P_{C_2H_6}$ (kPa)	$r_1 \times 10^{-7}$ (mol m^{-2} s^{-1})	$r_2 \times 10^{-8}$ (Mol m^{-2} s^{-1})	P_{N_2O} (kPa)	$r_1 \times 10^{-7}$ (mol m^{-2} s^{-1})	$r_2 \times 10^{-8}$ (mol m^{-2} s^{-1})
0.67	0.88	2.46	0.67	0.91	1.89
1.33	1.37	3.18	1.33	1.52	3.68
2.00	1.81	4.84	2.00	2.46	6.57
2.66	2.21	5.24	2.66	2.82	7.60
3.33	2.61	6.90	3.33	3.20	8.59
3.99	2.69	7.03	3.99	3.73	9.96
4.66	2.76	7.43	4.66	4.23	11.79
5.32	2.86	7.77	5.32	4.44	12.65

TABLE 3.4.1.B The effects of component partial pressures on the rate of the O_2/C_2H_6 reaction at 573 K over Mn_2O_3.

$P_{C_2H_6}$ (kPa)	$r_2 \times 10^{-8}$ (mol m^{-2} s^{-1})	P_{O_2} (kPa)	$r_2 \times 10^{-8}$ (mol m^{-2} s^{-1})
0.67	4.84	0.67	5.20
1.00	6.00	1.00	6.95
1.33	7.20	1.33	8.15
2.00	8.97	2.00	9.34
2.66	10.59	2.66	10.59
3.33	12.61	3.33	12.19
3.99	15.53	3.99	12.86
4.66	18.65	4.66	13.43
5.32	21.03	5.32	14.29

Water vapour

The addition of from 0.04 to 1.5 kPa of water vapour had no effect upon reaction rates.

The experimental rate of reaction was therefore represented by the expressions:

$$r = k \; P_{N_2O}^{0.8} \; P_{C_2H_6}^{0.7} \qquad [3.4.1]$$

for $0.67 < P_{C_2H_6} < 3.33$ kPa and

$$r = k \; P_{N_2O}^{0.8} \; P_{C_2H_6}^{0.2} \qquad [3.4.2]$$

for $3.33 < P_{C_2H_6} < 5.32$ kPa,

where r and k represent either r_1 and k_1 or r_2 and k_2.

3.4.2 *The effect of temperature*

Steady catalytic activity was obtained after 2 h exposure to the standard mixture of 2.66 kPa each of nitrous oxide and ethane at 673 K. Reaction rate constants were calculated by integration of the rate equation [3.4.1] as a function of concentration from 673 to 573 K. Two apparent activation energies were obtained using r_1, namely 133 ±4 kJ mol^{-1} from 673 to 623 K and 106 ±4 kJ mol^{-1} from 613 to 573 K, Figure 3.4.2. The pre-exponential factors were 6.35×10^8 and 3.27×10^6 $mol^{-0.5} \; \ell^{0.5} \; m^{-2} \; s^{-1}$, respectively. From r_2 a single value of activation energy, 130 ±4 kJ mol^{-1}, was determined over the region 673 to 573 K with the pre-exponential factor 9.72×10^7 $mol^{-0.5} \; \ell^{0.5} \; m^{-2} \; s^{-1}$. The data are summarized in Table 3.4.2.

3.4.3 *The effects of reaction conditions on catalyst properties*

The catalyst surface area was not altered by the nitrous oxide/ethane reaction at 673 K after exposure periods up to 48 h. Under the scanning electron microscope, the catalyst surface also appeared unaffected

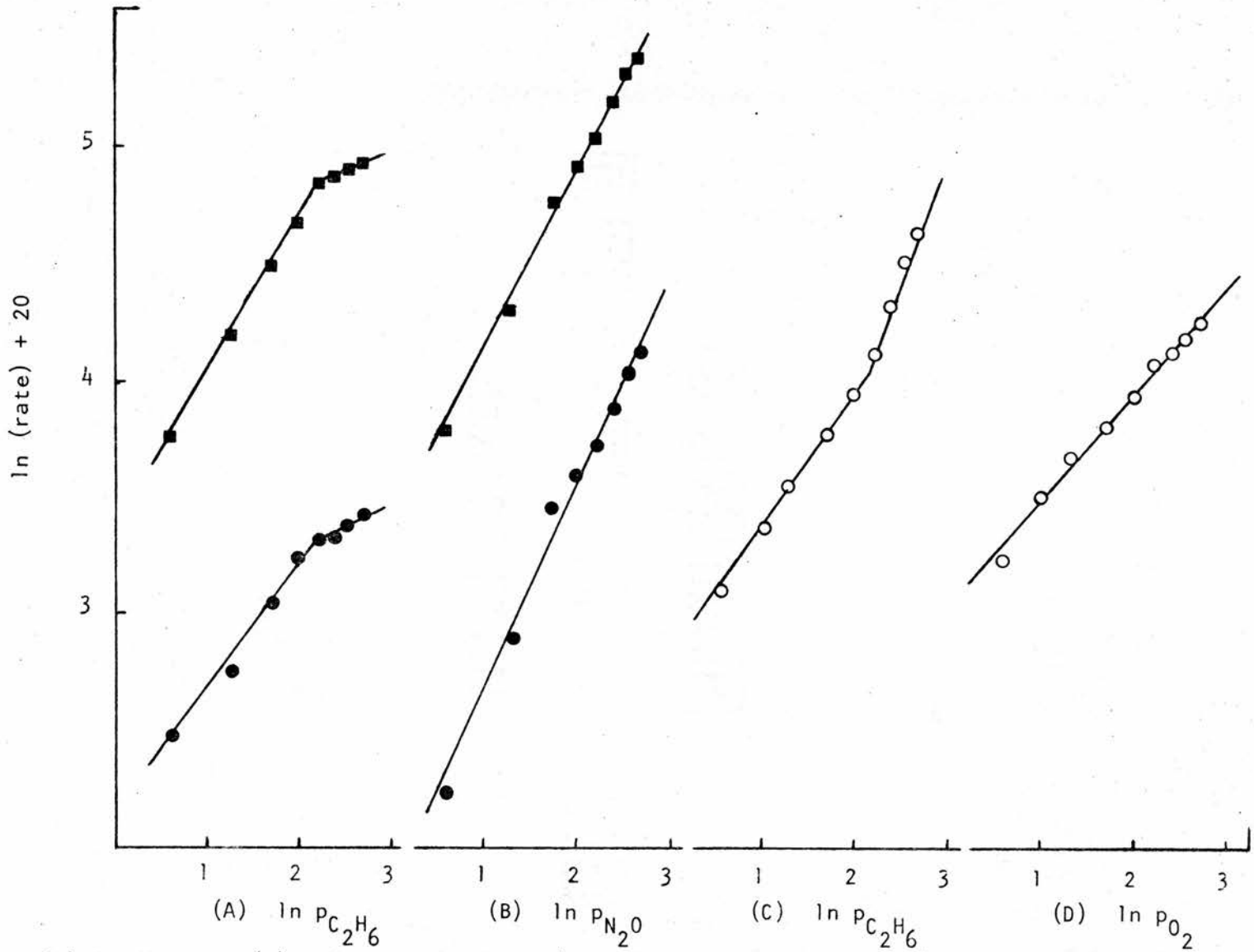

Figure 3.4.1 Nitrogen (■) and carbon dioxide (● in A and B, ○ in C and D) rate dependency on variations in the partial pressures of nitrous oxide (A) and ethane (B) in the N_2O/C_2H_6 catalytic reaction over Mn_2O_3 at 623 K; and oxygen (C) and ethane (D) in the O_2/C_2H_6 reaction at 573 K.

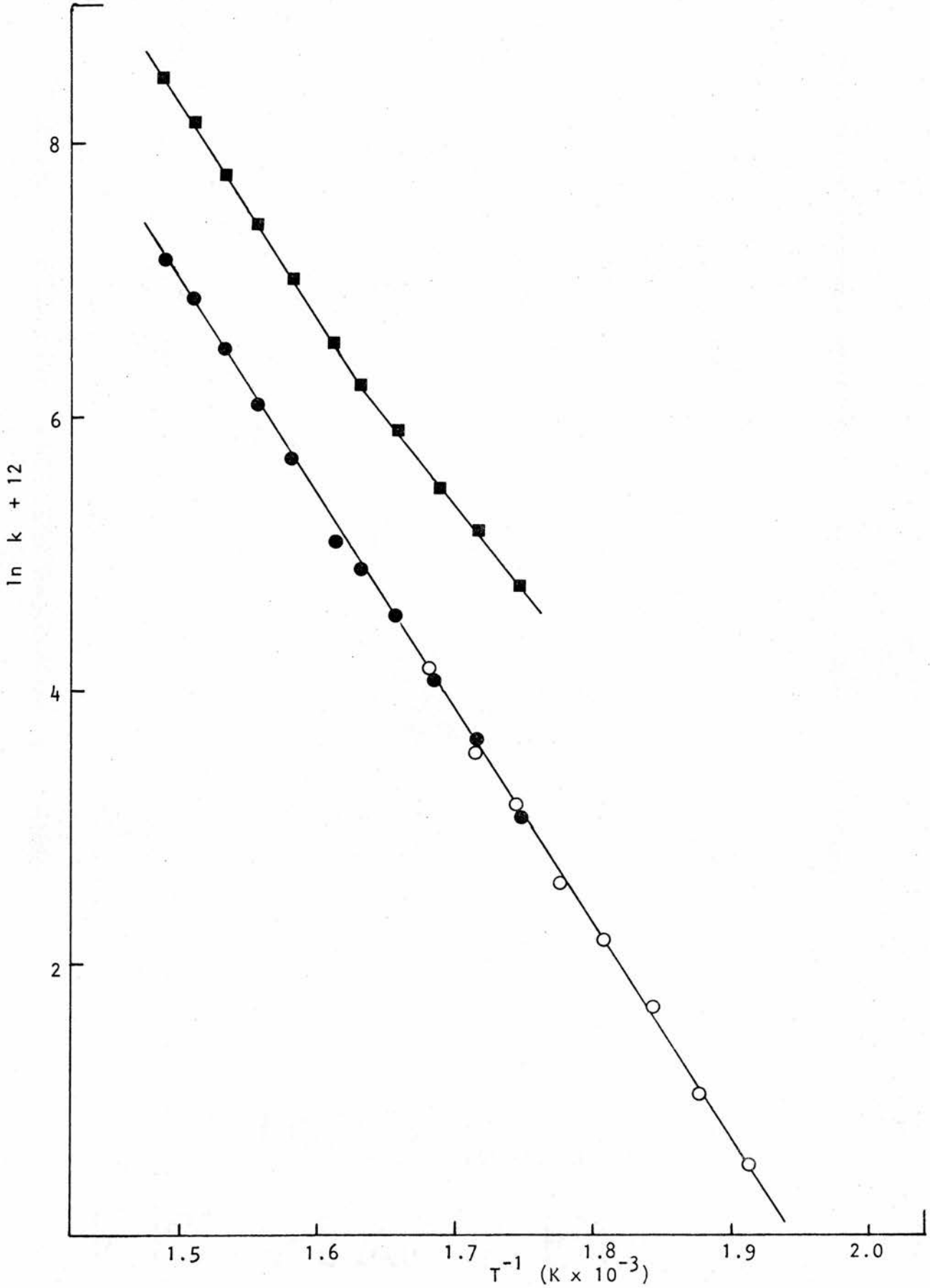

Figure 3.4.2 Arrhenius plots for the N_2O/C_2H_6 (■ k_1; ● k_2) and O_2/C_2H_6 (Q k_2) catalytic reactions over Mn_2O_3.

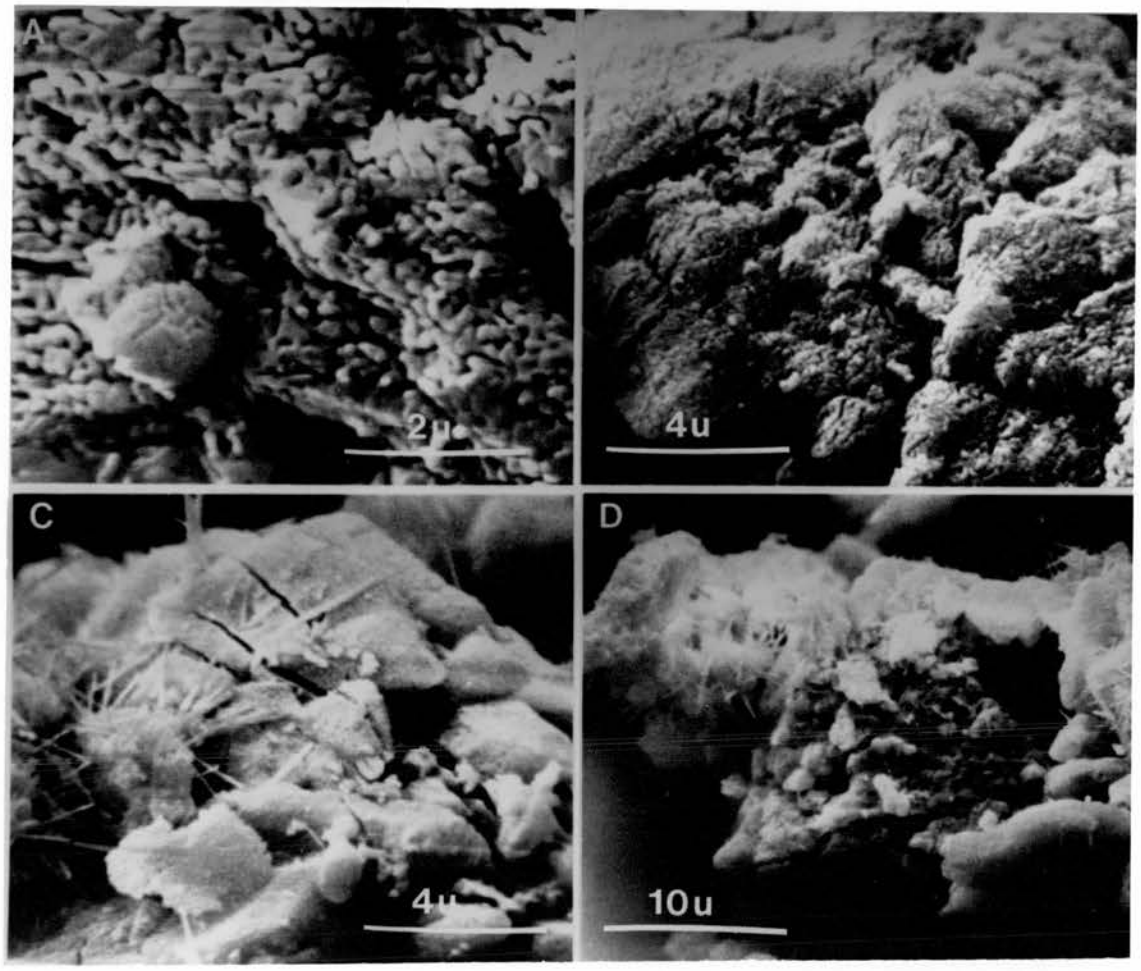

Figure 3.4.3 Scanning electron micrographs of Mn_2O_3 after the catalytic N_2O/C_2H_6 reaction; at 673 K, A and B; and at 673 K with an excess of water vapour added, C and D.

by reaction, Figure 3.4.3 A and B. When a large excess of water vapour was passed over the oxide with 2.66 kPa of nitrous oxide and ethane, needle-like growths appeared on the surface, Figure 3.4.3 C and D.

The infrared spectra of the manganese(III) oxide after catalysis at 673 K for 48 h and at temperatures from 673 to 573 K gave absorption bands at 615 (s), 490 (s), 425 (m) and 350 (m) cm^{-1}. With the exception of the absence of any nitrate bands, the spectra were similar to those observed previously from samples used in the nitric oxide/ethane reaction.

Chemical analysis indicated 69.6% w/w manganese in the catalyst after reaction at 673 K and the oxide remained black in colour.

X-ray powder diffraction gave the following d-spacings in order of decreasing relative intensity:

2.48, 2.74, 3.08, 1.543, 1.558, 1.80, 2.08.

X-ray photoelectron results indicated O(1S) and Mn(2p 3/2) values similar to those found for the unreacted manganese(III) oxide, Table 3.3.4.

3.5 *The oxygen/ethane reaction over manganese(III) oxide*

The catalytic reaction rate increased for the first 30 min of reaction at 593 K and thereafter remained constant for at least 48 h. The products of reaction were those of complete oxidation - carbon dioxide and water - with a 15% ethane conversion at 593 K.

3.5.1 *Reaction rate orders*

Reaction rate orders for the oxygen/ethane reaction over manganese(III) oxide were measured at 573 K.

Oxygen

The dependence of the reaction rate (r_2) on variations in the oxygen partial pressure from 0.67 to 5.32 kPa was examined with ethane

partial pressure maintained at 2.66 kPa. A reaction rate order of 0.5 was obtained, Figure 3.4.1.

Ethane

With the partial pressure of oxygen held at 2.66 kPa, the rate order with respect to ethane partial pressure was 0.6 from 0.67 to 2.66 kPa and 0.85 from 2.66 to 5.32 kPa, Figure 3.4.1.

Carbon dioxide

When the carbon dioxide partial pressure was varied from 0.20 to 5.32 kPa with oxygen and ethane partial pressures maintained at 2.66 kPa, no changes in the steady-state concentrations of oxygen, ethane or water were observed. Therefore the rate order with respect to carbon dioxide was zero.

Water vapour

With oxygen and ethane partial pressures kept at 2.66 kPa, the reaction rate was zero order with respect to water vapour partial pressure from 0.04 to 1.5 kPa.

On the basis of these results, the rate of reaction was expressed as:

$$r_2 = k_2 P_{O_2}^{0.5} P_{C_2H_6}^{0.6} \qquad [3.5.1]$$

where $0.67 < P_{C_2H_6} < 2.66$ kPa and

$$r_2 = k_2 P_{O_2}^{0.5} P_{C_2H_6}^{0.85} \qquad [3.5.2]$$

where $2.66 < P_{C_2H_6} < 5.32$ kPa.

3.5.2 *The effect of temperature*

After catalyst pretreatment with 2.66 kPa oxygen and 2.13 kPa ethane at 593 K for 3 hr, the rate of carbon dioxide formation was determined from 593 K to 523 K at 10 K intervals. Rate constants were calculated from the integrated form of equation [*3.5.1*], Table 3.4.1 and plotted in the Arrhenius fashion, Figure 3.4.2. The results lay on the same straight line as those for the rate of carbon dioxide formation in the nitrous oxide/ethane reaction. The apparent activation energy was 130 ±4 kJ mol^{-1} and the pre-exponential factor, 9.72×10^{7} $mol^{-0.1} \ell^{0.1} m^{2} g^{-1}$.

3.5.3 *The effects of reaction conditions on catalyst properties*

No change in surface area was noted after reaction at 593 K for 48 h. Similarly, no change in the catalyst surface structure was apparent from scanning electron microscopy.

The infrared spectrum of manganese(III) oxide after catalysis at 573 K was identical to that observed for the same oxide after the nitrous oxide/ethane reaction. This consisted of bands at 615 (s), 490 (s), 425 (m) and 350 (m) cm^{-1}.

Analysis of the catalyst after reaction at 573 K indicated 69.8% w/w manganese present.

The X-ray powder diffraction pattern was similar to those obtained in previous studies with the calculated d-spacings:

2.48, 2.74, 3.08, 1.543, 1.558, 1.80, 2.08.

X-ray photoelectron results, Table 3.3.4, did not vary greatly from those found for the original unreacted catalyst, Table 3.3.4.

3.6 *The nitric oxide/1-butene reaction over manganese(III) oxide*

When the catalyst was exposed to 3.06 kPa nitric oxide and 2.32 kPa 1-butene at 673 K, the initial rates of nitrogen and carbon dioxide formation were very high, Figure 3.6.1. These rates quickly decreased to steady

values in approximately 5 h. The rate of nitrous oxide production increased in the first hour and then decreased to reach a constant value after 5 h. Under these experimental conditions, the rate of reaction remained constant for up to 48 h and the conversion of 1-butene reached 13% at 723 K.

3.6.1 *Reaction rate orders*

Rate orders were determined at 673 K after catalyst pretreatment under standard conditions of 2.89 kPa nitric oxide and 2.35 kPa 1-butene for 12 h.

Nitric oxide

The partial pressure of nitric oxide was adjusted from 0.17 to 8.17 kPa with 1-butene maintained at 2.60 kPa. A reaction rate order of 0.5 with respect to nitric oxide partial pressure was found from logarithmic plots of nitrogen and carbon dioxide experimental rates, Figure 3.6.2. For the rate of nitrous oxide formation, a rate order of 1.35 with respect to nitric oxide partial pressure was calculated.

1-Butene

A zero order rate dependency with respect to 1-butene partial pressure variations from 0.92 to 7.49 kPa was observed, Table 3.6.1, with the partial pressure of nitric oxide constant at 3.05 kPa.

Nitrogen

With the partial pressures of nitric oxide and 1-butene maintained at 2.41 and 2.57 kPa, respectively, the nitrogen partial pressure was altered from 0.55 to 6.94 kPa. This had no effect on the rate of reaction, r_2 or r_3, and therefore the rate order was zero with respect to nitrogen concentration.

Carbon dioxide

Variations in the carbon dioxide partial pressure from 0.82 to

7.15 kPa had no effect on the rate of nitrogen or nitrous oxide formation. The reaction was zero order with respect to carbon dioxide concentration with nitric oxide and 1-butene partial pressures maintained at 2.41 and 2.57 kPa, respectively.

Water vapour

The reactant partial pressures were held constant as described in the preceding paragraph while the water vapour concentration was altered from 0.07 to 2.41 kPa. This had no effect on the experimental rates of reaction and the reaction was zero order with respect to water vapour partial pressure.

From the preceding results, the rate of reaction was given by:

$$r = kP_{NO}^{0.5} \qquad [3.6.1]$$

for r_1 and r_2 and

$$r_3 = k_3 P_{NO}^{1.35} \qquad [3.6.2]$$

3.6.2 *The effect of temperature*

Specific rate constants were calculated from the integrated forms of equations [*3.6.1 and .2*] with respect to concentration at temperatures from 723 to 623 K. The catalyst was pretreated with 2.89 kPa nitric oxide and 2.35 kPa 1-butene for 12 h. Apparent activation energies, determined from Arrhenius plots, Figure 3.6.3, were found to be 69 ±4, 78 ±4 and 30 ±4 kJ mol^{-1} from nitrogen, carbon dioxide and nitrous oxide rates, respectively. The corresponding pre-exponential factors were 1.72×10^{-1} and 1.16 and 1.99×10^{-2}. $mol^{0.5} \ell^{-0.5} m^2 g^{-1}$, and 1.99×10^{-2} $mol^{-0.35} \ell^{0.35} m^2 g^{-1}$.

3.6.3 *The effects of reaction conditions on catalyst properties*

After a 48 h exposure to 3.06 kPa nitric oxide and 2.32 kPa 1-butene at 673 K, the catalyst surface area remained 15.5 $m^2 g^{-1}$. Under the scanning electron microscope, catalyst particles exhibited a separate

TABLE 3.6.1 The effects of component partial pressures on the NO/C_4H_8 reaction over Mn_2O_3

$P_{C_4H_8}$ (kPa)	$r_1 \times 10^{-8}$ (mol m^{-2} s^{-1})	$r_2 \times 10^{-8}$ (mol m^{-2} s^{-1})	$r_3 \times 10^{-8}$ (mol m^{-2} s^{-1})
0.92	3.39	3.00	2.55
1.32	3.26	2.68	2.93
1.44	3.39	2.48	3.19
1.63	3.39	2.74	2.90
2.77	3.26	3.16	3.16
2.84	3.29	3.55	2.81
3.22	2.87	2.80	3.19
3.72	3.10	2.81	2.90
5.50	3.26	2.81	2.58
6.09	3.26	2.74	3.12
7.49	3.19	2.95	2.68
P_{NO} (kPa)			
0.17	0.56	0.98	0.07
0.55	1.08	1.78	0.49
0.98	1.43	2.40	1.11
1.52	2.19	3.03	1.84
2.34	2.41	3.94	3.53
4.15	3.00	5.23	7.54
5.75	3.78	6.30	11.25
8.17	5.26	7.54	18.55

TABLE 3.6.2 The effect of temperature on reaction rate constants for the NO/C_4H_8 reaction over Mn_2O_3

Temperature (k)	$k_1 \times 10^{-7}$	$k_2 \times 10^{-7}$	$k_3 \times 10^{-5}$
723	17.1	27.2	14.5
713	14.8	22.3	13.6
703	12.4	18.4	12.8
693	10.9	15.2	11.9
683	8.91	12.7	11.0
673	7.58	10.2	10.2
663	6.19	8.35	9.44
653	5.05	6.74	8.66
643	4.16	5.28	7.98
633	3.40	4.27	7.28
623	2.72	3.35	6.59

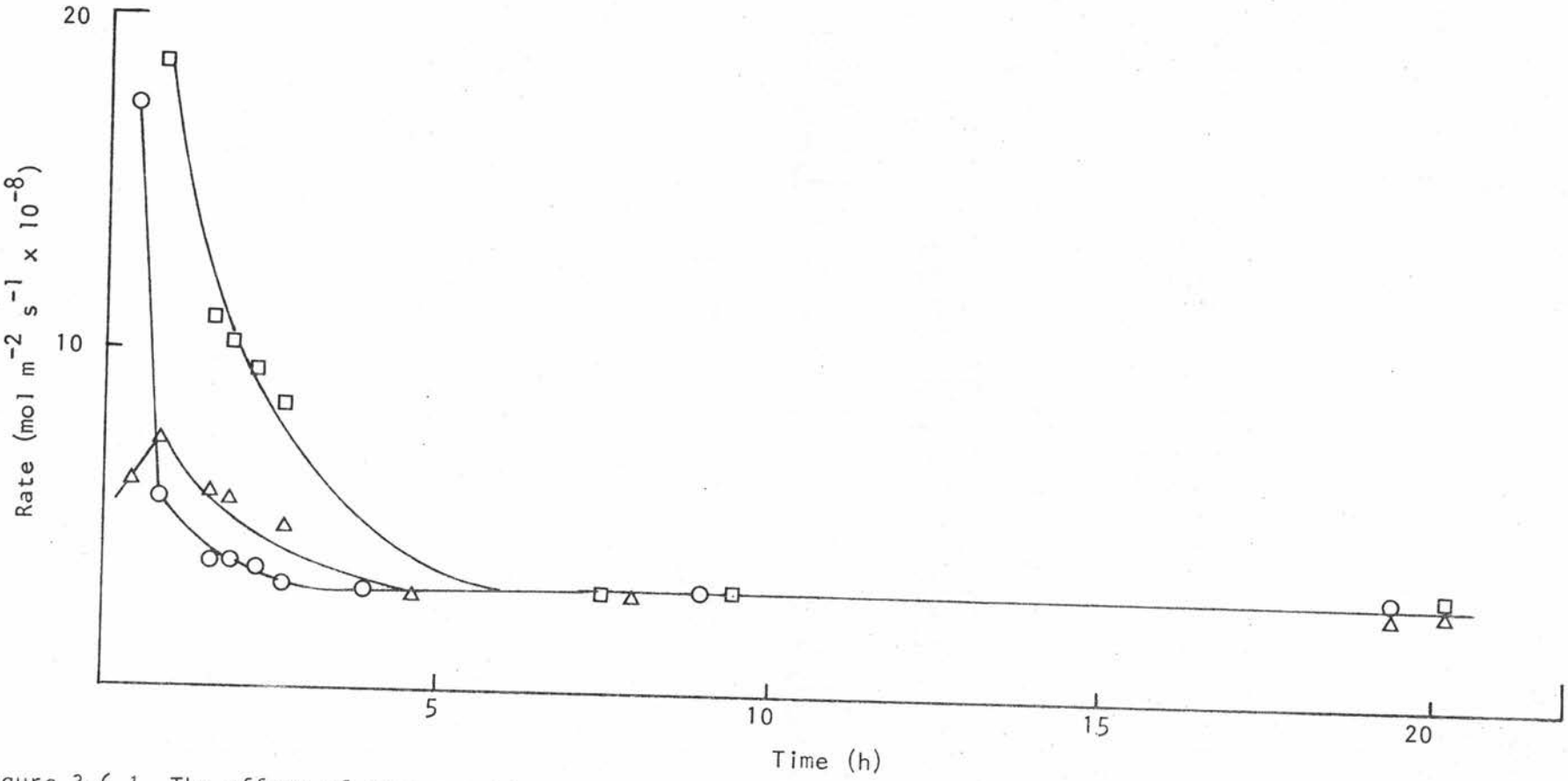

Figure 3.6.1 The effect of exposure time on the NO/C_4H_8 reaction over Mn_2O_3; □ r_1, ○ r_2, △ r_3.

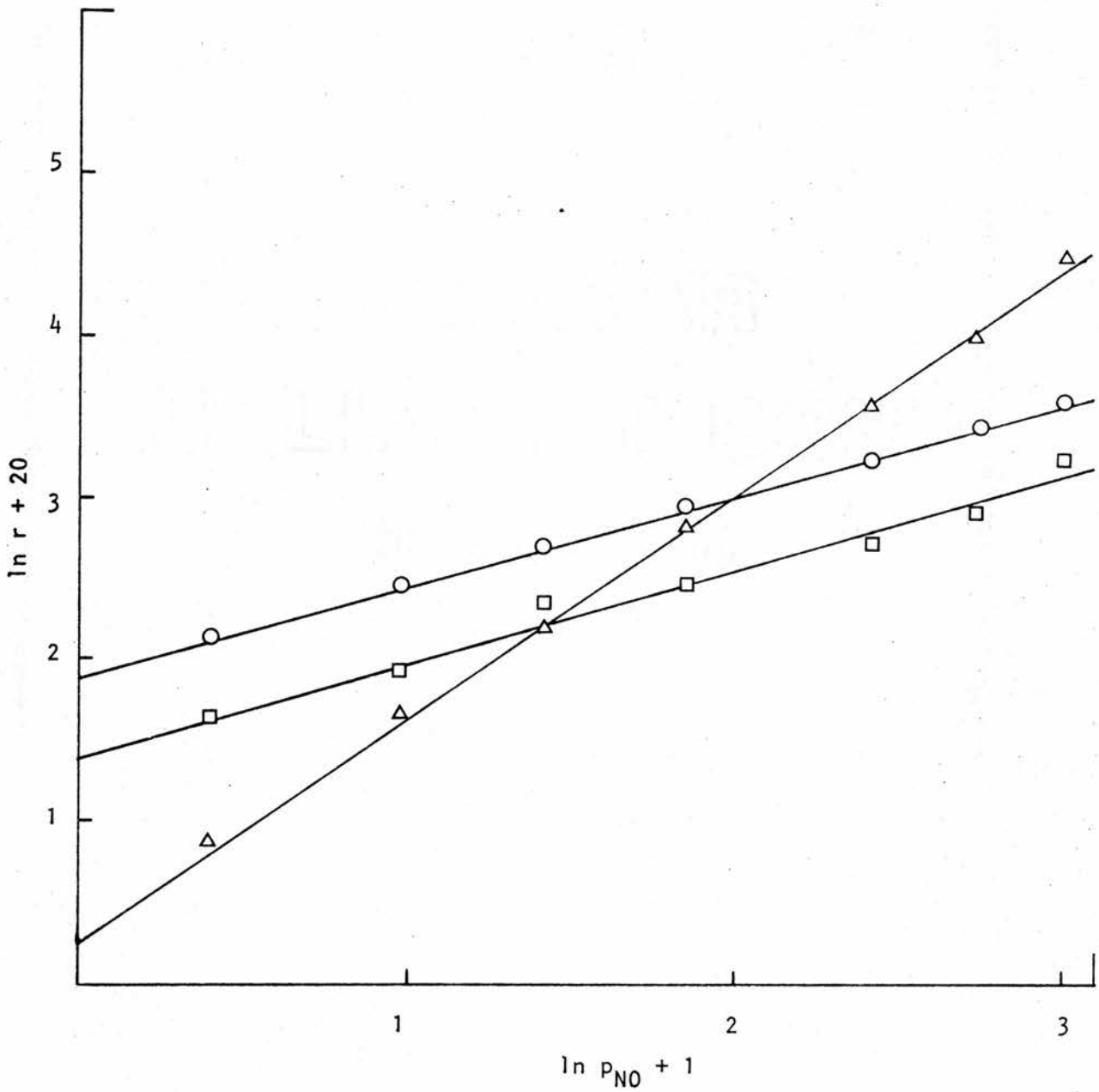

Figure 3.6.2 Effect of component partial pressure on the NO/C_4H_8 reaction over Mn_2O_3; p_{NO}, □ r_1, ○ r_2, △ r_3.

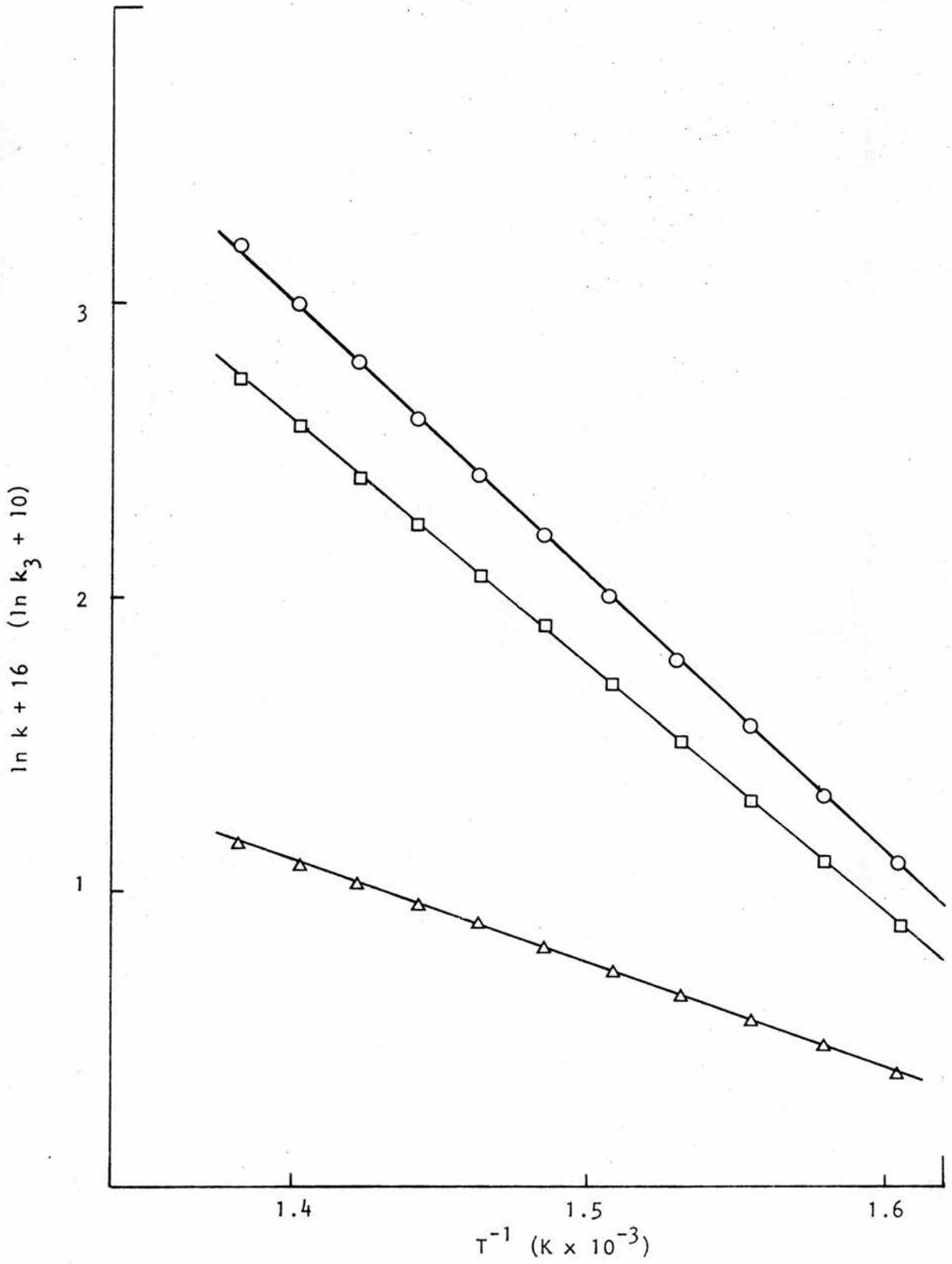

Figure 3.6.3 Arrhenius plot for the NO/C_4H_8 reaction over Mn_2O_3; □ k_1, ○ k_2, △ k_3.

crystalline phase on parts of their surface as in Figure 3.3.3, while the remainder of the surface appeared unaffected as in Figure 3.4.3 A and B.

The infrared spectrum of manganese(III) oxide after catalysis appeared similar to that observed for the same catalyst after the nitric oxide/ethane reaction, Figure 3.3.4 C. This included absorption bands at 1630, 1390 and 845 cm^{-1} indicative of a nitrate species along with bands at 615, 490, 425 and 350 cm^{-1}.

Chemical analysis indicated 69.0% w/w manganese in the used catalyst which remained black in colour. X-ray powder diffraction produced d-spacings corresponding to gamma manganese(III) oxide - 2.48, 2.74, 3.08, 1.543, 1.558, 1.81 and 2.06 Å.

3.7 *The nitrous oxide/1-butene reaction over manganese(III) oxide*

The rate of the catalytic reaction, measured as the rate of nitrogen or carbon dioxide production, decreased slightly for the first hour of reaction at 673 K and remained constant thereafter for a minimum of 24 h. The conversion of 1-butene at this temperature amounted to 18% with only nitrogen, carbon dioxide and water as the products of reaction.

3.7.1 *Reaction rate orders*

After catalyst pretreatment with 2.66 kPa nitrous oxide and 2.66 kPa 1-butene for 3 h, rate orders were determined at 623 K.

Nitrous oxide

With the partial pressure of 1-butene maintained at 3.05 kPa, the effects of from 0.30 to 4.93 kPa nitrous oxide on the experimental reaction rates were observed. The rate order with respect to nitrous oxide concentration was 0.5 for partial pressures <2.60 kPa. As shown in Figure 3.7.1, plots of ln (rate) against ln p_{N_2O} were linear at low pressures and increased with an increase in nitrous oxide partial pressure above 2.60 kPa.

1-Butene

The partial pressure of 1-butene was altered from 0.43 to 8.27 kPa while nitrous oxide partial pressure was maintained at 2.49 kPa. The rate order with respect to the concentration of 1-butene was 0.4, Figure 3.7.1.

Carbon dioxide

The partial pressures of nitrous oxide and 1-butene were held at 2.48 and 2.58 kPa, respectively, and that of carbon dioxide was adjusted from 0.62 to 8.33 kPa. This had no effect on the rate of nitrogen formation, $r_1 \propto P^0_{CO_2}$, and the reaction was zero order with respect to carbon dioxide concentration.

Water vapour

Variations in the partial pressure of water vapour from 0.09 to 2.10 kPa with nitrous oxide (2.48 kPa), and 1-butene (2.58 kPa), partial pressures held constant had no effect on the experimental rate of reaction; r_1, $r_2 \propto P^0_{H_2O}$.

Based on these results, the rate of reaction was expressed by:

$$r = k\, P^{0.5}_{N_2O}\; P^{0.4}_{C_4H_8} \qquad [3.7.1]$$

for both r_1 and r_2 where $0.30 < P_{N_2O} < 2.60$ kPa.

3.7.2 *The effect of temperature*

The catalyst was first exposed to 2.23 kPa nitrous oxide and 2.78 kPa 1-butene at 673 K for 3 h. Reaction rate constants were calculated at 10 K intervals from 673 to 573 K from the integrated form of equation [3.7.1]. The specific rate constant data are summarized in Table 3.7.2. When plotted in the Arrhenius fashion, the data yielded apparent activation energies from k_1 and k_2 of 117 ±4 and 126 ±4 kJ mol^{-1} with pre-exponential factors 6.09×10^5 and 1.94×10^6 $mol^{0.1}\ \ell^{-0.1}\ m^{-2}\ s^{-1}$

TABLE 3.7.1 The effects of component partial pressures on the N_2O/C_4H_8 reaction over Mn_2O_3

$P_{C_4H_8}$ (kPa)	$r_1 \times 10^{-7}$ (mol m^{-2} s^{-1})	$r_2 \times 10^{-7}$ (mol m^{-2} s^{-1})
0.43	1.42	0.768
0.94	1.84	1.13
1.25	2.10	1.21
1.72	2.19	1.33
2.67	2.62	1.51
3.04	3.02	1.81
3.66	3.12	1.78
4.13	3.26	1.85
6.67	3.74	2.00
8.27	3.97	2.38
P_{N_2O} (kPa)		
0.30	1.07	0.549
0.40	1.19	0.676
0.44	1.28	0.700
0.83	1.69	0.933
1.28	2.13	1.15
1.85	2.36	1.35
2.69	3.00	1.76
2.90	3.17	1.95
3.26	3.66	2.20
3.74	4.48	2.72
4.05	5.21	3.13
4.47	6.04	3.84
4.93	8.79	7.71

TABLE 3.7.2 The effect of temperature on reaction rate constants for the N_2O/C_4H_8 reaction over Mn_2O_3

Temperature (K)	$k_1 \times 10^{-5}$	$k_2 \times 10^{-5}$
673	46.7	35.5
663	35.4	24.6
653	28.8	18.1
643	21.4	12.6
633	14.2	8.46
623	8.90	5.70
613	6.76	3.92
603	4.60	2.60
593	3.08	1.71
583	1.97	1.11
573	1.30	0.711

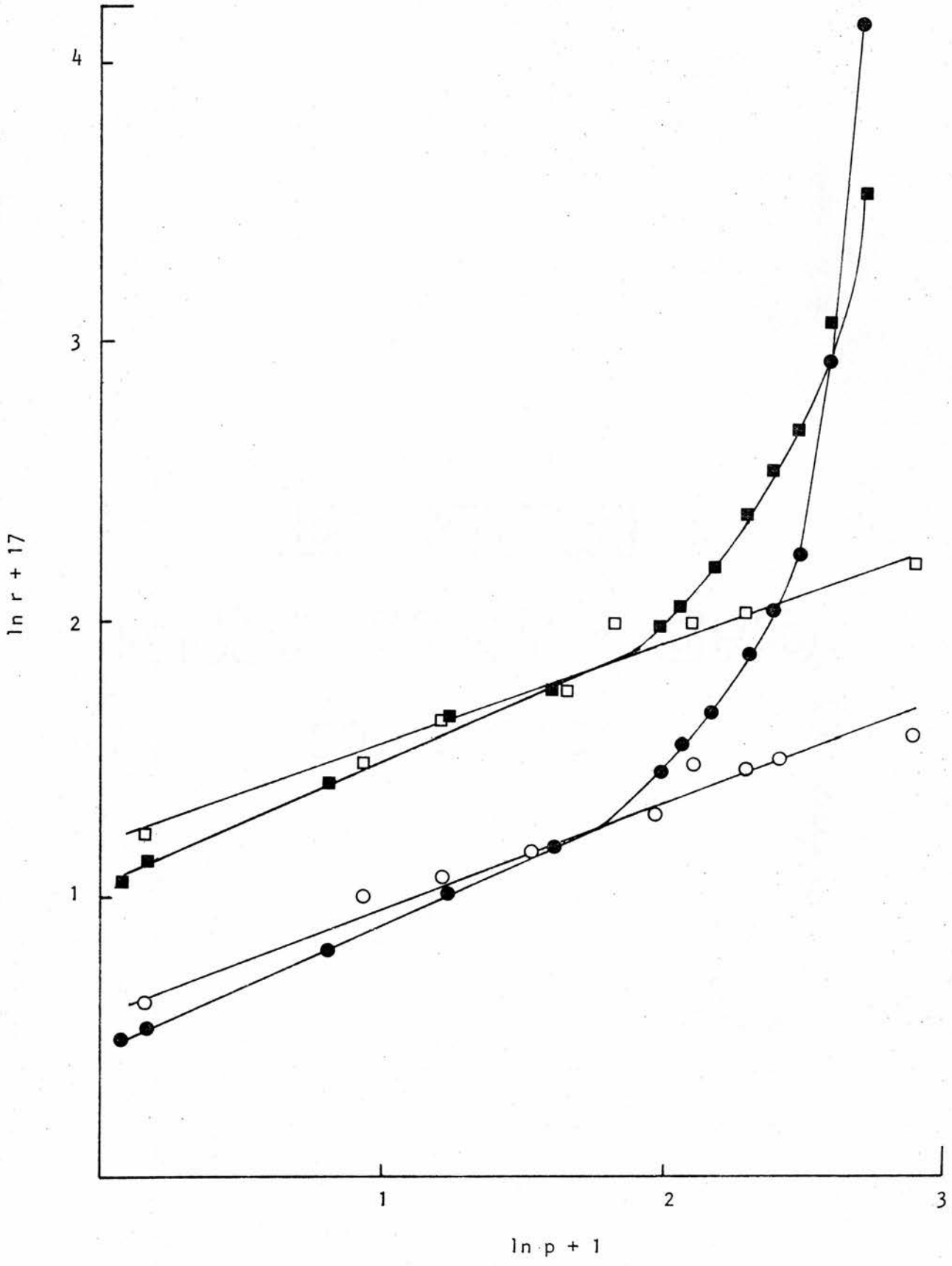

Figure 3.7.1 Effects of component partial pressures on the N_2O/C_4H_8 reaction over Mn_2O_3; $p_{C_4H_8}$, □ r_1, ○ r_2; p_{N_2O}, ■ r_1, ● r_2.

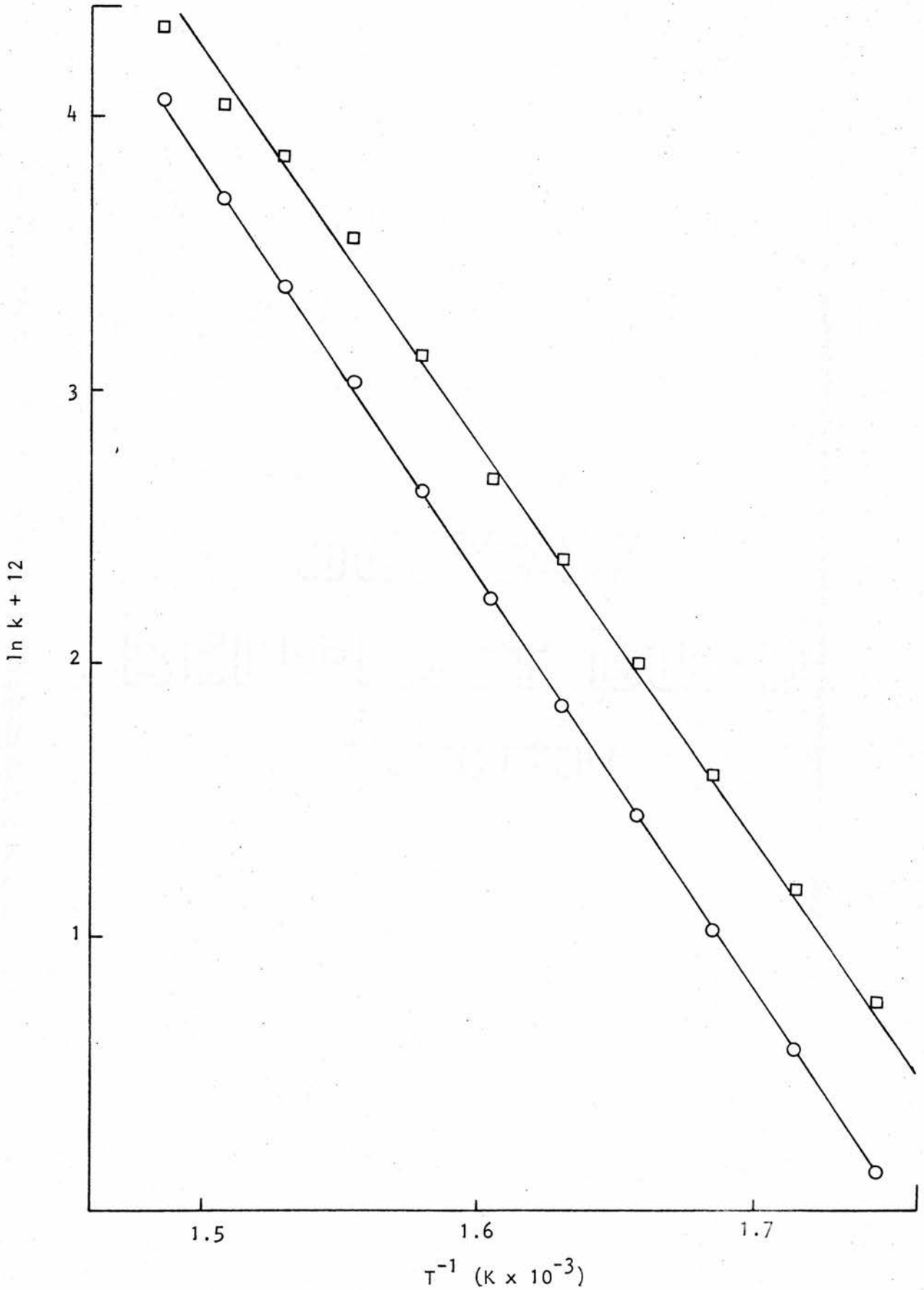

Figure 3.7.2 Arrhenius plot for the N_2O/C_4H_8 reaction over Mn_2O_3; □ k_1, ○ k_2.

3.7.3 *The effects of reaction conditions on catalyst properties*

Exposure to 2.48 kPa nitrous oxide and 2.58 kPa 1-butene for periods of up to 24 h at 673 K had essentially the same effects as noted in previous sections. The surface area remained 15.5 $m^2 g^{-1}$ and infrared absorption bands appeared at 615, 490, 425 and 350 cm^{-1}. Chemical analysis indicated 69.2% w/w manganese and d-spacings corresponding to gamma manganese(III) oxide - 2.48, 2.74, 3.08, 1.542, 1.556, 1.80, 2.06 Å - were determined from X-ray diffraction studies.

3.8 *The oxygen/1-butene reaction over manganese(III) oxide*

With 2.12 kPa oxygen and 2.35 kPa 1-butene, the catalytic reaction rate increased slightly for the first 30 min of reaction and then remained constant for at least 24 h at 523 K where the conversion of 1-butene was 13%. Prior to any catalytic studies, then, the catalyst was pretreated under these conditions for 3 h.

3.8.1 *Reaction rate orders*

Rate orders for the oxygen/1-butene reaction over manganese(III) oxide were determined at 473 K.

Oxygen

The partial pressure of oxygen was altered from 0.48 to 4.95 kPa with that of 1-butene maintained at 2.77 kPa. For oxygen partial pressure <2.20 kPa, the rate order with respect to oxygen was found to be 0.4, Figure 3.8.1. The rate order increased with an increase in partial pressure above this point.

1-Butene

With oxygen partial pressure maintained at 2.18 kPa, the rate order was 0.3 with respect to 1-butene concentrations from 0.46 to 7.88 kPa, Figure 3.8.1.

Carbon dioxide

Variations in the partial pressure of carbon dioxide from 0.55 to 6.45 kPa had no effect on experimental reaction rate with oxygen and 1-butene partial pressures held constant at 2.16 and 2.71 kPa, respectively. Hence, the rate order with respect to carbon dioxide concentration was zero.

Water vapour

With the partial pressures of oxygen and 1-butene maintained at 2.16 and 2.71 kPa, respectively, the rate order was zero with respect to water vapour partial pressure from 0.08 to 2.33 kPa.

On the basis of the rate order results, the catalytic rate of reaction was expressed as:

$$r_2 = k\, P_{O_2}^{0.4}\, P_{C_4H_8}^{0.4} \qquad [3.8.1]$$

for $0.48 < P_{O_2} < 2.20$ kPa.

3.8.2 *The effect of temperature*

Rate constants were calculated from the integrated form of equation [3.8.1] at temperatures from 523 to 433 K, Table 3.8.2. When plotted as ln k versus T^{-1} as shown in Figure 3.8.2, two linear regions were apparent. The Arrhenius plot gave rise to two apparent activation energies 183 ±4 and 88 ±4 kJ mol^{-1} for the temperature ranges 523 to 503 K and 503 to 433 K. The corresponding pre-exponeitial factors were 1.74×10^{15} and 2.94×10^{5} $mol^{0.3}\ \ell^{-0.3}\ m^{-2}\ s^{-1}$.

3.8.3 *The effects of reaction conditions on catalyst properties*

The oxide surface area remained 15.5 $m^2\ g^{-1}$ after reaction at 523 K for 24 h and the infrared spectrum, with absorption bands at 615, 490, 425 and 350 cm^{-1}, was similar to that obtained for the same manganese(III) oxide catalyst in previous related studies, sections 3.4.3, 3.5.3 and 3.7.3. Further analyses yielded 69.3% w/w manganese and d-spacings were 2.48, 2.74, 3.08, 1.544, 1.558, 1.80 and 2.08 as determined by X-ray diffraction.

TABLE 3.8.1 The effects of component partial pressures on the O_2/C_4H_8 reaction over Mn_2O_3

$P_{C_4H_8}$ (kPa)	$r_2 \times 10^{-8}$ (mol m^{-2} s^{-1})	P_{NO} (kPa)	$r_2 \times 10^{-8}$ (mol m^{-2} s^{-1})
0.46	3.67	0.48	3.96
0.87	4.53	0.98	4.90
1.11	4.90	1.31	5.34
1.55	5.29	1.69	5.99
2.03	5.78	2.00	6.07
2.68	6.15	2.26	6.56
3.40	7.11	2.81	7.69
4.92	7.69	3.23	8.65
6.45	8.41	3.46	9.38
7.88	9.07	3.86	12.5
		4.10	13.9
		4.95	45.6

TABLE 3.8.2 The effect of temperature on the reaction rate constant for the O_2/C_4H_8 reaction over Mn_2O_3

Temperature (K)	$K_2 \times 10^{-6}$
523	140
513	61.0
503	26.3
493	18.9
483	10.7
473	6.76
463	4.22
453	2.63
443	1.51
433	0.900
423	0.498

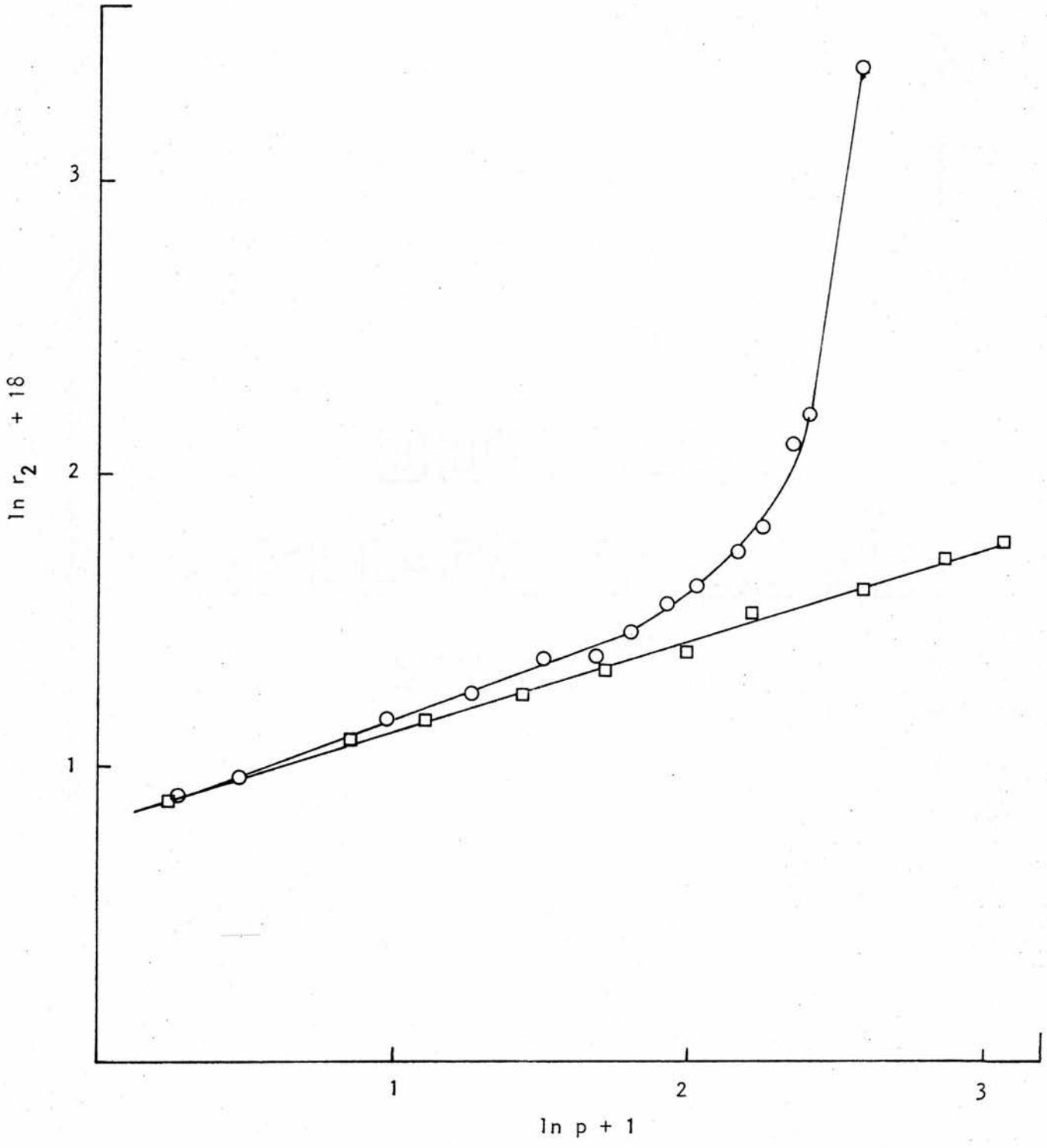

Figure 3.8.1 Effect of component partial pressure on the rate of the O_2/C_4H_8 reaction over Mn_2O_3; p_{O_2}, O r_2; $p_{C_4H_8}$, □ r_2.

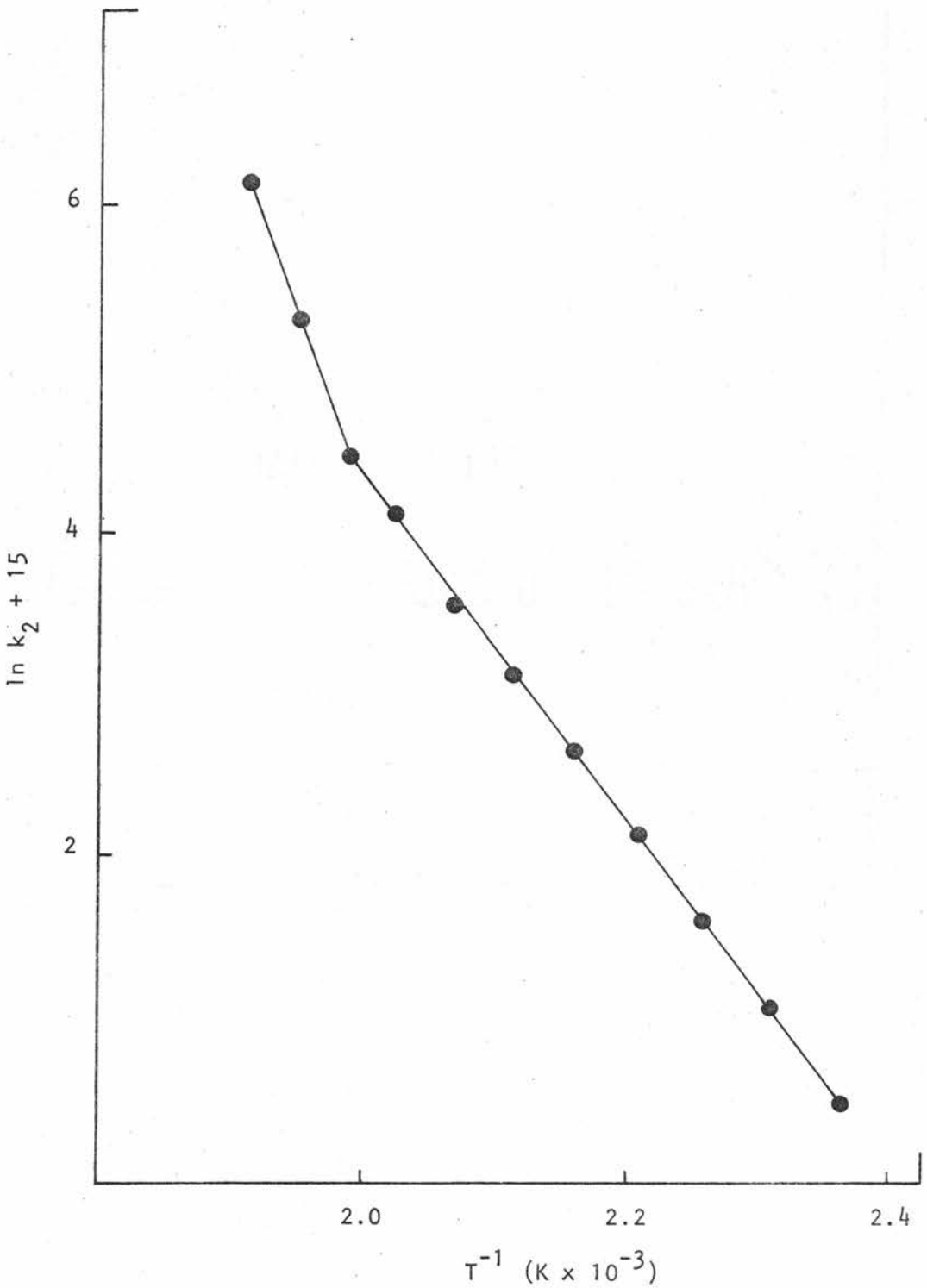

Figure 3.8.2 Arrhenius plot for the O_2/C_4H_8 reaction over Mn_2O_3; ● k_2.

3.9 *The nitrous oxide/1-butene reaction over related oxides*

A number of metal oxides - Sc_2O_3, TiO_2, V_2O_5, Cr_2O_3, Mn_2O_3, Fe_2O_3, NiO, CuO, ZnO, and SnO - were evaluated as possible catalysts for the nitrous oxide/1-butene reaction. The catalytic reaction generally produced nitrogen, carbon dioxide and water in measureable quantities at temperatures >623 K.

The catalytic activity of each oxide was assessed by determining the rates of nitrogen and carbon dioxide formation at 673 K. As in previous studies, 1 g catalyst samples were used and the total gas flow rate was 350 $dm^3\ min^{-1}$. The catalysts were pretreated with nitrous oxide and 1-butene, both at 2.66 kPa partial pressure for 12 h at 673 K. Each reactant was passed separately over the catalyst to ensure that no reaction occurred until both were present.

Surface areas were determined after reaction and are presented in Table 3.9.1 along with the experimental rate data. Also included in the table are the results obtained with Modmor fibres impregnated with copper, nickel and manganese from 10% w/w nitrate solutions, section 2.11.3.

3.10 *Carbon fibre catalyst supports*

The surface areas of the original carbon fibres were 0.4 $m^2\ g^{-1}$ for Grafil and 1.8 $m^2\ g^{-1}$ for Modmor fibres. Initial studies were aimed towards "activating" or increasing the surface areas of these fibres without seriously affecting their fibrous nature.

3.10.1 *Activation*

Treating carbon fibres in a microwave discharge as described in section 2.11 had no measureable effects on sample weight or surface area. Steam activation, however, of 10 cm lengths of Grafil at 1173 K in nitrogen plus water vapour (12.3 kPa) at a flow rate of 200 $dm^3\ min^{-1}$ produced a 44% weight loss in 48 h, Figure 3.10.1. The surface area of this residue was 2.2 $m^2\ g^{-1}$. Prolonged treatment (5 days) under these conditions produced a 96% weight loss and the residue surface area was 2.6 $m^2\ g^{-1}$.

TABLE 3.9.1 Catalyst activity series for the N_2O/C_4H_8 reaction at 673 K.

CATALYST	S A ($m^2\ g^{-1}$)	EXPERIMENTAL RATES ($mol\ m^{-2}\ s^{-1}$)	
		r_1	r_2
CuO	4.1	6.82×10^{-6}	3.28×10^{-6}
Modmor + Cu	4.6	2.51×10^{-6}	1.62×10^{-6}
Fe_2O_3	6.0	1.58×10^{-6}	9.10×10^{-7}
NiO	2.5	6.72×10^{-7}	3.19×10^{-7}
Modmor + Ni	4.6	2.35×10^{-7}	1.17×10^{-7}
Mn_2O_3	15.5	2.20×10^{-7}	9.74×10^{-8}
Modmor + Mn	4.6	5.45×10^{-8}	1.72×10^{-8}
Cr_2O_3	3.1	4.85×10^{-8}	-
TiO_2	9.0	2.48×10^{-8}	-
Sc_2O_3	2.3	1.41×10^{-8}	-
SnO	9.0	1.36×10^{-8}	-
ZnO	11.7	1.04×10^{-8}	-
V_2O_5	6.1	8.77×10^{-9}	-
Al_2O_3	2.8	7.68×10^{-9}	-

Grinding the Grafil fibre with a mortar and pestle produced a fine powder with surface area 5.0 $m^2\ g^{-1}$. Steam activation under the same conditions produced a 97% weight loss after only 90 min. Observation by scanning electron microscopy indicated that the ground fibre consisted of a number of small, irregularly-shaped particles and no further studies were conducted on this sample.

The Modmor fibre was much more reactive to steam activation as shown in Figure 3.10.2. Treatment of 10 cm lengths with nitrogen plus water vapour (12.3 kPa) at 200 $dm^3\ min^{-1}$ and 773 K gave an 80% weight loss after 60 min. After a 50% weight loss by steam activation, the fibre surface area was 4.2 $m^2\ g^{-1}$, while the same loss in air produced a residue surface area of 3.2 $m^2\ g^{-1}$.

Scanning electron micrographs of Modmor fibres after various treatments are shown in Figure 3.10.3. The relatively smooth surface of normal Modmor fibres is shown in A. Modmor fibre impregnated with manganese in a 10% nitrate solution as in section 2.11.3 and further treated at 773 K in nitrogen plus water vapour (12.3 kPa) at 200 $dm^3\ min^{-1}$ for 20 min is shown in Figure 3.10.3 B. Modmor fibre impregnated with manganese and further treated in air at 773 K for 3 h is shown in C. Steam activation appears to involve surface etching and pitting at discrete sites while air oxidation appears to involve indiscriminate attack of the fibre sheath even at low exposure time. The surface roughness after steam treatment for 30 min at 773 K is apparent in D. This sample had lost 46% of its original weight and the surface area was 4.6 $m^2\ g^{-1}$.

Dynamic thermogravimetric analysis of Modmor fibres indicated that the major weight loss in air began at 750 K and the rate of weight loss increased with temperature to yield a 99.5% loss at 900 K, Figure 3.10.4. Fibres impregnated with manganese from a 10% (w/w) nitrate solution and dried at 378 K exhibited the same thermal behaviour. When the treated sample was first heated in nitrogen at 773 K for 2 h, the weight loss curve was the same as that for original Modmor fibres up to 873 K. Above

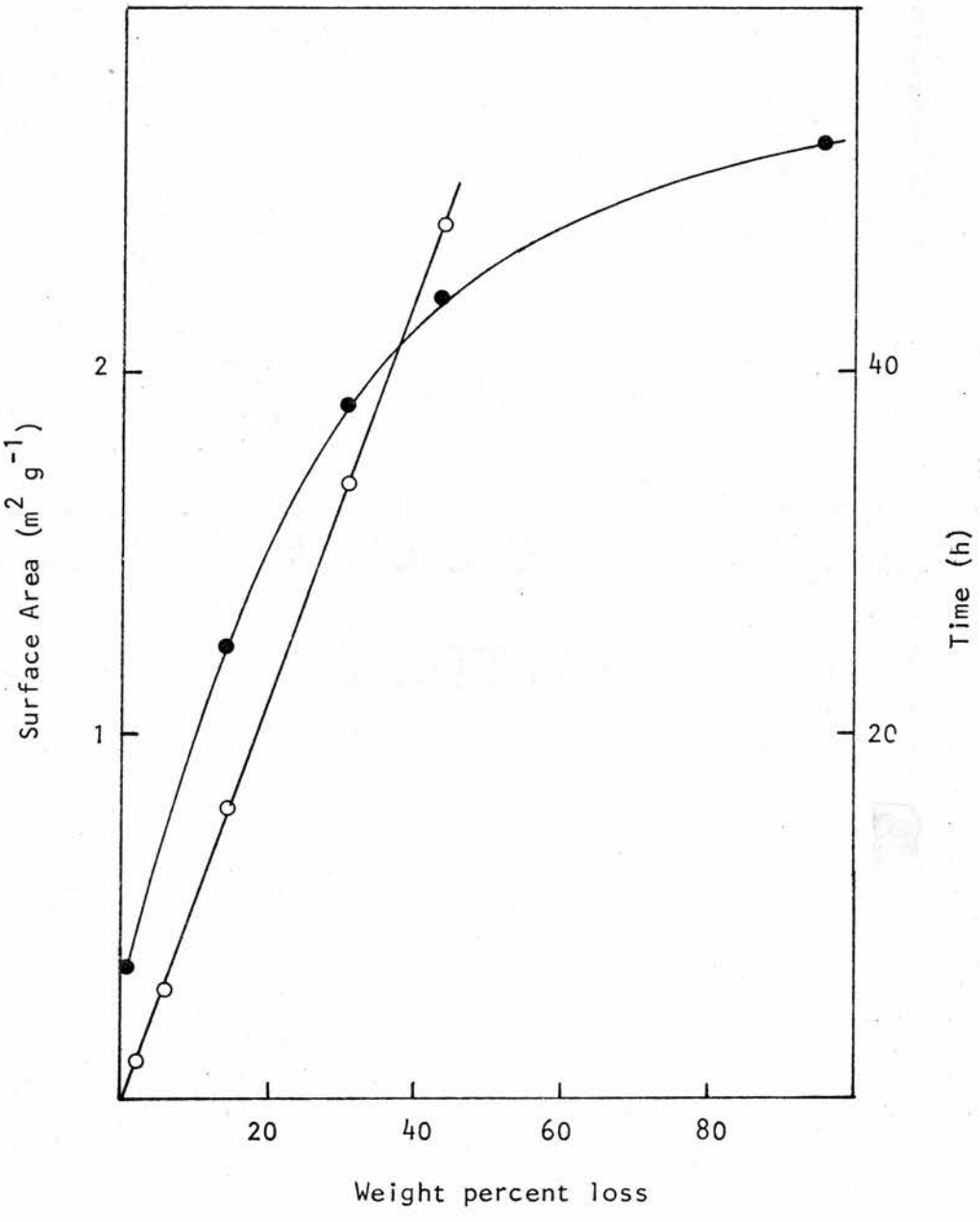

Figure 3.10.1 Steam activation (12.3 kPa) of **Grafil** fibres at 1173 K at 200 dm^3 min^{-1}; ● surface area (m^2 g^{-1}), ○ time to % loss (h).

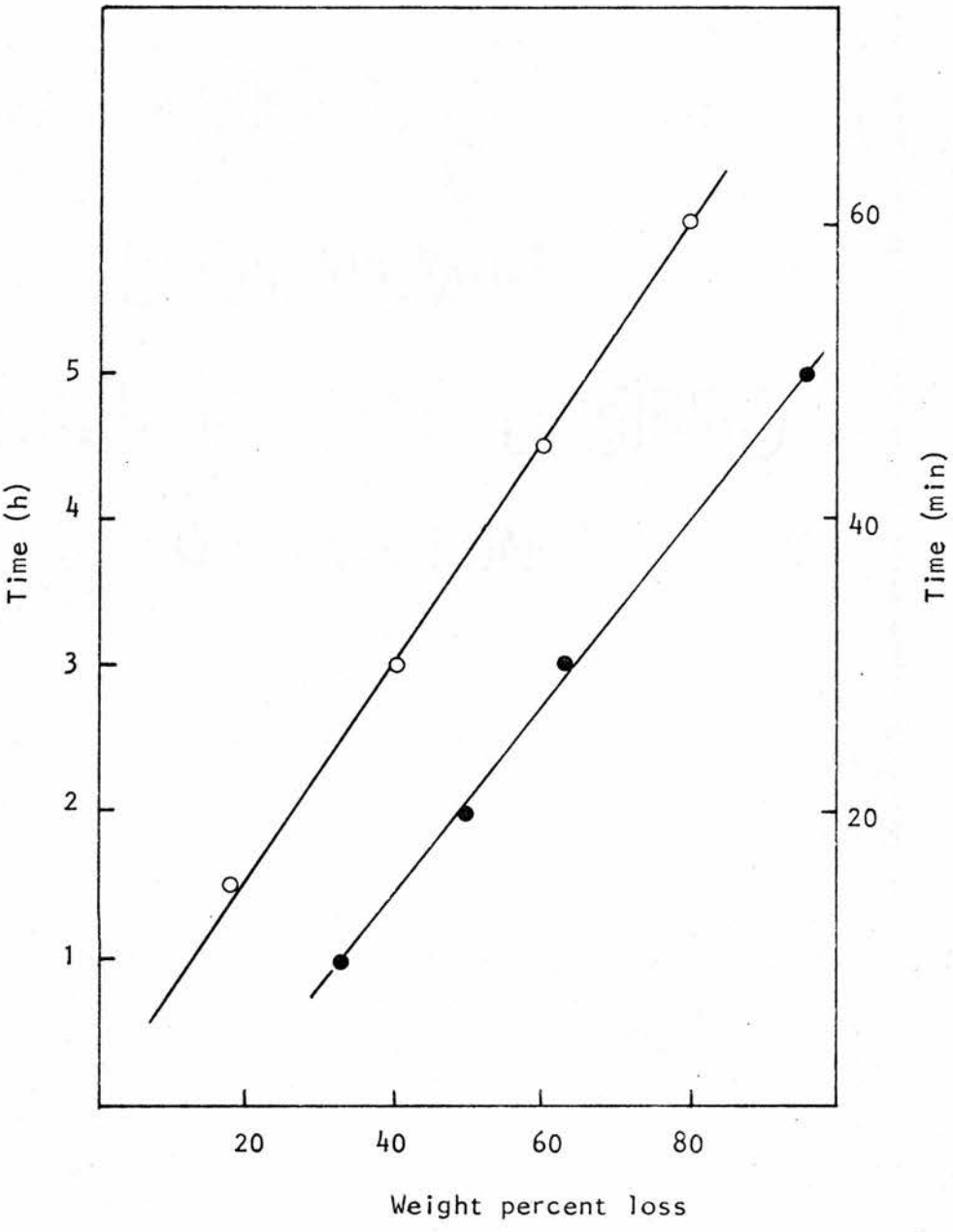

Figure 3.10.2 Activation of Modmor fibres at 773 K in N_2 + H_2O (12.3 kPa) at 200 dm^3 min^{-1}, o ; and at 773 K in air, ● .

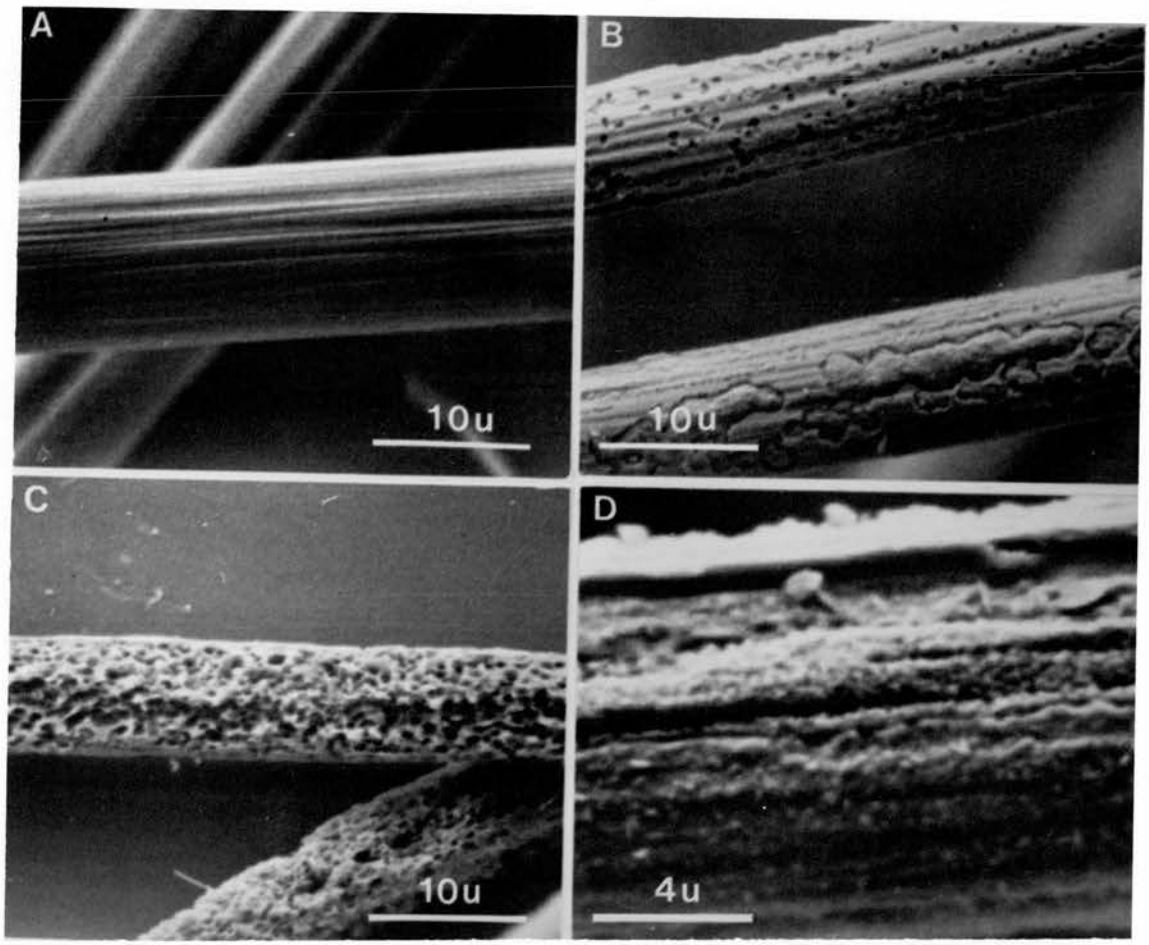

Figure 3.10.3 Scanning electron micrographs of Modmor fibres; unreacted, A; in N_2/H_2O (12.3 kPa) at 773 K and 200 dm^3 min^{-1} (NTP) for 30 min, B and D; and in air at 773 K for 3 h, C.

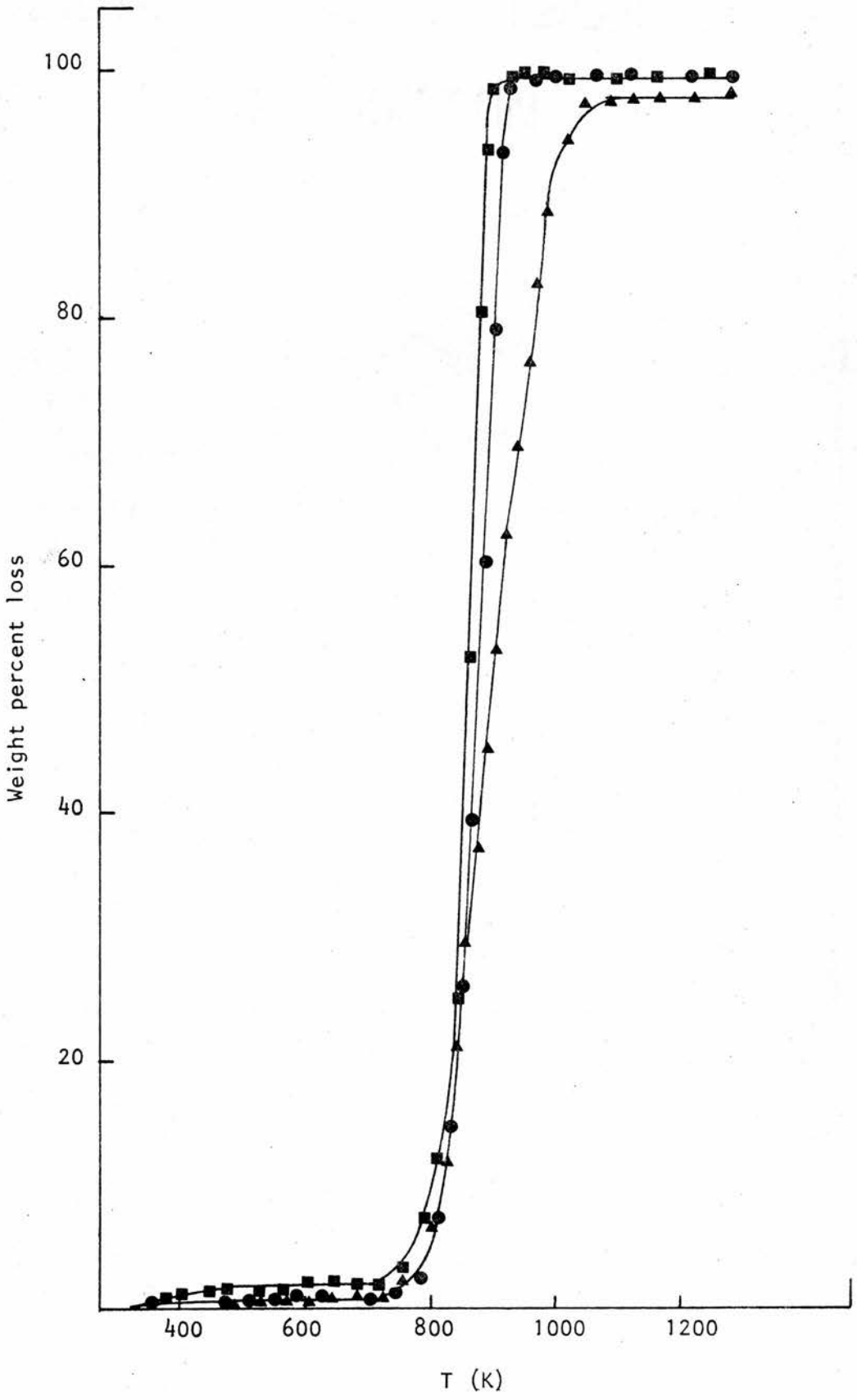

Figure 3.10.4 TG analysis of Modmor fibres (10 cm lengths) in air; ● Modmor, ■ Modmor + $Mn(NO_3)_2$, ▲ Modmor + $Mn(NO_3)_2$ treated at 773 K.

TABLE 3.10.1 Kinetic evaluation of carbon fibre supported catalysts

CATALYST	TEMPERATURE (K)	EXPERIMENTAL RATES (mol m^{-2} s^{-1})		EXPERIMENTAL Ea (kJ mol^{-1})		EXPERIMENTAL A (mol $\ell^{-1} m^2 g^{-1}$)	
		r_1	r_2	From r_1	From r_2	From r_1	From r_2
N_2O/C_2H_6							
Grafil/Cu	673	3.35×10^{-7}	-	89		2.61	
	723	7.20×10^{-7}	-				
	773	2.69×10^{-6}	2.75×10^{-7}				
Modmor/Cu	673	1.79×10^{-7}	-	142		1.97×10^{4}	
	723	9.55×10^{-7}	6.86×10^{-7}		170		1.39×10^{6}
	773	4.84×10^{-6}	4.29×10^{-6}				
N_2O/C_4H_8							
Grafil/Cu	673	6.73×10^{-7}		164		3.99×10^{6}	
	723	5.61×10^{-6}	5.66×10^{-7}		315		3.29×10^{16}
	773	3.00×10^{-5}	1.68×10^{-5}				
Modmor/Cu	673	2.51×10^{-6}	1.62×10^{-6}	63		19.5	
	723	7.31×10^{-6}	5.27×10^{-6}		81		3.42
	773	1.05×10^{-5}	1.05×10^{-5}				
Grafil/Co	673	6.82×10^{-6}	3.28×10^{-6}	45		2.01×10^{-2}	
	723	1.90×10^{-6}	1.06×10^{-5}		50		2.52×10^{-2}
	773	4.26×10^{-5}	2.54×10^{-5}				
Modmor/Ni	673	2.35×10^{-7}	1.17×10^{-7}	130		3.75×10^{3}	
	723	2.96×10^{-6}	2.76×10^{-6}		145		3.29×10^{4}
	773	4.52×10^{-6}	3.15×10^{-6}				
Modmor/Mn	673	5.45×10^{-8}	1.72×10^{-8}	161		1.87×10^{5}	
	723	6.96×10^{-7}	4.70×10^{-7}		206		2.20×10^{8}
	773	2.17×10^{-6}	1.95×10^{-6}				
Modmor/Mn	573	5.43×10^{-8}	2.82×10^{-8}	70		0.228	
(sprayed)	673	4.89×10^{-7}	2.77×10^{-7}		73		0.134

this temperature, the rate of weight loss slowly decreased to give 98% loss at 1073 K.

CHN analysis indicated that Grafil fibres contained 97.32% carbon and 1.29% nitrogen (w/w) while Modmor fibres contained 92.7% carbon and 5.83% nitrogen. Modmor fibres impregnated with manganese from a 10% (w/w) nitrate solution and heat treated at 773 K contained 95.44% carbon and 1.92% nitrogen.

3.10.2 *Evaluation of carbon fibre catalysts*

Experiments were carried out using Modmor supported transition metals in the nitrous oxide/ethane and nitrous oxide/1-butene reactions. Impregnation was accomplished by adsorption from a nitrate solution as discussed in section 2.11.3. Before kinetic measurements were undertaken, the catalysts were pretreated at 673 for 12 h with 2.66 kPa nitrous oxide and 2.66 kPa hydrocarbon at a total flow rate of 350 dm^3 min^{-1} (NTP).

The surface area of the Grafil catalysts was 0.5 m^2 g^{-1} after reaction while that of the Modmor catalysts was 4.6 m^2 g^{-1}. The experimental rates of nitrogen and carbon dioxide formation were determined at 673, 723 and 773 K, Table 3.10.1. When plotted in the Arrhenius fashion as ln (rate) against T^{-1}, the data yielded values for the experimental activation energy and pre-exponential factor for each reaction as summarized in Table 3.10.1.

3.11 *The oxygen/ethane reaction over Modmor fibres plus manganese*

The catalyst was prepared by spraying a 50% w/w manganese(II) nitrate solution on to 10 cm lengths of Modmor as described in section 2.11.3. The catalyst contained 9.5% w/w manganese and had a surface area of 3.8 m^2 g^{-1}.

When the catalyst was exposed to 2.63 kPa oxygen and 2.62 kPa ethane at 673 K, the initial rate of carbon dioxide formation was very high, possibly due to oxidation of the carbon fibre itself. The rate of product

formation quickly decreased to 1.11×10^{-6} mol m^{-2} s^{-1} after 3 h, whereupon it remained constant for at least 48 h. At 673 K, the percentage conversion of ethane was 6.5% and the only products of reaction were those of complete oxidation-carbon dioxide and water vapour. The surface area of used catalyst was 6.9 m^2 g^{-1}.

3.11.1 *Reaction rate orders*

Rate order data for the oxygen/ethane reaction over a Modmor/manganese catalyst were determined at 623 K in terms of the rate of carbon dioxide production.

Oxygen

A reaction rate order of 0.3 with respect to oxygen concentration was determined, Figure 3.11.1, by altering the partial pressure from 0.31 to 14.15 kPa. The partial pressure of ethane was maintained at 2.57 kPa for this study.

Ethane

With the partial pressure of oxygen held constant at 2.47 kPa, the partial pressure of ethane was adjusted from 0.69 to 10.05 kPa. The rate order with respect to ethane concentration was found to be 0.4 from the linear ln (rate) versus ln (partial pressure) plot, Figure 3.11.1.

Carbon dioxide

Variations in the carbon dioxide partial pressure of from 0.67 to 6.44 kPa had no effect on the rate of reaction with oxygen and ethane partial pressure maintained at 2.68 and 2.74 kPa, respectively. Therefore, the rate order was zero with respect to carbon dioxide concentration.

Water vapour

Oxygen and ethane concentrations were held at 2.63 and 2.71 kPa, respectively, while the partial pressure of water vapour was altered from

0.06 to 2.11 kPa. A rate order of zero with respect to water vapour partial pressure resulted, $r_2 \propto P_{H_2O}^{0}$.

The rate of the oxygen/ethane reaction at 623 K over the Modmor/manganese catalyst was therefore expressed by:

$$r = k\, P_{O_2}^{0.4}\, P_{C_2H_6}^{0.3} . \qquad [3.11.1]$$

3.11.2 *The effect of temperature*

After catalyst pretreatment with 2.63 kPa oxygen and 2.76 kPa ethane at 673 K for 4 h, rate constants were calculated at 10 K intervals from 673 to 573 K. The data, Table 3.11.2, when plotted in the Arrhenius fashion, Figure 3.11.2, gave rise to an apparent activation energy of 108 kJ mol^{-1} and a pre-exponential factor of 5.42×10^4 $mol^{0.3}$ $\ell^{-0.3}$ m^{-2} s^{-1}.

3.11.3 *The effects of reaction conditions on catalyst properties*

The surface area of the catalyst increased from 3.8 m^2 g^{-1} to 6.9 m^2 g^{-1} after reaction. The concentration of manganese in the sample, 9.5%, did not alter appreciably after catalysis at 673 K for 48 h. The description of catalyst particles when observed by scanning electron microscopy is the same as that given in section 3.12.3.

3.12 *The oxygen/1-butene reaction over Modmor fibres plus manganese*

Upon exposure of the catalyst to the reaction mixture, 2.69 kPa oxygen and 3.04 kPa 1-butene, a great deal of carbon dioxide was liberated at 573 K. This was most likely due to oxidation of the carbon fibre and the rate of production decayed over 24 h to a steady state. The initial high rate of carbon dioxide formation persisted at temperatures as low as 323 K in the initial 24 h period. Only carbon dioxide and water were produced by the reaction and at 573 K the conversion of ethane was 8%.

TABLE 3.11.1 The effects of component partial pressures on the O_2/C_2H_6 reaction over Modmor plus Mn

$P_{C_2H_6}$ (kPa)	$r_2 \times 10^{-8}$ (mol m^{-2} s^{-1})	P_{O_2} (kPa)	$r_2 \times 10^{-8}$ (mol m^{-2} s^{-1})
0.69	6.16	0.31	5.00
0.82	6.49	0.40	5.05
1.05	7.02	1.20	7.55
1.45	7.99	1.52	8.08
1.47	8.32	2.34	9.12
2.04	9.55	3.81	10.36
2.58	11.14	4.37	11.11
4.28	12.74	6.05	12.93
5.23	14.57	8.77	14.19
5.71	15.73	14.15	16.54
6.21	16.49		
7.16	16.26		
8.01	18.08		
10.05	19.96		

TABLE 3.11.2 The effect of temperature on the reaction rate constant for the O_2/C_2H_6 reaction over Modmor plus Mn

Temperature	$k_2 \times 10^{-5}$
673	26.0
663	20.5
653	13.4
643	9.55
633	7.07
623	5.16
613	3.61
603	2.48
593	1.91
583	1.31
573	0.922

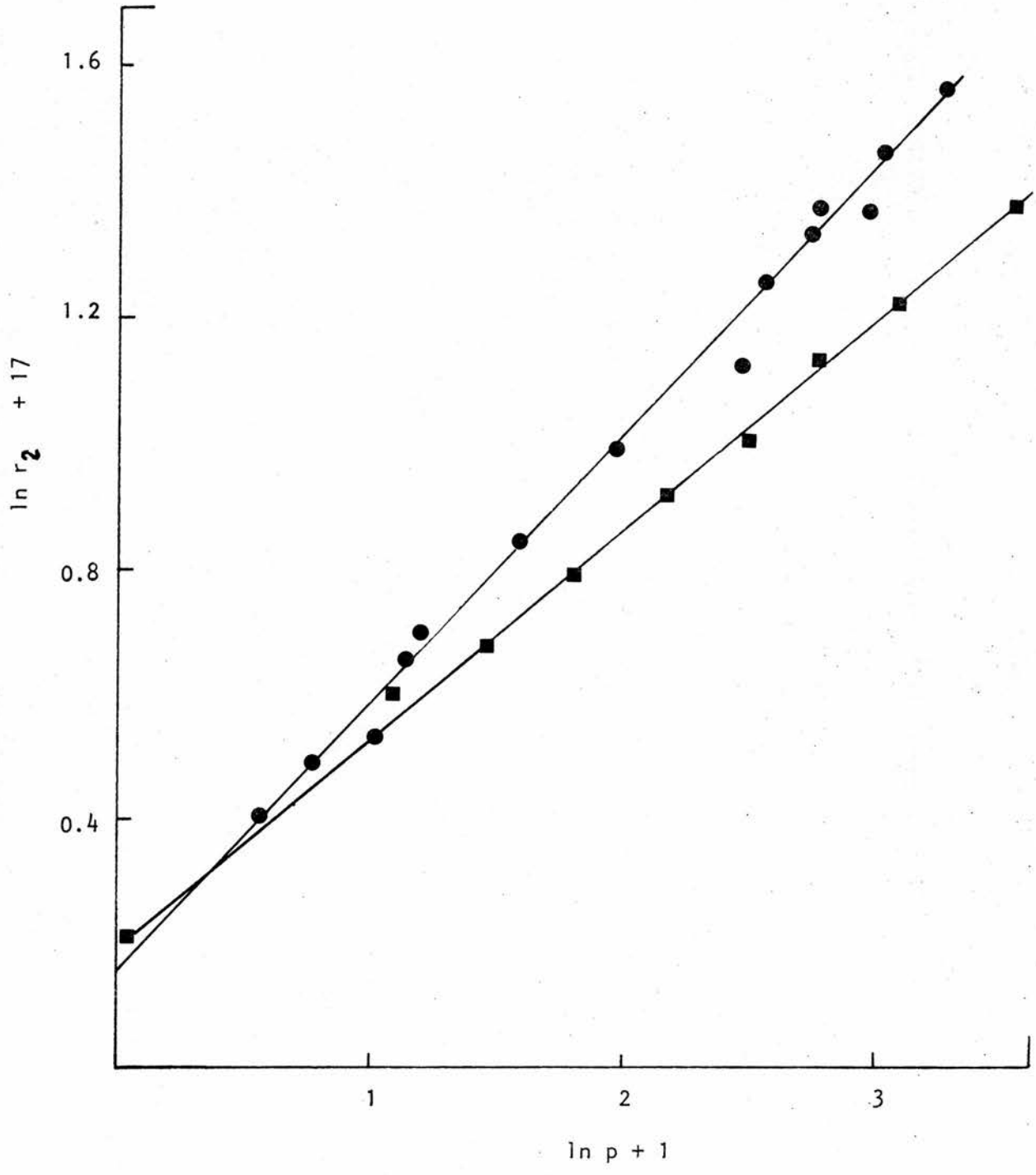

Figure 3.11.1 The effects of component partial pressures on the O_2/C_2H_6 reaction over Modmor + Mn; p_{O_2}, ■ r_2; $p_{C_2H_6}$, ● r_2.

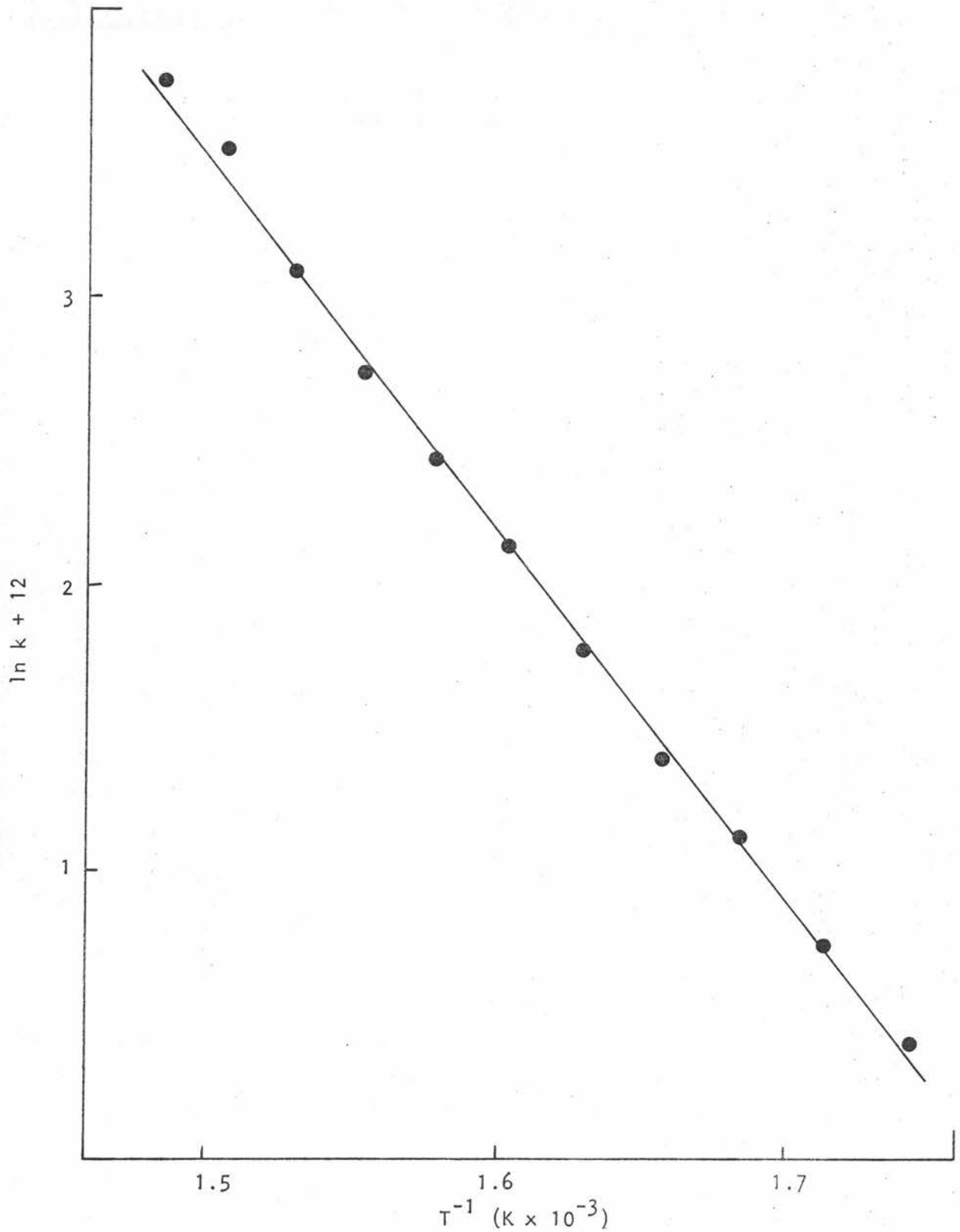

Figure 3.11.2 Arrhenius plot for the O_2/C_2H_6 reaction over Modmor + Mn; ● k_2.

3.12.1 *Reaction rate orders*

Rate orders were determined at 523 K for the oxygen/1-butene reaction over a Modmor/manganese catalyst. The catalyst surface area was 11.1 $m^2\ g^{-1}$ after reaction.

Oxygen

With 1-butene partial pressure maintained at 2.68 kPa, the oxygen concentration was adjusted from 0.32 to 7.36 kPa. The rate order with respect to oxygen concentration was 0.4, Figure 3.12.1.

1-Butene

The partial pressure of 1-butene was altered from 0.82 to 7.15 kPa and a rate order of 0.4 was obtained, $r_2 \propto P_{C_4H_8}^{0.4}$, while oxygen partial pressure was held at 2.46 kPa. The data are summarized in Table 3.12.1.

Carbon dioxide

The partial pressures of oxygen and 1-butene were maintained at 2.61 and 2.69 kPa, respectively, and the effects of from 0.50 to 9.31 kPa of carbon dioxide were observed. A rate order of zero was obtained with respect to carbon dioxide concentration.

Water vapour

The partial pressure of water vapour was adjusted from 0.09 to 2.50 kPa in the reaction mixture of 2.57 kPa oxygen and 2.81 kPa 1-butene. A rate order of zero with respect to water vapour partial pressure was determined, $r_2 \propto P_{H_2O}^{0}$.

The rate of reaction, r, was therefore given by:

$$r = k\ P_{O_2}^{0.4}\ \ P_{C_4H_8}^{0.4}\ . \qquad [3.12.1]$$

3.12.2 *The effect of temperature*

The effects of total gas flow rate on the catalytic oxygen/1-butene reaction rate was examined at 473, 523 and 573 K. Experimental activation energies were obtained from the Arrhenius-type plot of ln (rate) against T^{-1}. With 2.69 kPa oxygen and 3.04 kPa 1-butene, experimental activation energies of from 72 to 82 kJ mol^{-1} were derived for total gas flow rates from 250 to 450 dm^3 min^{-1} (NTP). As indicated in Table 3.12.2, the rate of reaction was essentially constant over the flow rate range from 300 to 400 dm^3 min^{-1} (NTP). The experimental activation energy did not vary systematically with flow rate. These results indicate that gas phase diffusion and heat and mass transfer effects were minimal.

After catalyst pretreatment for 24 h at 573 K with 2.47 kPa oxygen and 2.71 kPa 1-butene, rate constants were calculated from the integrated form of equation [*3.12.1*] over the temperature range from 573 to 473 K. When plotted in the Arrhenius fashion, Figure 3.12.2, the data yielded an apparent activation energy of 81 ±4 kJ mol^{-1} and pre-exponential factor, 2.16×10^4 $mol^{0.2}$ $\ell^{-0.2}$ m^{-2} s^{-1}.

3.12.3 *The effects of reaction conditions on catalyst properties*

The Modmor/manganese catalyst surface area increased from 3.8 to 11.1 m^2 g^{-1} after reaction at 573 K. Scanning electron micrographs, Figure 3.12.3, showed the effects of reaction on the Modmor fibres. It appears that the outer sheath and central core of the fibre remain while the middle of the fibre, the radial continuum (121), has been oxidized. In most cases, the ends of the fibres appear hollow, Figure 3.12.3 C, and the fibre surface appears rough and pitted, D. The outer sheath appeared to have peeled away from many fibres.

TABLE 3.12.1 The effects of component partial pressures on the O_2/C_4H_8 reaction over Modmor plus Mn

$P_{C_4H_8}$ (kPa)	$r_2 \times 10^{-7}$ (mol m^{-2} s^{-1})	P_{O_2} (kPa)	$r_2 \times 10^{-7}$ (mol m^{-2} s^{-1})
0.82	2.48	0.32	1.72
0.91	2.66	0.54	2.06
1.18	3.12	0.88	2.36
1.43	3.23	1.14	2.58
1.61	3.43	1.23	2.83
1.83	3.58	1.73	3.05
2.06	3.80	1.92	3.48
2.51	3.98	2.47	3.55
3.44	4.86	2.70	3.74
3.71	4.85	4.49	4.51
4.45	5.07	4.67	4.77
4.97	5.19	7.15	5.15
6.26	5.61	7.36	5.25
7.15	6.35		

TABLE 3.12.2 The effect of total gas flow rate on the $O_2C_4H_8$ reaction over Modmor plus Mn

Flow Rate (dm^3 min^{-1})	$r_2 \times 10^{-7}$ (mol m^{-2} s^{-1})			Experimental Ea (kJ mol^{-1})
	473 K	523 K	573 K	
250	0.528	3.59	12.8	72
300	0.613	4.11	16.2	74
350	0.614	4.55	17.7	76
400	0.549	4.50	19.9	81
450	0.786	5.10	21.8	75

TABLE 3.12.3 The effect of temperature on the reaction rate constant for the O_2/C_4H_8 reaction over Modmor plus Mn

Temperature (K)	$k_2 \times 10^{-5}$
573	95.3
563	66.2
553	48.8
543	36.1
533	27.3
523	18.7
513	13.4
503	9.34
493	5.71
483	4.08
473	2.46

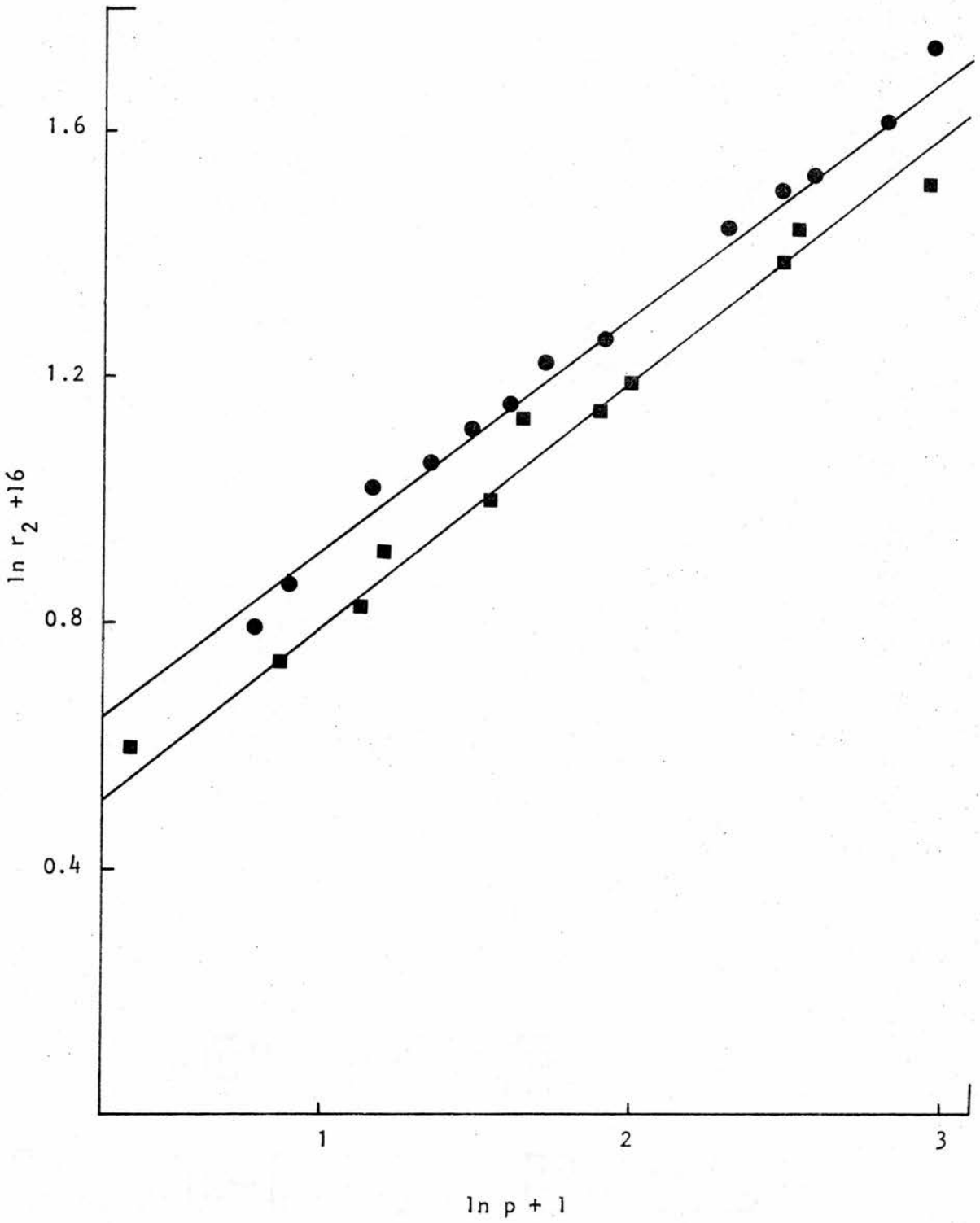

Figure 3.12.1 The effects of component partial pressures on the O_2/C_4H_8 reaction over Modmor + Mn; p_{O_2}, ■ r_2; $p_{C_4H_8}$, ● r_2.

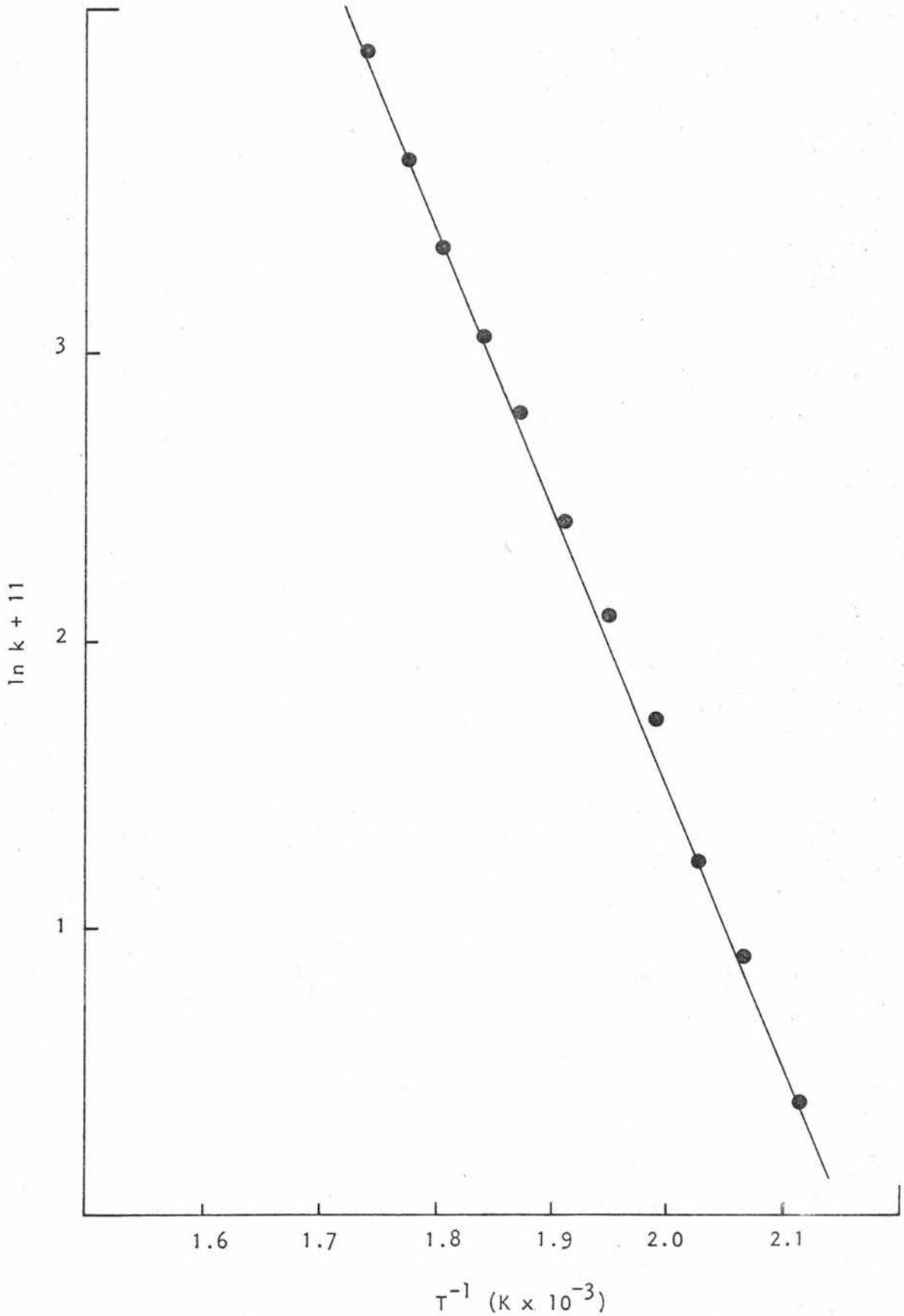

Figure 3.12.2 Arrhenius plot for the O_2/C_4H_8 reaction over Modmor + Mn; ● k_2.

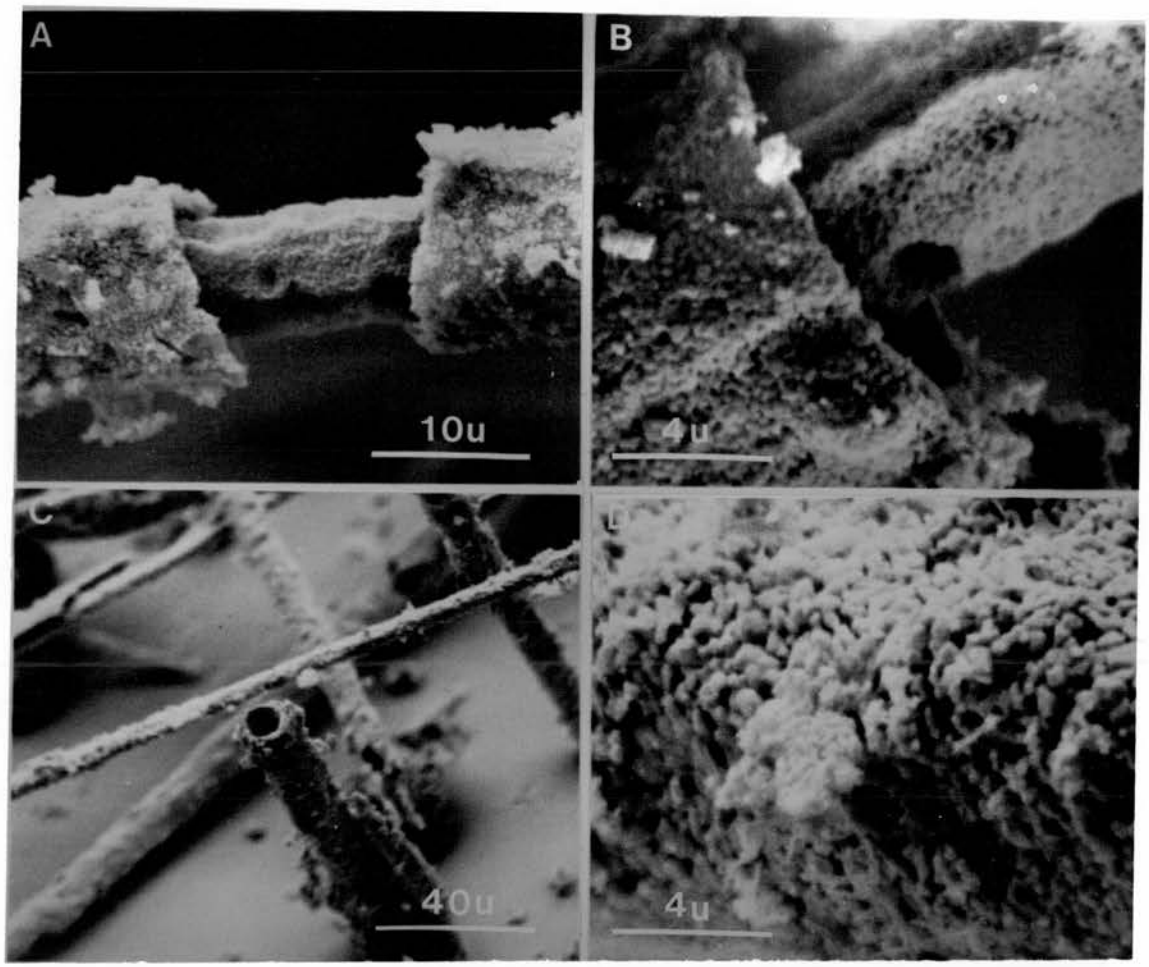

Figure 3.12.3 Scanning electron micrographs of Modmor fibres plus manganese after the catalytic O_2/C_4H_8 reaction.

CHAPTER IV

DISCUSSION

4.1 *Diffusion effects*

Concentration gradients which may occur at the catalyst surface because of diffusion effects may make the transport of reactants and products increasingly important as the temperature increases. The analysis of diffusion phenomena has resulted in the development of experimental methods to assess the influence of transport processes (164-167,172) and these have been used in the present study.

It has been shown that the total gas flow rate can affect the concentration gradients at the catalyst surface (167) and the flow rate experiments described in section 3.2 were conducted to establish conditions such that the catalytic reaction rate was independent of flow rate (space velocity) or transport effects. In the cases of the nitric oxide/ethane and the nitrous oxide/ethane reactions, the reaction rate appeared to be independent of the total gas flow rate in the range 300 to 400 $dm^3\ min^{-1}$ (NTP) at 573, 623 and 673 K. In all cases, the experimental reaction rate increased with flow rate from 200 to 300 $dm^3\ min^{-1}$ (NTP) and again from 400 to 450 $dm^3\ min^{-1}$ (NTP). This effect was most apparent at 673 K.

Dowden and Bridger (167) have shown that under the influence of gas-phase diffusion, variation of the flow rate would be expected to affect the activation energy of reaction. Neither the nitric oxide/ethane nor the nitrous oxide/ethane reactions exhibited significant deviation in the experimental activation energy from 573 to 673 K with flow rates 200 to 450 $dm^3\ min^{-1}$ (NTP), Table 3.2.1.

Molecular diffusion within pores in a solid catalyst could restrict reaction on the accessible internal surface (164). Such diffusion has been

shown to reduce the activation energy and increase the reaction rate (167). A large increase in manganese(III) oxide particle size from 0.037 to 0.149 mm had little effect on the reaction rates at 623 and 673 K, Table 3.2.2. The experimental activation energies derived from two point Arrhenius-type plots were similarly unaffected by particle size. Hence, in subsequent experiments the catalyst particle size was <0.037 mm and kinetic studies were conducted at a total gas flow rate of 350 $dm^3\ min^{-1}$ (NTP).

The principal conclusion from these studies was that external and internal diffusion effects were minimized under the chosen experimental conditions. Diffusion studies for subsequent systems were simplified and involved the measurement of reaction rates at two temperatures only with flow rates of 300, 350 and 400 $dm^3\ min^{-1}$ (NTP). In all cases, no major variation of catalytic reaction rate was observed with flow rate changes.

4.2 *Langmuir-Hinshelwood kinetics expressions*

The interpretation of kinetic data by application of the extended Langmuir-Hinshelwood theory to describe possible surface mechanisms has been documented (174-176). The rate expression (53) is usually given as:

$$r = \frac{k \prod_{i}^{i} C_i^{a_i}}{[1 + \sum_{i} (K_i C_i)^m]^n} \qquad [4.2.1]$$

where k is the rate constant and a_i the order of reaction with respect to the concentration (C) of component i. The denominator expresses the competition for sites by the components of the system; K_i is the Langmuir equilibrium adsorption constant for the i th component. The exponents m and n often have the value 1, although for dissociative chemisorption m = 0.5 and n = 2.

The validity of equation [4.2.1] has been questioned on the basis of the simplifying assumptions made in deriving the Langmuir adsorption model. For example, Weller (176) pointed out that interactions involving

adsorbed species may not necessarily be negligible as is expected from the Langmuir adsorption isotherm, while the assumption that the adsorption of one gas from a mixture always caused decreased adsorption of the second component was not always correct (177-179).

In spite of the known limitations of the idealized Langmuir-Hinshelwood model, it is still continuously applied to heterogeneous catalytic reactions. According to Boudart (180) for example, an assumed mechanism with or without substantiation may still lead to some understanding and control of catalyst behaviour.

4.3 *The nitric oxide/ethane reaction over manganese(III) oxide*

Several mechanistic schemes were evaluated by computer tests of the rate order results in kinetic expressions related mainly to the Langmuir-Hinshelwood model (26,174). The significance of such statistical criteria in the evaluation of the step-by-step nature of the catalytic process has been frequently analysed (181-183) and recently reviewed (184). The approach was adopted here to obtain a broad guide to the interpretation of kinetic results.

The approach assumes that the driving force for reaction is the concentration of species in the gas phase:

$$r \alpha k C_A^a \; C_B^b \; C_C^c \ldots \qquad [4.3.1]$$

although it would be more logical to use the surface concentrations:

$$r \alpha k^1 \Theta_A^a \; \Theta_B^b \; \Theta_C^c \ldots \qquad [4.3.2]$$

where Θ_A represents the fraction of surface covered by species A. The various Θ values were usually determined in terms of the appropriate partial pressures involved in the Langmuir, Temkin or Freundlich adsorption isotherms (185,186). In most cases, these involved the use of a Langmuir-Hinshelwood or Hougen-Watson rate expression (25,26).

Usually, four types of reactions were considered:

$$A \rightleftharpoons R \qquad [4.3.3]$$

$$A \rightleftharpoons R + S \qquad [4.3.4]$$

$$A + B \rightleftharpoons R \qquad [4.3.5]$$

$$A + B \rightleftharpoons R + S \qquad [4.3.6]$$

and various rate-controlling mechanisms were assumed. Yang and Hougen (174) considered several surface mechanisms and developed tables from which rate expressions were determined by three terms:

$$r = \frac{\text{(kinetic term) x (driving force)}}{\text{(adsorption term)}^n} .$$

Each expression is usually tested by plotting the appropriate functions of reaction rate and partial pressure (26,51,53,17).

Only one kinetic expression clearly accomodated the rate order data in each case:

$$r = \frac{kaP_{NO} + bP_{C_2H_6}}{(1 + aP_{NO} + bP_{C_2H_6})^2} \times (P_{NO}\, P_{C_2H_6}) \qquad [4.3.7]$$

where a and b are adsorption coefficients. As shown in Figure 4.3.1, plots of P versus $P/r^{0.5}$ were linear for nitric oxide, ethane and nitrous oxide rate order results. The form of equation [*4.3.7*] is consistent with that for an irreversible bimolecular reaction between reactive species adsorbed on the same type of site (187). The reaction rate is proportional to the probability that the reactants are adsorbed on neighbouring sites, and thus proportional to the product of the fraction of surface covered by each reactant, Θ_{NO} and $\Theta_{C_2H_6}$. Thus:

$$r = k^1\, \Theta_{NO}\, \Theta_{C_2H_6} \qquad [4.3.8]$$

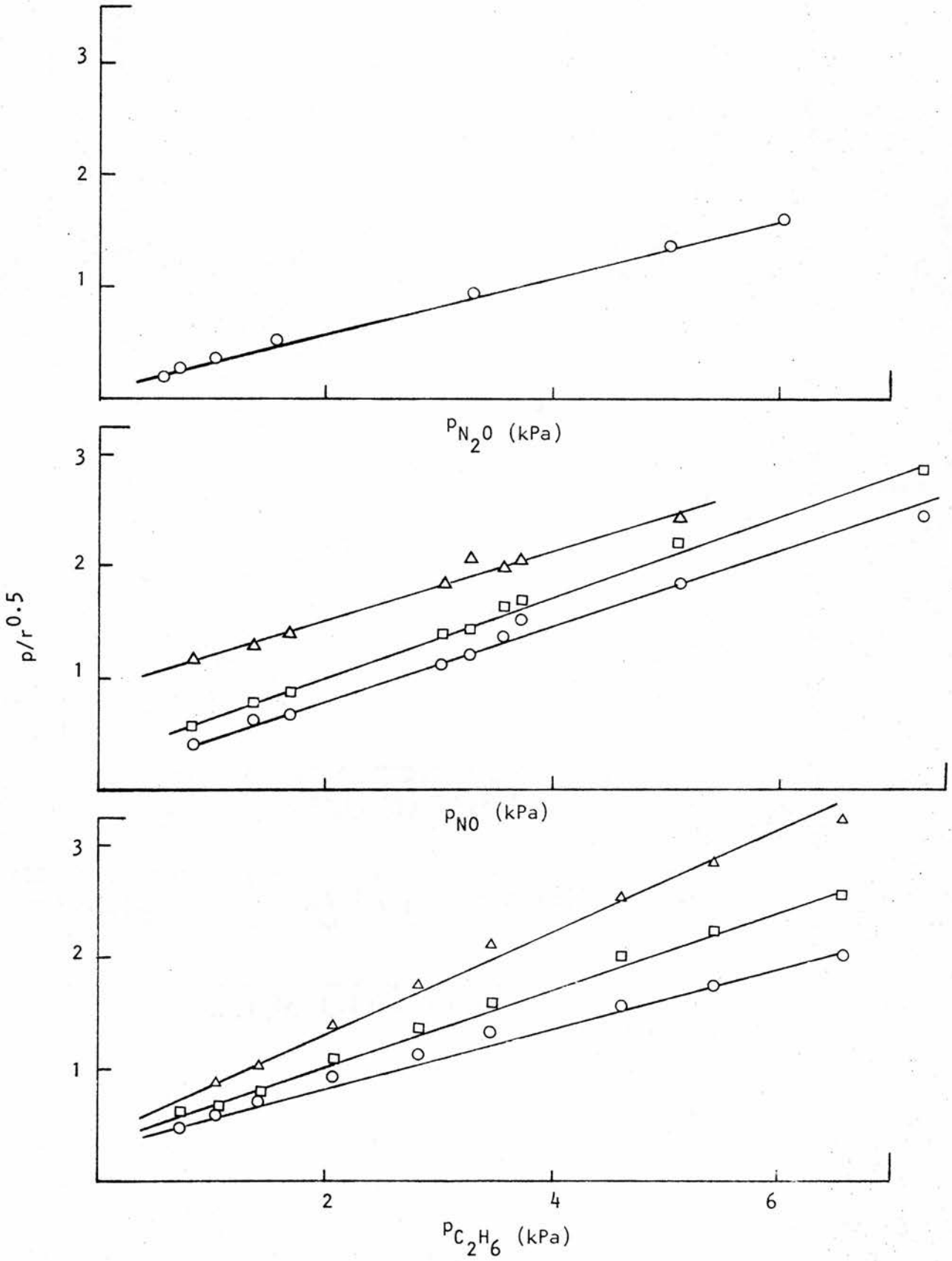

Figure 4.3.1 Reduced plots of the Langmuir-Hinshelwood expression [4.3.7] for the NO/C_2H_6 reaction at 623 K over Mn_2O_3, □ r_1, ○ r_2, △ r_3.

where $$\Theta_{NO} = \frac{K_{NO} P_{NO}}{(1 + K_{NO} P_{NO} + K_{C_2H_6} P_{C_2H_6})} \qquad [4.3.9]$$

and $$\Theta_{C_2H_6} = \frac{K_{C_2H_6} P_{C_2H_6}}{(1 + K_{NO} P_{NO} + K_{C_2H_6} P_{C_2H_6})} . \qquad [4.3.10]$$

The additional $(P_{NO} P_{C_2H_6})$ multiplier term in equation [4.3.7] indicates that at the steady state, the catalytic reaction includes additional interactions involving nitric oxide and ethane molecules either from the gas phase or as weakly chemisorbed species.

The limitations inherent in the method of deriving mechanistic schemes from the correlation of statistical relationships and the Langmuir-Hinshelwood surface reaction model have been documented (176, 180-182) Equation [4.3.7] was thus regarded as a general guide to the interpretation of the kinetic results. Various schemes were tested in a systematic fashion and rejected for good reasons. The best available scheme consistent with the evidence was postulated:

$$C_2H_{6(g)} \rightleftharpoons C_2H_{6(ads)} \qquad [4.3.11]$$

$$NO_{(g)} \rightleftharpoons NO_{(ads)} \qquad [4.3.12]$$

$$C_2H_{6(ads)} + NO_{(ads)} \longrightarrow C_2H_{5(ads)} + HNO_{(ads)} \qquad [4.3.13]$$

$$2HNO_{(ads)} \longrightarrow N_2O_{(ads)} + H_2O_{(ads)} . \qquad [4.3.14]$$

The formation of nitrous oxide and water from adsorbed HNO species as in equation [4.3.14] has previously been described in observations of the reduction of nitric oxide by both hydrazine (188) and ammonia (189).

The chemisorption of ethane on iron(III) and nickel(II) oxides has been shown to involve C-H bond rupture (89) while studies of ethane oxidation on nickel(II) oxide indicated that the hydrocarbon was adsorbed

prior to any surface reaction with pre-adsorbed oxygen (90). Both of the preceding studies invoked the formation of a $C_2H_{5(ads)}$ species.

In the nitric oxide/methane reaction (42), C-H bond rupture was described as the rate-limiting step. The formation of nitrous oxide occurred through the reaction of two nitric oxide molecules in the same manner as that proposed for the nitric oxide/carbon monoxide reaction (35). A similar mechanism was suggested for the oxidation of manganese(II) oxide to manganese(III) oxide (194) by nitric oxide:

$$2NO_{(ads)} + [\ ] + Mn^{2+} \longrightarrow N_2O_{(ads)} + [O^-] + Mn^{3+}. \quad [4.3.15]$$

The nitrous oxide produced could subsequently react with adsorbed ethane to eventually produce nitrogen, carbon dioxide and water.

In a current review of nitric oxide surface reactions (31), evidence obtained from IR, EPR and oxygen-exchange experiments was cited in favour of the proposal that adsorption of nitric oxide on transition metal oxides occurred through partial co-ordination to a surface oxygen ion. An intermediate surface nitrate or nitro complex was invoked and a similar species was identified from infrared spectra in the present study, section 3.3.4.

In earlier related work on manganese(II) oxide, the rate order of the water-gas shift reaction was zero with respect to water vapour (7). This was explained by either a rapid saturation of adsorption sites specific to water or a slow water desorption step. The dehydrogenation of 2-propanol on a similar catalyst was also essentially zero order in water vapour (1) although dehydration was inhibited.

According to the kinetic description, there would seem to be further reactions involving nitric oxide and ethane, some of which may be quite complex but could be represented by:

$$C_2H_6 + [O] \longrightarrow C_2H_{5(ads)} + [OH] \quad [4.3.16]$$

$$2C_2H_{5(ads)} + 12NO + [O] \longrightarrow 4CO_2 + 5H_2O + 6N_2 \qquad [4.3.17]$$

and

$$2C_2H_{5(ads)} + 13N_2O \longrightarrow 4CO_2 + 5H_2O + 13N_2 \cdot \qquad [4.3.18]$$

Studies of the nitric oxide/carbon monoxide reaction on platinum (191,192) indicated that the dissociation of nitric oxide may be rate-limiting:

$$NO_{(ads)} \longrightarrow N_{(ads)} + O_{(ads)} \qquad] \qquad [4.3.19]$$

followed by nitrogen formation:

$$N_{(ads)} + N_{(ads)} \longrightarrow N_{2(ads)} \cdot \qquad [4.3.20]$$

The adsorbed oxygen ion from [*4.3.19*] or [*4.3.15*] could act as a hydrocarbon oxidation source. The reaction of nitric oxide with ethane is quite complex and does not appear to occur by a simple two-step process involving first the formation of nitrous oxide followed by ethane oxidation. This is evidenced by the rates of product formation, Table 3.4.2, where the rate of carbon dioxide production was approximately twenty to thirty times that for nitrogen compared with three to four times in the nitrous oxide/ethane reaction.

In the present study, the rate of formation of nitrous oxide appeared to be constant from 573 to 673 K. Nitrous oxide has been observed as a gaseous intermediate (29) in the nitric oxide/carbon monoxide reaction on various supported oxides and mixed oxides, but not when reaction took place over supported manganese(III) oxide. In most cases, nitrous oxide was observed to reach a maximum concentration at various temperatures from a low of 453 K for $CuCr_2O_4$ to a high of 623 K for Co_3O_4.

The values of the apparent activation energies, Table 3.3.2, were similar to those obtained for the water-gas shift reaction on manganese (II) oxide (7) which was believed to involve an active surface species, perhaps $Mn^{3+}— O^-$. A two-step Arrhenius plot was also observed from 673

to 623 K and 613 to 573 K with activation energies 67 and 46 kJ mol^{-1}, respectively. The effect might be related to the presence of two forms of chemisorbed oxygen (58) or to a change in surface oxygen mobility at the Curie transition temperature (7).

Studies of the reaction of nitric oxide with propane (43) and propylene (45) produced apparent activation energies of 37.5 and 25 kJ mol^{-1}. In both cases, the catalytic rate of reaction was proportional to the partial pressure of nitric oxide and hydrocarbon both to the one-half order.

The mechanism of the decomposition of nitrous oxide on manganese oxides (58) has been explained by a redox scheme where oxidation was enhanced by conditions which preserved the 3+ oxidation state of the metal atom. And, although the proposed chemisorbed oxygen species were not identified, it was suggested that a weak form such as O_2^- or O_2^{2-}, could be sustained during catalysis. Oxygen desorption studies from manganese(IV) oxide have also indicated the presence of two surface states (193) for which the activation energies for absorption were 67 and 126 kJ mol^{-1}.

X-ray powder diffraction studies indicated that the original catalyst, alpha manganese(III) oxide, was altered by the reaction, but it was difficult to distinguish between gamma manganese(III) oxide and manganese (II,III) oxide as shown in Table 3.3.3. X-ray photoelectron studies could not readily separate manganese(II) from manganese(III) oxide either since Mn2p3/2 for the oxides is 641.7 and 641.8 eV, respectively (194). However, this evidence combined with other results gives a good indication that the surface manganese was in the 3+ oxidation state and that the catalyst had undergone a phase change to gamma manganese(III) oxide. The infrared spectrum after catalysis, with bands at 615, 490, 425 and 350 cm^{-1}, Figure 3.3.4, along with the X-ray diffraction data do not indicate the extent of this phase change, however.

4.4 *The nitrous oxide/ethane reaction over manganese(III) oxide*

A Langmuir-Hinshelwood treatment of the kinetic data was again

adopted within the context of the discussions by Weller (176,182) and Boudart (180,181). Computer analysis of the nitrous oxide and ethane rate order results yielded only one model with good correlation for all the data. The expression was the same as that found for the nitric oxide/ethane reaction:

$$r = \frac{k\ a\ P_{N_2O}\ b\ P_{C_2H_6}}{(1+a\ P_{N_2O}+b\ P_{C_2H_6})^2} \times (P_{N_2O}\ P_{C_2H_6}) \cdot \qquad [4.4.1]$$

Plots of $p/r^{0.5}$ versus p were linear, Figure 4.4.1.

The kinetic expression may be interpreted to represent an irreversibl bimolecular reaction between reactive species adsorbed on the same type of surface site (187). The rate of this reaction would be proportional to the fraction of surface covered by each reactant. The addition of the $(P_{N_2O}\ P_{C_2H_6})$ term complicates the model and suggests that additional interactions involve nitrous oxide and ethane molecules.

On a test/reject basis, a surface mechanism consistent with equation [4.4.1] may be formulated:

$$N_2O_{(g)} \rightleftharpoons N_2O_{(ads)} \qquad [4.4.2]$$

$$C_2H_{6(g)} \rightleftharpoons C_2H_{6(ads)} \qquad [4.4.3]$$

$$C_2H_{6(ads)} + N_2O_{(ads)} + [O] \longrightarrow C_2H_{5(ads)} + [OOH] + N_2 \qquad [4.4.4]$$

$$C_2H_6 + [OOH] \longrightarrow C_2H_{5(ads)} + [O] + H_2O \qquad [4.4.5]$$

$$2C_2H_{5(ads)} + 13N_2O \longrightarrow 4CO_2 + 5H_2O + 13N_2 \qquad [4.4.6]$$

with an overall stoichiometry:

$$2C_2H_6 + 14N_2O \longrightarrow 4CO_2 + 6H_2O + 14N_2 \qquad [4.4.7]$$

Examination of the rates of nitrogen and carbon dioxide formation, Table 3.4.2, indicates that nitrogen is formed at a rate (mol m^{-2} s^{-1}) which is 3 to 4 times that of carbon dioxide in accordence with the overall equation

for the reaction, [4.4.7].

Previously, a mechanism for the oxidation of hydrocarbons has been postulated to occur through the initial interaction of chemisorbed hydrocarbon species with either gaseous or chemisorbed oxygen, followed by a complex sequence of steps which invokes surface radical reactions (74). The formation of intermediate C_2H_5 species in ethane oxidation reactions has been described (85,89,90,101). The rate-limiting step may be the adsorbtion of ethane as a C_2H_5 radical or the interaction of an adsorbed oxygen species with gas phase or adsorbed ethane through attack at the C-H bond (89,101). In the homogeneous oxidation of ethane by oxygen, the formation of C_2H_5 and HO_2 radicals was postulated as the initial step (86,87); indeed, peroxide species are often formed in hydrocarbon oxidation reactions.

It seems likely then that the rate-determining step in the nitrous oxide/ethane reaction over manganese(II) oxide involves the formation of an adsorbed C_2H_5 species, which may occur through the interaction of adsorbed ethane with adsorbed nitrous oxide, equation [4.4.4], or through the action of a surface peroxide radical with gas phase or weakly adsorbed ethane, equation [4.4.5].

The apparent activation energies are in reasonable agreement with those determined for the nitrous oxide/carbon monoxide reaction, 493 to 573 K (11), the decomposition of isopropyl alcohol, 483 to 638 K (1), and the dehydration of formic acid, 523 to 573 K (8), all over a manganese(II) oxide catalyst. These, together with the water-gas shift reaction (7), all appear to involve both Mn^{2+} and Mn^{3+} reactive surface species in the c catalytic cycle.

The results of examination of the catalyst after reaction, section 3.4.4, indicate that the oxide has undergone a phase change to gamma manganese (III) oxide. This particular phase has been described as a defect structure which closely resembles manganese (II,III) oxide (159).

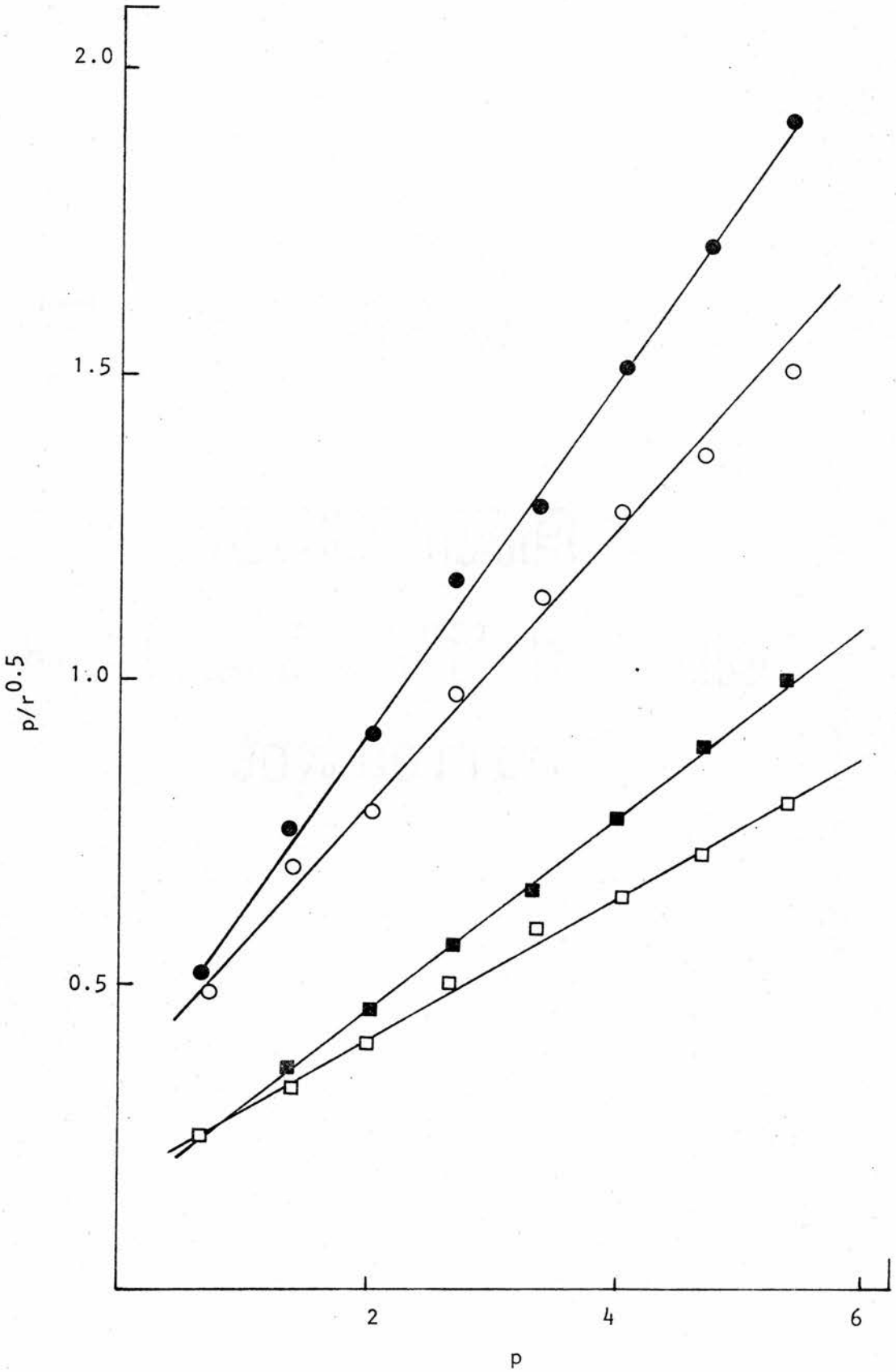

Figure 4.4.1 Reduced plots corresponding to equation [4.4.1] for the N_2O/C_2H_6 reaction at 623 K over Mn_2O_3; □ r_1, ○ r_2 for p_{N_2O}, ■ r_1, ● r_2 for $p_{C_2H_6}$.

4.5 *The oxygen/ethane reaction over manganese(III) oxide*

Analysis of the oxygen and ethane rate order results, section 3.5.1, yielded only one Langmuir-Hinshelwood kinetic expression which could accommodate the data, Figure 4.5.1. The expression was the same as that for the nitric oxide / and nitrous oxide/ethane reactions:

$$r = \frac{k\ a\ P_{O_2}\ \ b\ P_{C_2H_6}}{(1 + a\ P_{O_2}\ \ b\ P_{C_2H_6})^2} \times (P_{O_2}\ P_{C_2H_6}) \cdot \qquad [4.5.1]$$

Following the preceding sections, the mechanism of the catalytic oxygen/ethane reaction may be considered to involve an irreversible bimolecular reaction, where the rate is proportional to the fraction of surface covered by each reactant, followed by more complex reactions involving gaseous or weakly adsorbed oxygen and ethane molecules. That is:

$$r = k^1\ \Theta_{O_2}\ \Theta_{C_2H_6} \times (P_{O_2}\ P_{C_2H_6}) \cdot \qquad [4.5.2]$$

A plausible surface mechanism consistent with the results was postulated:

$$O_{2(g)} \rightleftharpoons O_{2(ads)} \qquad [4.5.3]$$

$$C_2H_{6(g)} \rightleftharpoons C_2H_{6(ads)} \qquad [4.5.4]$$

$$C_2H_{6(ads)} + O_{2(ads)} \longrightarrow C_2H_{5(ads)} + [OOH]_{ads} \qquad [4.5.5]$$

$$C_2H_6 + [OOH]_{ads} \longrightarrow C_2H_{5(ads)} + [O]_{ads} + H_2O \qquad [4.5.6]$$

$$2C_2H_{5(ads)} + [O]_{ads} + 6O_2 \longrightarrow 4CO_2 + 5H_2O \qquad [4.5.7]$$

with an overall stoichiometry:

$$2C_2H_6 + 7O_2 \longrightarrow 4CO_2 + 6H_2O \cdot \qquad [4.5.8]$$

The rate of carbon dioxide formation in the oxygen/ethane reaction

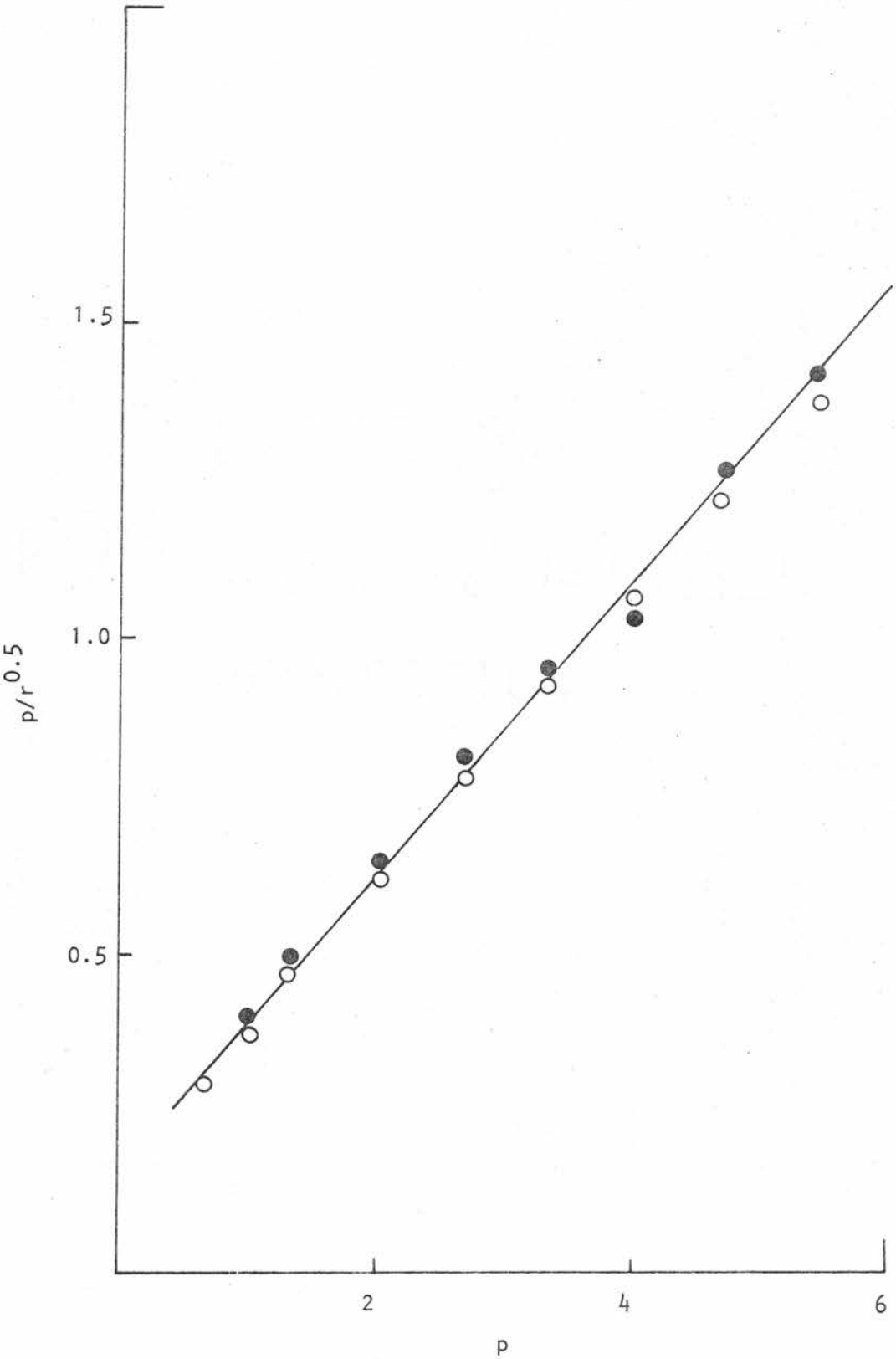

Figure 4.5.1 Reduced plots of the Langmuir-Hinshelwood expression [4.5.1] for the O_2/C_2H_6 reaction at 573 K over Mn_2O_3; ● r_2 for $p_{C_2H_6}$, ○ r_2 for p_{O_2}.

was the same as that for the nitrous oxide/ethane reaction, Table 3.4.2, over the same catalyst in the overlapping temperature region, 573 to 593 K. This may imply that the rate-controlling step is the same in both reactions. As mentioned in section 4.4, the formation of an adsorbed C_2H_5 species may be involved.

Although the activation energy, 130 kJ mol^{-1}, is in agreement with that for other reactions on manganese oxides (1,8,11), it is higher than that found for ethane oxidation by oxygen over palladium (93), 84 kJ mol^{-1} from 671 to 719 K, or nickel(II) oxide (101), 71 kJ mol^{-1} from 543 to 673 K. The complete oxidation of propane over hydrated manganese(IV) oxide was reported to have an activation energy of 90 kJ mol^{-1} and the rate order was zero with respect to both carbon dioxide and water vapour concentrations (97). However, the same reaction over other catalysts (99,100) was shown to be inhibited reversibly by water vapour, $r \propto P_{H_2O}^{-0.35}$. The rates of the water-gas shift reaction (7) and the dehydrogenation of 2-propanol (1) over manganese(II) oxide catalysts were also zero order in water vapour. This effect was thought to be due to the slow desorption of water from the surface (7,93).

The catalyst after reaction was identical to that from the nitrous oxide/ethane reaction, section 3.5.4. A phase change to gamma manganese(III) oxide may have taken place.

4.6 *The nitric oxide/1-butene reaction over manganese(III) oxide*

Various Langmuir-Hinshelwood-type kinetic expressions - (26, 51,53,178) were tested, and the equation which gave the best statistical correlation coefficient for all of the rate order data was adopted.

As shown by the linear plots of $P_{NO}^{0.5}$ against $(P_{NO}^{1.5}/r)^{0.5}$, Figure 4.6.1, only one expression accomodated the nitric oxide rate order results:

$$r = \frac{k\ a\ P_{NO}^{0.5}}{(1 + a\ P_{NO}^{0.5})^2} \times P_{NO} \quad . \qquad [4.6.1]$$

The square root relationship on the partial pressure of nitric oxide implies that this species is adsorbed and reacts on two surface sites. The zero order rate dependency on 1-butene concentration suggests that adsorption and reaction of 1-butene is very rapid compared to the reactions of nitric oxide.

A surface mechanism consistent with the experimental results was formulated:

$$C_4H_{8(g)} \rightleftharpoons C_4H_{8(ads)} \qquad [4.6.2]$$

$$NO + S + C_4H_{8(ads)} \longrightarrow C_4H_{7(ads)} + HNO_{(ads)} \qquad [4.6.3]$$

$$2HNO_{(ads)} \longrightarrow N_2O_{(ads)} + H_2O_{(ads)} \qquad [4.6.4]$$

where S is a surface site. These reactions account for the formation of nitrous oxide as in section 4.3. Further reactions involve nitric oxide as indicated by the P_{NO} term in equation [*4.6.1*] and these might be represented by:

$$2C_4H_{7(ads)} + 22NO + [O] \longrightarrow 8CO_2 + 7H_2O + 11N_2 \quad . \qquad [4.6.5]$$

As was the case in the nitric oxide/ethane reaction, the rate of nitrogen production was less than that of carbon dioxide, Table 3.6.2. This suggests that a disproportionation reaction may occur between two nitric oxide molecules to give nitrous oxide and an oxygen ion (35,188) as suggested by Hu, Van-Lirsburg and Hightower in the nitric oxide/methane reaction over platinum (42).

The apparent activation energies, Table 3.6.2, were similar to those found in the nitric oxide/ethane reaction over the same catalyst, section 3.3.2, and to the nitric oxide/propane (43,44) and nitric oxide/

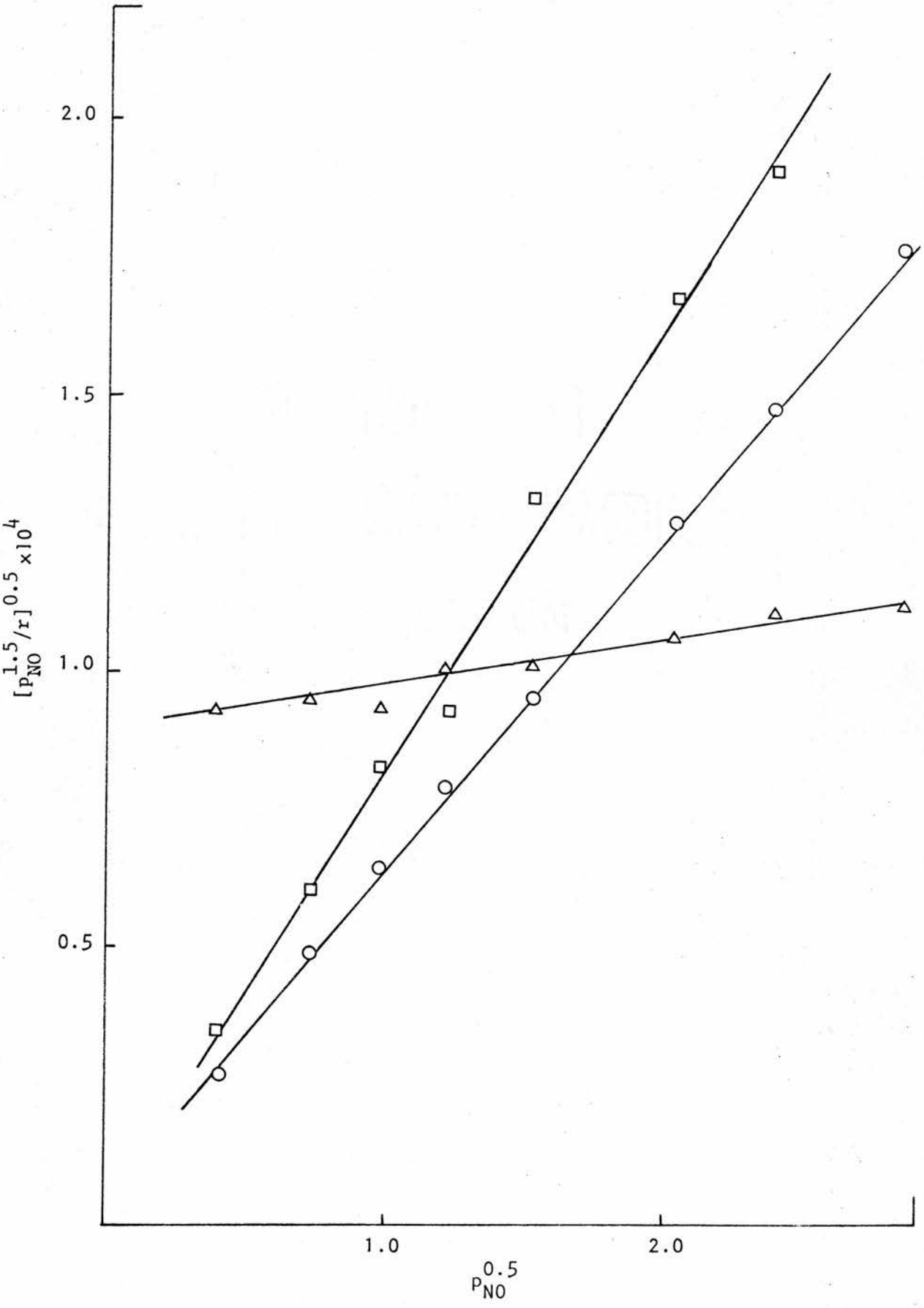

Figure 4.6.1 Reduced plots corresponding to equation [4.6.1] for the NO/C_4H_8 reaction at 673 K over Mn_2O_3, □ r_1, ○ r_2, △ r_3.

propylene (45) reactions over various catalysts. In the propane reaction (44) over bismuth phosphomolybdate, the activation energy was 92 kJ mol^{-1} for nitrogen formation and 55 kJ mol^{-1} for nitrous oxide while the corresponding results in the present work were 69 and 30 kJ mol^{-1}.

Infrared evidence again showed the presence of a nitrate species with absorption bands at 1630, 1390 and 845 cm^{-1}. The catalyst appeared to have undergone a phase change from alpha to gamma manganese(III) oxide. The extent of this change is not known, although the fact that it occurs indicates that surface oxygen ions are actively involved in reaction.

Nitric oxide has been shown to exist as $(NO)_2$ or as a nitro species on different surfaces (47-50) and this species may be involved in the disproportionation reaction. The nitrous oxide thus produced may also be involved in the oxidation of 1-butene, although in the nitric oxide/methane reaction in a static system (42), methane oxidation by nitrous oxide only occurred when all of the nitric oxide was consumed. It seems more likely that the oxygen ion produced by disproportionation would be involved in 1-butene oxidation.

4.7 *The nitrous oxide/1-butene reaction over manganese(III) oxide*

Computer analysis of the nitrous oxide and 1-butene rate order results as described in section 4.3 yielded only one expression which fits all of the data:

$$r = \frac{k\ a\ P_{N_2O}^{0.5}\ \ b\ P_{C_4H_8}^{0.5}}{(1 + a\ P_{N_2O}^{0.5} + b\ P_{C_4H_8}^{0.5})^2} \times (P_{N_2O}\ P_{C_4H_8}) . \qquad [4.7.1]$$

As shown in Figure 4.7.1, plots of $P^{0.5}$ versus $(P^{1.5}/r)^{0.5}$ were linear.

This relationship may be regarded as a Langmuir-Hinshelwood expression and was used as an initial guide to the interpretation of the kinetic results.

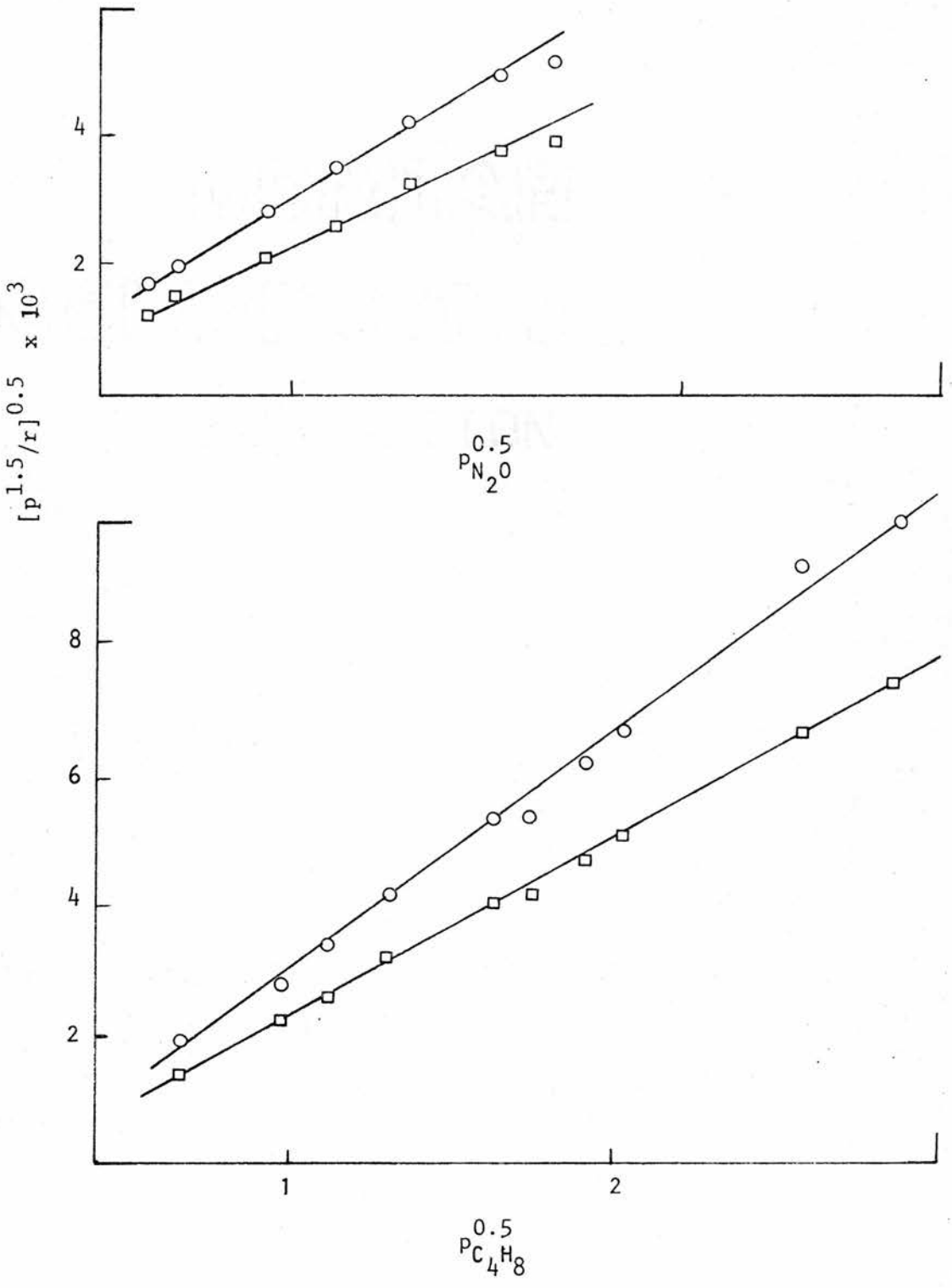

Figure 4.7.1 Reduced plots of the Langmuir-Hinshelwood expression [4.7.1] for the N_2O/C_4H_8 reaction at 623 K over Mn_2O_3; □ r_1, ○ r_2.

The form of this equation suggests that an irreversible bimolecular reaction occurs between adsorbed reactants where each species is adsorbed on two surface sites (187). Further steps involving the interaction of nitrous oxide and 1-butene, as indicated by the P_{N_2O} and $P_{C_4H_8}$ terms in the numerator of equation [*4.7.1*], produce a more complex overall surface process. Various mechanisms were examined on a test/reject basis and a surface mechanism consistent with the experimental results was formulated:

$$C_4H_{8(g)} + 2S \rightleftharpoons C_4H_{8(ads)} \qquad [4.7.2]$$

$$N_2O + [O] + C_4H_{8(ads)} \longrightarrow C_4H_{7(ads)} + [OOH] + N_2 \qquad [4.7.3]$$

$$C_4H_8 + S + [OOH] \longrightarrow C_4H_{7(ads)} + [O] + H_2O \qquad [4.7.4]$$

with further reactions represented by:

$$2C_4H_{7(ads)} + 23N_2O \longrightarrow 8CO_2 + 7H_2O + 23N_2 + 4\,S \qquad [4.7.5]$$

The activation energy determined for the nitrous oxide/1-butene reaction over manganese(III) oxide, 117-126 kJ mol^{-1}, was very close to that found for the nitrous oxide/ethane reaction on a similar catalyst, section 3.4.2. The initial step in the catalytic oxidation of 1-butene over bismuth molybdate also involved C-H bond rupture (111, 112) as in equation [*4.7.3*]. The decomposition of nitrous oxide over similar manganese oxide catalysts produced activation energies of 118 (58) and 146 kJ mol^{-1} (60).

Cimino and Indovina (58) observed a relationship between catalyst activity towards nitrous oxide decomposition and the strength of the oxygen-surface bond. The same investigators described the formation of peroxides from nitrous oxide as in [*4.7.3*]. In the complete oxidation of propylene, it was observed (110) that cleavage of the metal-oxygen surface bond may be involved in the rate-limiting step. Equation [*4.7.5*] necessarily involves a complex series of steps which may include surface radical reactions (74).

4.8 *The oxygen/1-butene reaction over manganese(III) oxide*

A number of kinetic expressions were examined using the rate order results for oxygen and 1-butene, section 3.8.1. The best correlations were obtained with the equation:

$$r = \frac{k\ a\ P_{O_2}^{0.5}\ \ b\ P_{C_4H_8}^{0.5}}{(1 + a\ P_{O_2}^{0.5} + b\ P_{C_4H_8}^{0.5})^2} \times (P_{O_2}\ P_{C_4H_8}) \qquad [4.8.1]$$

which is the same expression as that found for the nitrous oxide/1-butene reaction over manganese(III) oxide, section 4.7. The reduced plots are shown in Figure 4.8.1.

Once again, the equation suggests that an irreversible bimolecular reaction occurs between adsorbed species (187), and each species is adsorbed on two surface sites as indicated by the one-half order exponents. Additional reactions involve both oxygen and 1-butene as indicated by the $(P_{O_2}\ P_{C_4H_8})$ term.

Considering the discussions of Weller (176,182) and Boudart (180 181) on the application of kinetic modeling studies and with equation [4.8.1] as a general guide, a plausible surface mechanism was proposed:

$$C_4H_{8(g)} + 2S \rightleftharpoons C_4H_{8(ads)} \qquad [4.8.2]$$

$$O_2 + [\ ] + C_4H_{8(ads)} \longrightarrow C_4H_{7(ads)} + [OOH] \qquad [4.8.3]$$

$$C_4H_8 + S + [OOH] \longrightarrow C_4H_{7(ads)} + [O] + H_2O\ . \qquad [4.8.4]$$

Additional reactions may be represented by:

$$2C_4H_{7(ads)} + 11O_2 + [O] \longrightarrow 8CO_2 + 7H_2O + [\ ] + 4S\ . \qquad [4.8.5]$$

The square root relationships in equation [4.8.1] with respect to 1-butene and oxygen are rationalized in steps [4.8.2] and [4.8.3] respectively.

The change in apparent activation energy from 88 kJ mol^{-1}, 433 to 503 K, to 183 kJ mol^{-1}, 503 to 523 K, occurs at the temperature

at which the conversion of oxygen exceeds 15%. As the temperature is increased above 503 K, the conversion of oxygen increases rapidly compared to 1-butene as expected from the overall stoichiometry:

$$2C_4H_8 + 12O_2 \longrightarrow 8CO_2 + 8H_2O \cdot \qquad [4.8.6]$$

The lower value for activation energy corresponds closely to that found in the complete oxidation of ethane on palladium (93) or nickel(II) oxide and propane oxidation on manganese(IV) oxide (97). Ethylene or benzene oxidation over supported manganese(III) oxide (103) were reported with activation energies of 57 kJ mol^{-1} while ethylene oxidation over copper(II) oxide gave values from 84 to 113 kJ mol^{-1} (104).

As described previously, the oxygen/ethane and nitrous oxide/ethane reactions occurred in the same temperature range with identical rate constants. The oxygen/1-butene reaction kinetics were measured from 433 to 523 K while the nitrous oxide/1-butene rates were measured from 573 to 673 K. The apparent activation energy for the latter reaction (126 kJ mol^{-1}) was closer to those found in the ethane oxidation reactions over the same manganese(III) oxide catalyst. In these reactions, C-H bond rupture may have been involved in the rate determining step as in equations [*4.7.3*] or [*4.7.4*]. The kinetic parameters for the oxygen/1-butene reaction correspond more closely to those from the reactions of nitric oxide with ethane, section 3.3.2, or with 1-butene, section 3.6.2.

In both the nitrous oxide/ and oxygen/1-butene catalytic reactions, the rate of reaction with respect to the oxidizing gas increased with partial pressure > 2.6 kPa. This may indicate that a steady state condition has been achieved with respect to the adsorption of 1-butene. The rate-limiting step in this case would be the adsorption and reaction of the oxidizing gas as in equations [*4.7.3*] or [*4.8.3*].

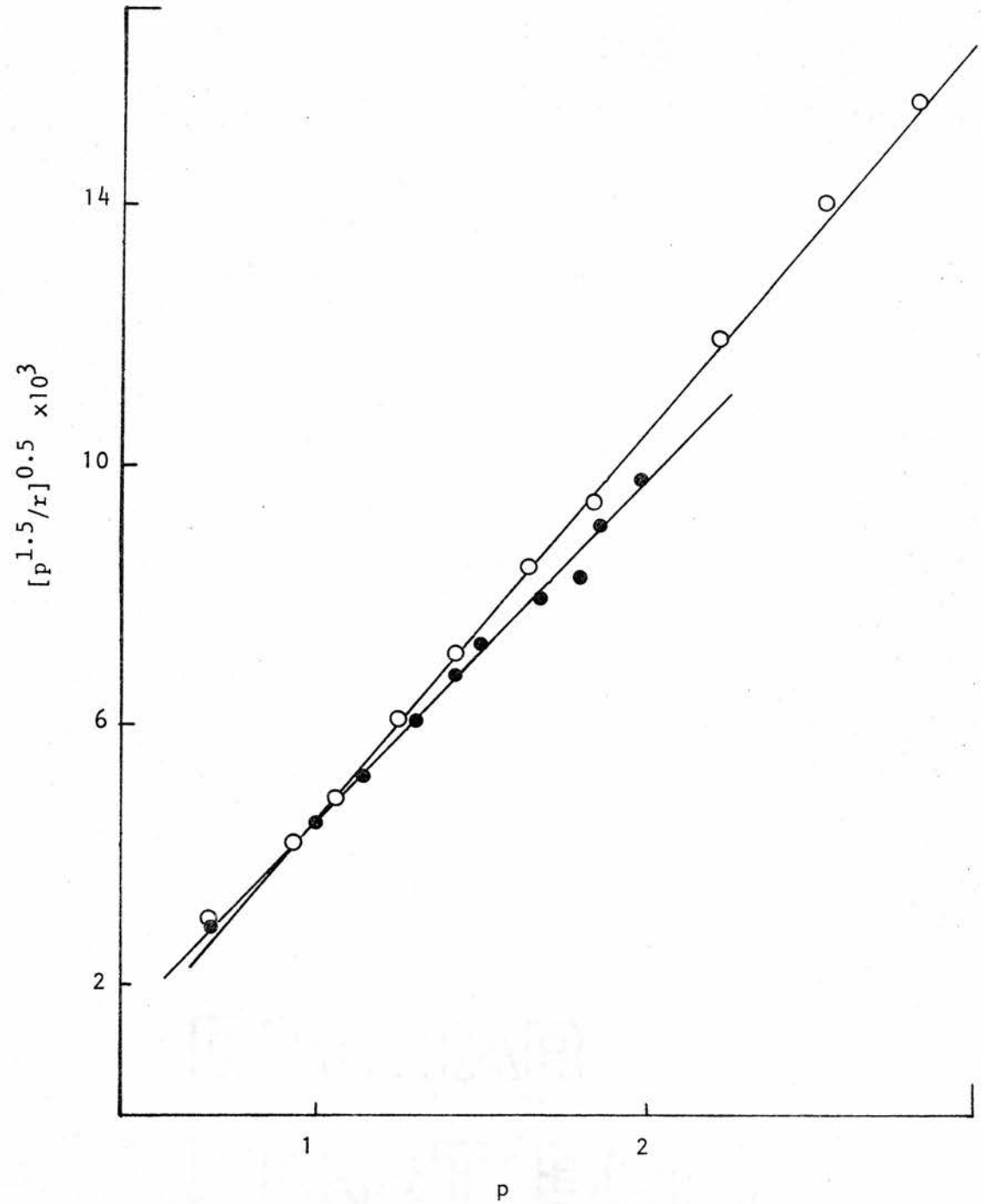

Figure 4.8.1 Reduced plots corresponding to equation [4.8.1] for the O_2/C_4H_8 reaction at 473 K over Mn_2O_3; ○ r_2 for $p_{C_4H_8}$, ● r_2 for p_{O_2}.

4.9 Correlation of catalytic activity

4.9.1 Catalyst activity series

The catalytic activity series for the nitrous oxide/1-butene reaction was determined by the empirical approach discussed in section 3.9. The overall sequence of reactivity in decreasing order was:

$$CuO > Fe_2O_3 > NiO > Mn_2O_3 > Cr_2O_3 > TiO_2 > Sc_2O_3 >$$

$$SnO > ZnO > V_2O_5 > Al_2O_3.$$

A close examination of Table 3.9.1 reveals that the difference in r_1 (used to determine activity) between titanium(IV) oxide and aluminum(III) oxide is of the same order of magnitude as that between each of the first five oxides in the series. Together with the low values of r_1 and the fact that r_2 could not be measured for these oxides, this suggests that the position of the last six members of the series are not as unequivocally determined as the first five.

Data obtained for carbon fibre supported copper, nickel or manganese indicated that these catalysts followed the same relative activity series in terms of reaction rates, Table 3.9.1, and experimental activation energies, Table 3.10.1.

The activity series is similar to those generally observed for catalytic oxidation reactions (195,196), with the exception of the position of iron(III) oxide. It resembles those found for the nitric oxide/carbon dioxide reaction (23), the nitrous oxide/carbon dioxide reaction (197), and the decomposition of nitric (17) and nitrous (55) oxides.

Possible relationships between the rate of the nitrous oxide/1-butene reaction at 673 K and various properties of the oxides were examined.

Heats of oxygen desorption, q, have been related to catalytic activity for a number of reactions over transition metal oxides (198-199) Good correlation was found between q and the activation energy of oxygen isotopic exchange (199) and the metal/oxygen bond energy in oxidation

reactions (195,196). The following activity series would arise:

$$Co_3O_4 > CuO > NiO > MnO_2 > Cr_2O_3 > Fe_2O_3 > V_2O_5 >$$

$$ZnO > TiO_2 .$$

Oxygen desorption was thought to occur in the rate-limiting step of the decomposition of nitric (200) and nitrous oxides (55). The heat of desorption was influenced by oxide stoichiometry (199) where q increased with the removal of surface oxygen, except for chromium(III) and iron(III) oxides.

Halpern and Germain (193) have shown that surface oxygen does not occupy a continuous distribution of states on the oxides, but that mobile oxygen may be present on discrete surface states. Correlations between catalytic activity and oxygen mobility, however, implies a knowledge of the oxygen states involved, and this state may change with temperature, time and reagent concentrations. A shift to higher states might therefore cause large distortions of the general activity series.

No clear correlation was discernible between the catalytic reaction rate and the metal/oxygen bond length (177) or the charge/radius ratio with respect to the cation (201,202).

4.9.2 *Rate order*

Examination of the rate order data for reactions over manganese(III) oxide and Modmor/manganese catalysts, Table 4.9.1 , indicated that the rate order with respect to both reactants was generally between zero and one, while that with respect to products was usually zero. Under the experimental conditions, the products did not inhibit reaction and the fact that the reaction rate orders with respect to both reactants were frequently very similar would indicate that both reactants contribute approximately equally to rate control, particularly in the reactions of nitrous oxide or oxygen with hydrocarbon.

TABLE 4.9.1 Rate order data

Catalyst	Reaction	Experimental Rate	RATE ORDERS Reactants NO	N_2O	O_2	C_2H_6	C_4H_6	Products N_2	N_2O	CO_2	H_2O	Temp. (K)
Mn_2O_3	NO/C_2H_6	r_1	0.5	-	-	0.5	-	0	0	0	0	623
		r_2	0.3	-	-	0.7	-	0	0.3	0	0	623
		r_3	1.2	-	-	0.5	-	0	0	0	0	623
Mn_2O_3	N_2O/C_2H_6	r_1	-	0.8	-	0.7	-	0	-	0	0	623
		r_2	-	0.8	-	0.7	-	0	-	0	0	623
Mn_2O_3	O_2/C_2H_6	r_2	-	-	0.5	0.6	-	-	-	0	0	573
Modmor/ manganese oxide	O_2/C_2H_6	r_2	-	-	0.3	0.4	-	-	-	0	0	623
Mn_2O_3	NO/C_4H_8	r_1	0.5	-	-	-	0	0	0	0	0	673
		r_2	0.5	-	-	-	0	0	0	0	0	673
		r_3	1.35	-	-	-	0	0	0	0	0	673
Mn_2O_3	N_2/C_4H_8	r_1	-	0.5	-	-	0.4	0	-	0	0	623
		r_2	-	0.5	-	-	0.4	0	-	0	0	623
Mn_2O_3	O_2/C_4H_8	r_2	-	-	0.4	-	0.3	-	-	0	0	473
Modmor/ manganese oxide	O_2/C_4H_8	r_2	-	-	0.4	-	0.4	-	-	0	0	523

In the nitric oxide/1-butene reaction, the reaction rate was zero order with respect to hydrocarbon concentration and this was associated with the rapid adsorption and reaction of this species compared to nitric oxide. In both nitric oxide reactions, the rate order with respect to nitric oxide was > 1 for nitrous oxide formation. This would be expected if a disproportionation reaction is involved in the formation of nitrous oxide.

4.9.3 *Compensation effect*

The kinetic parameters derived in this study are summarized in Table 4.9.2. A compensation effect was shown to occur as a plot of lnA against apparent activation energy, Figure 4.9.1, exhibited a linear relationship. This effect is often associated with the variation of kinetic parameters of either a heterogeneous reaction occurring on different solids or a group of related reactions on the same catalyst (186,203). A number of theoretical models have been proposed to explain the compensation effect, and these have been summarized by Galwey (204).

The compensation effect is expressed by the equation:

$$\ln A = m\,Ea + b \qquad [4.9.1]$$

which indicates that the influence of a change of one Arrhenius parameter on the reaction rate constant is offset by a corresponding change of the other Arrhenius parameter.

From Figure 4.9.1, values for m and b were calculated to be 0.24 and -12.38, respectively. A compensation effect also occurred in reactions of carbon fibre supported catalysts, Table 3.10.1, using experimental values for activation energy and pre-exponential factors, Figure 4.9.1.

The expression for the compensation effect can be compared to the Arrhenius equation of the form:

$$\ln A = \frac{Ea}{RT} + \ln k_o \qquad [4.9.2]$$

TABLE 4.9.2 Kinetic parameters

Catalyst	Reaction	Ea ($kJ\ mol^{-1}$)	Rate Constant	lnA	Temperature Range (K)
Mn_2O_3	NO/C_2H_6	78	k_1	3.97	673 - 613
		32	k_1	-4.61	613 - 573
		63	k_2	4.46	673 - 613
		22	k_2	-3.19	613 - 573
Mn_2O_3	N_2O/C_2H_6	133	k_1	20.27	673 - 623
		106	k_1	15.00	613 - 573
		130	k_2	18.38	673 - 573
Mn_2O_3	O_2/C_2H_6	130	k_2	18.38	593 - 523
Modmor/ manganese oxide	O_2/C_2H_6	108	k_2	10.93	673 - 573
Mn_2O_3	NO/C_4H_8	69	k_1	-1.76	723 - 623
		78	k_2	0.15	723 - 623
		30	k_3	-3.92	723 - 623
Mn_2O_3	N_2O/C_4H_8	117	k_1	13.32	673 - 573
		126	k_2	14.48	673 - 573
Mn_2O_3	O_2/C_4H_8	183	k_2	35.09	523 - 503
		88	k_2	12.59	503 - 433
Modmor/ manganese oxide	O_2/C_4H_8	81	k_2	9.98	573 - 473

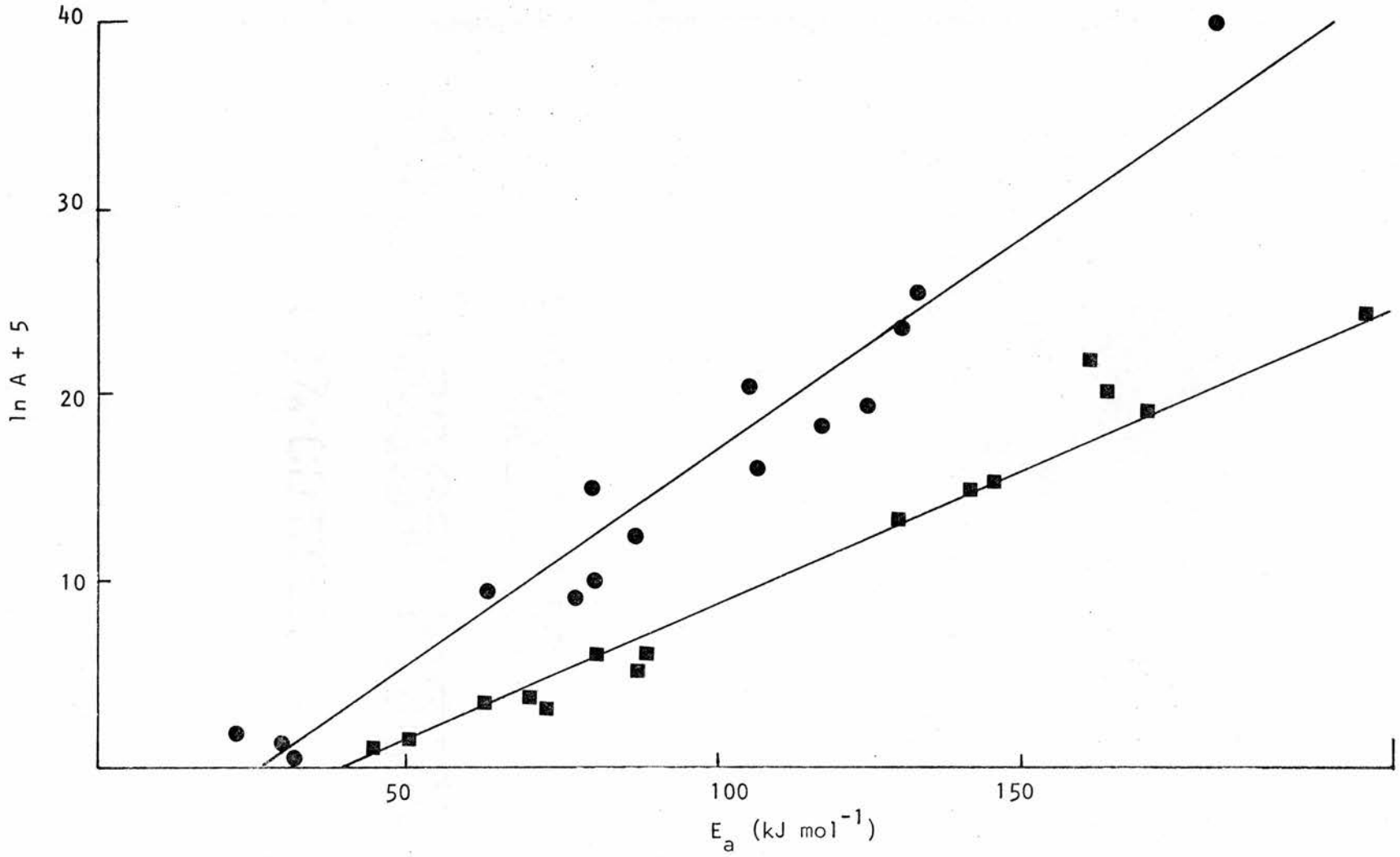

Figure 4.9.1 Compensation effect, ● the catalytic oxidation of C_2H_6 and C_4H_8 from Table 4.11.2; ■ from experimental rates from Table 3.10.1.

For a group of related reactions which obey equation [*4.9.1*], there exists a temperature β, the isokinetic temperature, at which the rates of these reactions are equal (205). The reaction rate constant at β = 501 K is given by k_o, 4.2×10^{-6} mol m^{-2} s^{-1}. The theoretical significance of the values of β and k_o remain unclear (206).

If the data are converted to the same units as in Galwey's description of the compensation effect (204), then:

$$\log A = \bar{B} + eE \qquad [4.9.3]$$

and e becomes 0.1042. This value is the same as that found in the oxidation reactions of propene (105) and acetylene (100) over various oxides (204). This pattern of kinetic behaviour indicates that the reactions probably involve the same rate-limiting step.

4.10 Modmor fibres plus manganese as catalysts

These catalysts were prepared by spraying the fibres with a manganese(II) nitrate solution as described in section 2.11.3. The air dried catalyst (9.5% w/w manganese) was heat treated at 773 K prior to reaction.

4.10.1 The oxygen/ethane reaction

Analysis of the oxygen and ethane rate order results, section 3.11.1, yielded only one Langmuir-Hinshelwood-type kinetic expression which could accommodate the data:

$$r = \frac{k\, a\, P_{O_2}^{0.5}\, b\, P_{C_2H_6}^{0.5}}{(1 + a\, P_{O_2}^{0.5} + b\, P_{C_2H_6}^{0.5})^2} \times (P_{O_2}\, P_{C_2H_6}) \qquad [4.10.1]$$

as indicated by the linear relationships of $P^{0.5}$ and $(P^{0.5}/r)^{0.5}$ in Figure 4.10.1.

The form of this equation (51) suggests that oxygen and ethane interact initially as two adsorbed species, each adsorbed on two surface

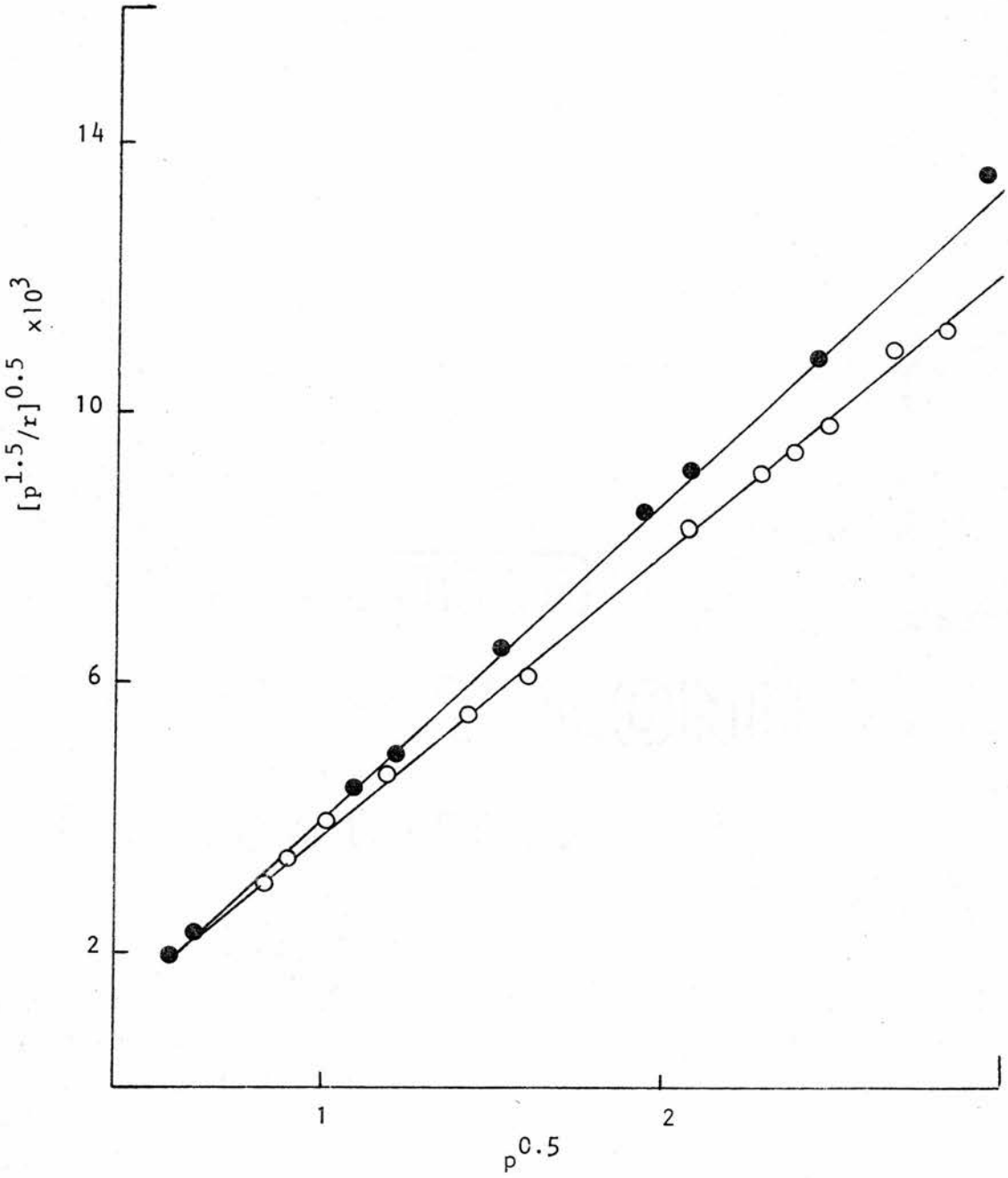

Figure 4.10.1 Reduced plots of the Langmuir-Hinshelwood expression [4.9.1] for the O_2/C_2H_6 reaction at 623 K over Modmor/marganese; ○ r_2 for $p_{C_2H_6}$, ● r_2 for p_{O_2}.

sites according to the square root relationships in equation [*4.10.1*]. The $(P_{O_2}\ P_{C_2H_6})$ term indicates that both oxygen and ethane interact in further steps involving a more complex overall reaction.

A plausible surface reaction scheme was formulated on a test/reject basis:

$$C_2H_6 + 2S \rightleftharpoons C_2H_{6(ads)} \qquad [4.10.2]$$

$$O_2 + [\ ] + C_2H_{6(ads)} \longrightarrow C_2H_{5(ads)} + [OOH]\ ] \qquad [4.10.3]$$

$$C_2H_6 + S + [OOH] \longrightarrow C_2H_{5(ads)} + [O] + H_2O \qquad [4.10.4]$$

with additional reactions given by:

$$2C_2H_{5(ads)} + 6O_2 + [O] \longrightarrow 4CO_2 + 5H_2O + [\ ] + 4S \qquad [4.10.5]$$

The rate constants derived for the oxygen/ethane reaction over manganese(III) oxide, Table 3.5.2, were approximately sixteen times greater than those found for the same reaction over a Modmor/manganese catalyst from 573 to 593 K, Table 3.11.2. The activation energy, 130 kJ mol^{-1}, determined for the former reaction was somewhat higher than that for the latter, 108 kJ mol^{-1}. Examination of Table 4.9.1 shows that the reaction rate orders with respect to oxygen and ethane were 0.5 and 0.6 for reaction over manganese(III) oxide at 573 K and 0.3 and 0.4 for reaction over Modmor/manganese at 623 K.

The mechanism presented for reaction over Modmor/manganese catalyst contains similar steps to that proposed for the same catalytic reaction over manganese(III) oxide, section 3.5. The basic differences occur in the adsorption and reaction of both reactants on two surface sites on the former catalyst and only one on manganese(III) oxide.

4.10.2 The oxygen/1-butene reaction

A Langmuir-Hinshelwood treatment (174-176) of the kinetic data provided only one expression which best fit the experimental results. This was the same expression as that determined in section 4.8 for the oxygen/

1-butene reaction over manganese(III) oxide:

$$r = \frac{k\ a\ P_{O_2}^{0.5}\ b\ P_{C_4H_8}^{0.5}}{(1 + a\ P_{O_2}^{0.5}\ b\ P_{C_4H_8}^{0.5})^2} \times (P_{O_2}\ P_{C_4H_8}) \cdot \qquad [4.10.6]$$

The reduced plots are shown in Figure 4.10.2. The same reaction scheme as presented in section 4.8 would also apply for this catalyst.

The activation energy for reaction over Modmor/manganese, 81 kJ mol^{-1}, was slightly less than that over manganese(III) oxide, 88 kJ mol^{-1}.

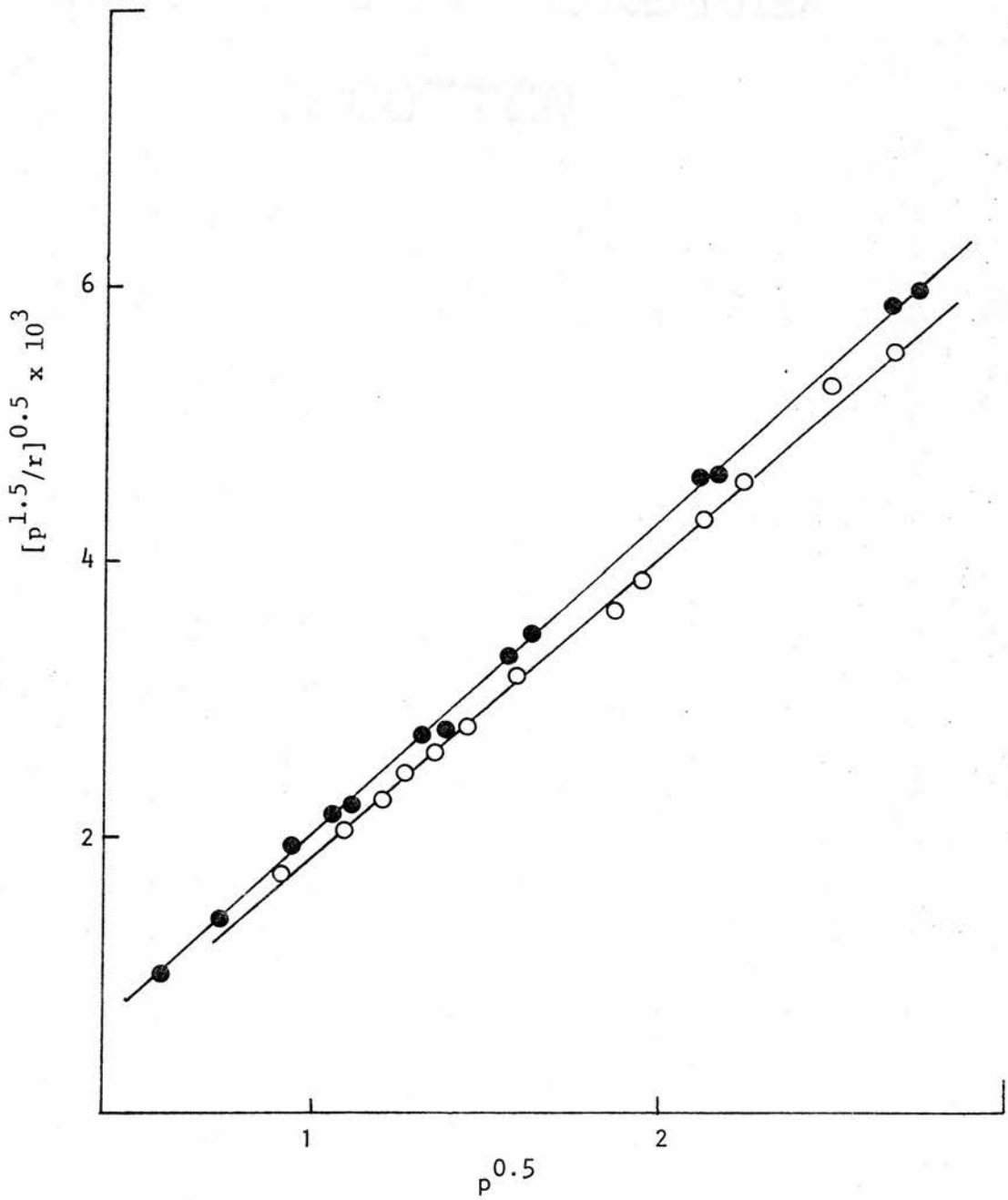

Figure 4.10.2 Reduced plots corresponding to equation [4.9.1] for the O_2/C_4H_8 reaction at 523 K over Modmor/manganese; O r_2 for $p_{C_2H_6}$, ● r_2 for p_{O_2}.

4.11 *Conclusions*

The main results of this study may be summarized:

(i) Only the products of complete oxidation were observed in studies of the catalytic reactions of nitric oxide, nitrous oxide or oxygen with ethane or 1-butene over manganese (III) oxide. These reactions may all occur in emission control systems which require the removal of NO_x and unburned hydrocarbons.

(ii) Reactions appeared to initiate from an irreversible bimolecular reaction between adsorbed species on the catalyst surface. Each reactant was adsorbed on one surface site in reactions with ethane. In reactions with 1-butene each reactant was adsorbed on two sites. The initial steps in the mechanism were thought to involve C-H bond rupture, although the strength of the metal/oxygen bond on the catalyst surface appeared to influence the rate-limiting steps.

(iii) Manganese (III) oxide underwent a phase change from the alpha to the gamma phase during catalysis. The extent of the change could not be determined accurately, however, this indicates that lattice or surface oxygen may be actively involved in the cataltic reactions.

(iv) The reactions of nitric oxide were more complex than those of nitrous oxide or oxygen. In the nitric oxide/hydrocarbon reactions, it was apparent that nitrous oxide was formed in one series of steps, and that a second sequence was responsible for hydrocarbon oxidation by nitric oxide and possibly by nitrous oxide as well. A nitro or nitrate species was identified on the catalyst surface after reaction.

(v) An activity series was developed for the nitrous oxide/1-butene reaction:

$$CuO > Fe_2O_3 > NiO > Mn_2O_3 > Cr_2O_3 > TiO_2 > Sc_2O_3 > SnO > ZnO > V_2O_5 > Al_2O_3.$$

There was no apparent enhancement of activity which could be related to semiconductivity type, however, the strength of the metal/oxygen bond appeared to be a factor.

(vi) Carbon fibres were found to be a useful catalyst support, or co-catalyst, in the oxidation of ethane or 1-butene by oxygen. A more active catalyst was prepared by spraying the fibres repeatedly with a manganese (II) nitrate solution than by adsorption from aqueous solution. The physical properties of these fibres appeared to be altered by catalysis.

4.12 *Suggestions for future work*

Langmuir-Hinshelwood-related expressions provided a clue to the nature of the surface mechanisms and corroborating information was obtained from infrared and ESCA studies as well as from the literature. However, methods such as temperature-programmed desorption and isotopic exchange would help to clarify some of the surface processes which occur during catalysis.

This study indicated that carbon fibres may be a useful support material in catalytic hydrocarbon oxidation reactions, however additional reactions should be examined using other hydrocarbons and oxidizing species. In addition, ESCA studies or infrared spectroscopy may be of specific value in identifying the active surface centres involved in catalysis. Further studies of the process of activating carbon fibres would help in evaluating their potential as catalyst supports.

APPENDIX

A.1 *Saturator efficiency*

The volume of water (ℓ) passing through a flow line in time t (h) with a carrier gas flow velocity V ($dm^3\ min^{-1}$) is given by:

$$\text{volume} = \frac{t\ V\ P_0 \times 6 \times 10^{-2}}{101.08} \qquad [A.1.1]$$

at 100% efficiency with the partial pressure of water in the saturators at P_0 (kPa). The number of moles of water vapour would therefore be:

$$\text{no. of moles} = \frac{t\ V\ P_0 \times 6 \times 10^{-2}}{22.415 \times 101.08} \qquad [A.1.2]$$

where one mole of water vapour at 101.08 kPa and 273 K occupies 22.415 ℓ, assuming ideal gas behaviour.

If the actual number of moles of water trapped is m, then saturator efficiency is given by:

$$\text{efficiency} = \frac{m \times 22.415 \times 101.08}{t\ V\ P_0 \times 6 \times 10^{-2}} \times 100\% \qquad [A.1.3]$$

When m is replaced by W/M, the weight of water divided by the molecular weight, the expression becomes:

$$\text{efficiency} = \frac{W \times 22.415 \times 101.08}{M\ t\ V\ P_0 \times 6 \times 10^{-2}} \times 100\% \qquad [A.1.4]$$

A.2 *Rate calculations*

The calculation of experimental rate data assumes ideal gas behaviour so that one mole of gas occupies 22.415 ℓ at STP (101.08 kPa and 273 K). Flow rate measurements were conducted at room temperature (296 K) where the volume of one mole of gas is 24.303 ℓ. When the partial pressure of one component (product) gas is X kPa and the total gas flow rate is

V dm^3 min^{-1} (NTP), the rate of reaction is given by:

$$r = \frac{X\ V\ T}{101.08 \times 24.303 \times 296 \times 6 \times 10^4 \times S.A.} \cdot \text{(mol } m^{-2}\ s^{-1}\text{)} \quad [A.2.1]$$

where T is the reactor temperature (K) and S.A., the surface area of the catalyst (m^2) in the reactor.

A.3 *Space velocity*

The term space velocity, SV, indicates the number of times that a unit volume of gas contacts the catalyst during a specified time interval at reactor temperature, T. If the catalyst volume is C_V (dm^3) for a one gram sample, then:

$$SV = \frac{V\ T}{C_V \times 296 \times 60} \quad [A.3.1]$$

at a total gas flow rate V (dm^3 min^{-1}). Generally, the space velocity is given as dm^3 gas per dm^3 catalyst per second, and this is usually abreviated to s^{-1}.

The catalyst volume C_V for oxide samples was measured in a graduated cylinder. The volume per gram was read directly after tapping the cylinder to pack the particles to the same state as in the reactor.

The specific volume of the carbon fibres was measured by the standard method using a pyknometer and found to be 0.68 dm^3 g^{-1} for Modmor fibres treated with manganese. This value did not change after catalysis, and it compares favourably with the values quoted for fibre density in section 1.5.

A.4 *Rate constants*

Using the ideal gas laws in a manner similar to that outlined in A.2, the concentration of any gas species at temperature T can be shown to be:

$$C = \frac{X\ T}{101.08 \times 24.303 \times 296} \quad \text{(mol } \ell^{-1}\text{)} \quad [A.4.1]$$

where X is the partial pressure (kPa).

The rate constant k was computed by integration of the experimental rate equation in terms of concentrations (mol ℓ^{-1}). This equation was of the form:

$$\frac{db}{dt} = k\ (a-b)^n\ b^m \qquad [A.4.2]$$

where a represents the initial concentration of reactant and b, that of the product formed as a result of reaction. Rate order exponents, n and m, were determined for reactants and products, respectively.

With conversion levels in this study kept below 15%, the rate equation was simplified to a power law expression:

$$\frac{db}{dt} = k\ a_1^{n_1}\ a_2^{n_2}\ b_1^{m_1}\ b_2^{m_2} \cdots \qquad [A.4.3]$$

where the rate order exponents for products were usually zero. The initial product concentration was zero, so that separating variable and integrating gave the equation:

$$\frac{b}{a_1^{n_1}\ a_2^{n_2}}_{o} = k\ \tau \qquad [A.4.4]$$

The contact time τ is proportional to the reciprocal of space velocity. The specific rate constant was therefore given by:

$$k = \frac{b}{a_1^{n_1}\ a_2^{n_2}} \times \frac{SV \times 10^{-3}}{S.A.} \qquad [A.4.5]$$

where the 10^{-3} factor converts the space velocity term to ℓ per dm^3 catalyst per second. The units for k and A, the pre-exponential factor in the Arrhenius equation, were therefore $(\text{mol}\ \ell^{-1})^{1-n_1-n_2}\ m^{-2}\ s^{-1}$. These rather cumbersome units where not always specified in the text, however, rate order exponents have been included such that the units of k and A are readily apparent.

A.5 Computer programmes

The following APL programmes were used in this thesis on a DEC 2020 computer:

```
      ∇KRRET[⎕]∇
    ∇  KRRET;ALPHA;BETA
[1]     'ENTER THE VALUE FOR, VB (IN MLS.), FOR THE TUBE USED.'
[2]     VB←⎕
[3]     'ENTER THE VALUE FOR, VC (IN MLS.), FOR THE TUBE USED.'
[4]     VC←⎕
[5]     ' ENTER THE NAME OF YOUR SAMPLE, MAKING SURE THAT IT IS ENCLOSED IN SING
      LE QUOTATION MARKS.'
[6]     NAME←⎕
[7]     'ENTER THE WEIGHT (IN GRAMS) OF THE SAMPLE USED.'
[8]     WT←⎕
[9]     ' WHAT IS THE INTERNAL DIAMETER OF THE TUBE USED (IN MM.), IF YOU DO NOT
      KNOW ENTER THE NUMBER ZERO. '
[10]    ID←⎕
[11]    →(ID=0)/END
[12]    VI←46.19
[13]    VA←21.82
[14]   C1:'HOW MANY POINTS HAVE YOU OBTAINED FOR THE R.F.T. PLOT.'
[15]    POINTS←⎕
[16]    'ENTER YOUR MCLEOD READINGS IN CM AS A VECTOR, FOR EXAMPLE:'
[17]    'PRESSURE FOR CHARGE 1,PRESSURE FOR MEASURE 1,PRESSURE FOR CHARGE 2, PRE
      SSURE FOR MEASURE 2,ETC. FOR ALL CHARGES'
[18]    CPR←TPR←⎕
[19]    CPR←TPR←(CPR×2)×0.00383
[20]    →(POINTS=(⍴TPR)÷2)/C2
[21]    'YOU HAVE ENTERED THE WRONG NUMBER OF PRESSURE READINGS FOR THE NUMBER O
      F POINTS YOU ARE PLOTTING.'
[22]    'RE-ENTER THE NUMBER OF POINTS YOU WISH TO PLOT AND THE CORRECT NUMBER O
      F PRESSURE READINGS.'
[23]    →C1
[24]   C2:J1←J2←J3←J4←J5←J6←J7←J8←2
[25]   C3:CPR[J1]←CPR[J1]-CPR[J1]×0.49÷(37.2×(ID×2)×CPR[J1]×2)+(14.5×ID×CPR[J1])
      +1
[26]    →((J1←J1+2)≤⍴)/C3
[27]    V←⍴⍳46.19
[28]   C4:V[J2]←VA+VB+VI
[29]    →((J2←J2+2)≤⍴)/C4
[30]    VNTP←0.00123×V×CPR
[31]    FA←VC×293÷77.5×760
[32]    VPNTP←TVOL←VIA←VSTS←VADS←PPO←TAX←⍳0
[33]   C5:VPNTP[J3]←CPR[J3]×FA
[34]    →((J3←J3+2)≤⍴)/C5
[35]   C6:TVOL[J4]←VNTP[J4]+VPNTP[J4]
[36]    →((J4←J4+2)≤⍴)/C6
[37]   C7:VIA[J5]←0.07475×CPR[J5]
[38]    →((J5←J5+2)≤⍴)/C7
```

Continued:

```
[39]    J←I←1
[40]    VSYS[J]←VNTP[J]
[41]  C8:J←J+2
[42]    VSYS[J]←VSYS[J-2]+VNTP[J]-VIA[J-1]
[43]    →(J<(Q-1))/C8
[44]  C9:VADS[J6]←VSYS[J6-1]-TVOL[J6]
[45]    →((J6←J6+2)≤Q)/C9
[46]    VG←VADS÷WT
[47]  C10:PPO[J7]←CPR[J7]÷1.754
[48]    →((J7←J7+2)≤Q)/C10
[49]  C11:TAX[J8]←PPO[J8]÷(VG[J8]×(1-PPO[J8]))
[50]    →((J8←J8+2)≤Q)/C11
[51]    'ROLL UP TO A NEW SHEET AND PRESS''RETURN'' KEY FOR TABLE.'
[52]    DUMMY←⍞
[53]    (↑'       THE DATA FOR THE P.E.T. PLOT FOR  '),(↑NAME),↑'  IS GIVEN IN TH
      E FOLLOWING TABLE.'
[54]    ' '
[55]    ' '
[56]    '    TRUE     CORRECTED  VOLUME     VOLUME     VOLUME      TOTAL     VOLUME
      VOLUME     VOLUME      P/PO       P/PO       VI+VA'
[57]    ' PRESSURE  PRESSURE    (MLS.)     AT NTP   UNDER LN2   VOLUME      IN
      ADSORBED  ADSORBED                 VG(1-P/PO)    (MLS)'
[58]    '   (TORR)     (TORR)                (MLS)      AT NTP     (MLS)     SYSTEM
      (MLS)     PER GRAM'
[59]    '                                                (MLS)                (MLS)
                (MLS/G.)'
[60]    N←'    -----   '
[61]  C12:' '
[62]    DISP← 10 6 PFT VEC←(TPR[I],CPR[I],V[1],VNTP[I],VPNTP[I],TVOL[I],VSYS[I],
      VADS[I],VG[I],PPO[I],TAX[I],VIA[I])
[63]    ZER←(⍳10),(0=VEC)/⍳⍴VEC
[64]    I2←1
[65]    DISP[(10×ZER[I2]-1)+⍳10]←N
[66]    →((I2←I2+1)≤⍴ZER)/¯1+⍳26
[67]    DISP
[68]    →((I←I+1)>Q)/0
[69]    →C12
[70]  END:'THE TUBE DIAMETER IS REQUIRED FOR THE THERMAL TRANSPIRATION CORRECTI
      ON FOR KRYPTON, WITOUT THIS'
[71]    '      CORRECTION THE RESULTS WILL BE SUBJECT TO ERROR.  WHEN USING THIS
      PROGRAMME NEXT MAKE SURE YOU'
[72]    '      HAVE THE INNER DIAMETER (IN MM.) OF THE TUBE.  THIS PROGRAMME WILL
       NOW TERMINATE.'
```

```
      ∇LINEFIT[⎕]∇
    ∇  X LINEFIT Y;R;MX;MY;SX2;SE2;N
[1]     →(2<(N←⍴X)/2+⌶26
[2]     →0,⍴⎕ ←'INSUFFICIENT NUMBER OF POINTS ENTERED, ANALYSIS CANNOT PROCEED.'
[3]     →(N=⍴Y)/3+⌶26
[4]     (⍕'YOU HAVE ENTERED '),(⍕N),(⍕' VALUES OF THE X VARIABLE AND '),(⍕⍴Y),⍕'
        VALUES OF Y. I QUIT.'
[5]     →0
[6]     SX2←+/(X-MX←+/X÷N←⍴X)*2
[7]     SL←(+/(X-MX)×(Y-MY←+/Y÷N))÷SX2
[8]     INT←MY-SL×MX
[9]     SE2←(+/(Y-(SL×X)+INT)*2)÷N-2
[10]    SA←(SE2÷SX2)*0.5
[11]    SB←(SE2×((÷N)+(MX*2)÷SX2))*0.5
[12]    R←(1-(+/(Y-(SL×X)+INT)*2)÷(+/(Y-MY)*2))*0.5
[13]    (⍕'LINE SLOPE IS : '),⍕SL
[14]    (⍕'LINE INTERCEPT IS : '),⍕INT
[15]    (⍕'THE CORRELATION COEFFICIENT IS : '),⍕R←R××SL
[16]    (⍕'THERE ARE '),(⍕N-2),⍕' DEGREES OF FREEDOM.'
[17]    'FIND THE ''''T''''VALUE FROM A TABLE, AND CONFIDENCE INTERVALS ARE:'
[18]    (⍕'+/- T X '),(⍕SA),⍕' FOR THE SLOPE, AND'
[19]    (⍕'+/- T X '),(⍕SB),⍕' FOR THE INTERCEPT.'
[20]    '      X                 Y(OBS)              Y(CALC)'
[21]    ⍉((3,N)⍴X,Y,((SL×X)+INT))
```

REFERENCES

1. Klissurski, D. G., E. F. McCaffrey and R. A. Ross, Can. J. Chem., 49, 3778(1971); J. Catal., 26, 380(1972).

2. Krupay, B. W. and R. A. Ross, Can. J. Chem., 52, 3063(1974).

3. Ross, R. A. and M. R. Jeanes, Ind. Eng. Chem., Prod. Res. Develop., 13, 102(1974).

4. Ross, R. A., G. D. Martin and W. G. Cook, Ind. Eng. Chem., Prod. Res. Develop., 14, 151(1975).

5. Ross, R. A. and S. P. Sood, Ind. Eng. Chem., Prod. Res. Develop., 16, 147(1977).

6. Fikis, D. V., W. J. Murphy and R. A. Ross, Can. J. Chem., 57, 2464(1979).

7. Krupay, B. W. and R. A. Ross, Can. J. Chem., 51, 3520(1973).

8. Krupay, B. W. and R. A. Ross, J. Catal., 39, 369(1975).

9. Krupay, B. W. and R. A. Ross, Z. Phys. Chem. N. F., 106, 83(1977).

10. Krupay, B. W. and R. A. Ross, J. Catal., 50, 220(1977).

11. Krupay, B. W. and R. A. Ross, Can. J. Chem., 56, 10(1978).

12. Krupay, B. W. and R. A. Ross, Can. J. Chem., 56, 2447(1978).

13. Krupay, B. W. and R. A. Ross, Can. J. Chem., 57, 718(1979).

14. Haas, L. A., C. F. Anderson and S. E. Khalafalla, Ind. Eng. Chem., Process Des. Develop., 18, 143(1979).

15. Trantz, M., Z. Elektrochem., 22, 104(1916).

16. Schuck, E. A. and E. R. Stephens, Adv. Environ. Sci., Vol. I, 73(1969).

17. Amirnazmi, J., J. E. Benson and M. Boudart, J. Catal., 30, 55(1973).

18. Howard, C. S. and F. Daniels, J. Phys. Chem., 62, 360(1958).

19. Boreskov, G. K., Disc. Faraday Soc., 41, 263(1966).

20. Andrew, S. P. S., Trans. Instn. Chem. Engrs., 54, 196(1976).

21. Shelef, M. and J. T. Kummer, AIChE Symp. Ser., 67, 74(1971).

22. Shelef, M., K. Otto and H. Gandhi, J. Catal., 12, 361(1968).

23. Alkhazov, T. G., G. Z. Gasan-Zade and M. Yu. Sultanov, Kinet. Katal., 17, 699(1976).

24. Lawson, A., J. Catal., 24, 297(1972).

25. Hougen, O. A. and K. M. Watson, Ind. Eng. Chem., 35, 529(1943).

26. Hougen, O. A. and K. M. Watson, "Chemical Process Principles, Part III", John Wiley and Sons, New York, 1966.

27. Peters, M. S. and R. J. Ayen, Ind. Eng. Chem., Process Des. Develop., 1, 205(1962).

28. Ayen, R. J. and Yu-Sim Ng, Intern. J. Air Water Pollution, 10, 1(1966).

29. Shelef, M. and K. Otto, J. Catal., 10, 408(1968).

30. London, J. W. and A. T. Bell, J. Catal., 31, 32(1973).

31. Shelef, M., Catal. Rev. Sci. Eng., 11, 1(1975).

32. Alkhazov, T. G., G. Z. Gasan-Zade, M. O. Osmanov and M. Yu. Sultanov, Kinet. Katal., 16, 1061(1975).

33. Unland, M. L., Science, 179, 567(1972); J. Phys. Chem., 77, 1952(1973); J. Catal., 31, 459(1973).

34. Solymosi, F., J. Sarkany and A. Schauer, J. Catal., 46, 297(1977).

35. Sazanova, I. S., G. M. Alikina, G. V. Glazoreva, N. P. Keier, N. E. Bogdanchikova and V. G. Devyatov, Kinet. Katal., 18, 441(1977).

36. Glazoreva, G. V., I. S. Sazanova and N. P. Keir, Dokl. Akad. Nauk. SSSR., 213, 364(1973).

37. Zecchina, A., L. Cerruti and E. Borello, J. Catal., 25, 55(1972).

38. Shelef, M., K. Otto and J. T. Kummer, Z. Phys. Chem. N. F., 72, 316(1970).

39. Hoffman, B. M. and N. J. Nelson, J. Chem. Phys., 50, 2598(1969).

40. Naccache, C., M. Che and Y. Ben-Taarit, Chem. Phys. Lett., 13, 109(1972).

41. Pozdnyakov, D. V. and V. N. Filimonov, Kinet. Katal., 14, 760(1973).

42. Hu, I., D. Van-Linsburg and J. W. Hightower, Kinet. Katal., 18, 545(1977).

43. Ault, J. W. and R. J. Ayen, AIChE Journal, 17, 265(1971).

44. Stelley, T. J. and J. B. Butt, Ind. Eng. Chem., Prod. Res. Develop., 11, 397(1972).

45. Chien, M. W. and K. Nobe, Amer. Chem. Soc., Div. Water, Air Waste Chem., Preprints, 11, 71(1971).

46. Kasaoki, S., H. Tsumaki and T. Kitamura, Nipon Kagaku Kaishi, 5, 1052(1973).

47. Blyholder, G. and M. C. Allen, J. Phys. Chem., 65, 3998(1965).

48. Pozdnyakov, D. V. and V. N. Filimonov, Adv. Mol. Relax. Proc., 5, 55(1973).

49. Lubezky, A. and M. Folman, Trans. Faraday Soc., 74, 2935(1978).

50. Morrow, B. A. and L. E. Moran, J. Catal., 62, 294(1980).

51. Clark, A., "The Theory of Adsorption and Catalysis", Academic Press, New York and London, 1970.

52. Thomas, J. M. and W. J. Thomas, "Introduction to the Principles of Heterogeneous Catalysis", Academic Press, New York and London, 1967.

53. Krylov, O. V., "Catalysis by Non-metals", Academic Press, New and London, 1970.

54. Garner, W. E., (ed.), "Chemistry of the Solid State", Butterworths, London, 1955.

55. Winter, E. R. S., J. Catal., 15, 144(1969); 19, 32(1970).

56. Winter, E. R. S., J. Catal., 34, 431(1974).

57. Dziewiecki, Z., Russ. J. Phys. Chem., 40, 1239(1966).

58. Cimino, A. and V. Indovina, J. Catal., 17, 54(1970).

59. Tanaki, K. and A. Ozaki, Bull. Chem. Soc. Japan, 40, 420(1967).

60. Rheaume, L. and G. Parravano, J. Phys. Chem., 63, 264(1959).

61. Bickley, R. I. and F. S. Stone, Trans. Faraday Soc., 64, 3393(1968).

62. Ben-Taarit, Y. and J. H. Lunsford, Proc. Int. Congr. Catal., 5th, (J.W. Hightower, ed.) North-Holland, Amsterdam, paper no. 106, (1973).

63. Schwab, G. -M. and J. Drikos, Z. Phys. Chem. A., 186, 348(1940).

64. Dell, R. M., F. S. Stone and P. F. Tiley, Trans. Faraday Soc., 49, 201(1953).

65. Tanaka, K. and G. Blyholder, J. Chem. Soc. D, Chem. Commun., 736(1971).

66. Leech, C. A. and M. S. Peters, AIChE Symp. Ser. 126, 68, 75(1972).

67. Hwang, S. T. and G. Parravano, J. Electrochem. Soc., 114, 482(1967).

68. Fuller, M. J. and M. E. Warwick, J. Catal., 39, 412(1975).

69. Kemball, C. and W. R. Patterson, Proc. Roy. Soc. A, 270, 219(1962).

70. Krylova, A. V., L. E. Derlyukova and L. Ya. Margolis, Dokl. Akad. Nauk SSSR, 178, 610(1968).

71. Cant, N. W. and W. K. Hall, J. Catal., 27, 70(1972).

72. Hinshelwood, C. N., "The Kinetics of Chemical Change", Oxford University Press, London, p. 207, 1949.

73. Mars, P. and D. W. van Krevelen, Chem. Eng. Sci., 3, 41(1954).

74. Lyubarskii, G. D., Dokl. Akad. Nauk SSSR, Otd. Khim. Nauk, 1173(1958).

75. Knox, J. H., Combust. Flame, 9, 297(1965).

76. Margolis, L. Ya., Adv. Catal., 14, 429(1963).

77. Voge, H. V. and C. R. Adams, Adv. Catal., 17, 151(1967).

78. Hucknall, D. J., "Selective Oxidation of Hydrocarbons", Academic Press, New York and London, 1974.

79. Haber, J., Z. Chem., 13, 241(1973); Pure Appl. Chem., 50, 923 (1978); Kinet. Katal., 21, 123(1980).

80. Dadyburjor, D. B., S. S. Tewar and E. Ruchenstein, Catal. Rev. Sci. Eng., 19, 293(1979).

81. Stein, K. C., J. J. Feenan, G. P. Thompson, J. F. Shultz, L. J. Hofer and R. B. Anderson, Ind. Eng. Chem., 52, 671(1960).

82. Anderson, R. B., K. C. Stein, J. J. Feenan and L. J. Hofer, Ind. Eng. Chem., 53, 809(1961).

83. Bone, W. A. and S. G. Hill, Proc. Roy. Soc. A, 129, 434(1930).

84. Averbukh, A. Ya., V. P. Shukin, T. I. Epova and V. I. Rutkovskii, Kinet. Mater. - Vses. Konf. Kinet. Katal. Reakts., 2nd, 1, 70(1975).

85. Avramenko, L. I. and R. V. Kolesnikova, Izv. Akad. Nauk SSSR, Ser. Khim., 12, 2693(1971).

86. Moshkina, R. I., S. S. Polyak, N. A. Sokolova and A. B. Nalbandyan, Kinet. Katal., 17, 1057(1976).

87. Moshkina, R. I., S. S. Polyak, N. A. Sokolova, I. F. Masterovoi and A. B. Nalbandyan, Int. J. Chem. Kin., 12, 315(1980).

88. Mahajan, S., W. R. Menzies and L. F. Albright, Prepr., Div. Pet. Chem., Amer. Chem. Soc., 19, 653(1974).

89. Thomas, W. J., Trans. Faraday Soc., 53, 1124(1957).

90. Thomas, W. J., Trans. Faraday Soc., 55, 624(1959).

91. Meshenko, N. T., V. V. Veselov, F. S. Shub and M. I. Temkin, Kinet. Katal., 18, 962(1977).

92. Battacharyya, S. K., K. Janakiram and N. D. Ganguly, J. Catal., 8, 128(1967).

93. Cullis, C. F. and T. G. Nevell, Proc. Roy. Soc. Lond. A, 349, 523(1976).

94. Economy, J., D. T. Meloon, Jr., and R. L. Ostrozynski, J. Catal., 4, 446(1965).

95. Falconer, J., D. Hoare and R. Overend, Combust. Flame, 21, 339(1973).

96. Nagiev, M., T. Nagiev, R. Babaev and Sh. A. Tagieva, Azerb-Khim. Zh., 5/6, 3(1973).

97. Zanevskaya, O. S., V. Ya. Vol'fson and O. T. Chugaeva, Kinet. Katal., 10, 8(1973).

98. Wanke, S. E., Can. J. Chem. Eng., 51, 454(1973).

99. Hoodless, I. M., R. A. Ross and R. Swaminathan, Can. J. Chem., 59, 865(1981).

100. Moro-Oka, Y., Y. Morikawa and A. Ozaki, J. Catal., 7, 23(1967).

101. Yu Yao, Y.-F. and J. T. Kummer, J. Catal., 28, 124(1973).

102. Kemball, C. and W. R. Patterson, J. Catal., 3 465(1963).

103. Dmuchovsky, B., M. C. Freerks and F. B. Zienty, J. Catal., 4, 577(1965).

104. Koutsoukas, E. P. and K. Nobe, Ind. Eng. Chem., Prod. Res. Develop., 4, 425(1965).

105. Moro-Oka, Y. and A. Ozaki, J. Catal., 5, 116(1966); 10, 84(1968).

106. Linde, V. R., Dokl. Akad. Nauk SSSR, 136, 860(1961).

107. Linde, V. R. and L. Ya. Margolis, Izv. Akad. Nauk SSSR, Otd. Khim. Nauk, 1723(1962).

108. Rubanik, M. Ya, K. M. Kholyavenko, A. V. Gershingorina and V. I. Lazukin, Kinet. Katal., 5, 666(1964).

109. Anderson, J. R. and A. B. Swanson, J. Catal., 8, 41(1967).

110. Panikarovskaya, A. N., K. P. Zhdanova, F. A. Mil'man, B. V. Timashkova and V. G. Lipovich, Kinet. Katal., 19, 190(1978).

111. Batist, Ph. S., B. C. Lippens and G. C. A. Schwit, J. Catal., 5, 55(1966).

112. Batist, Ph.A., C. J. Kaptijns, B. C. Lippens and G. C. A. Schuit, J. Catal., 7, 33(1967).

113. Kimkhai, O. N., V. V. Popovskii, G. K. Boreskov, T. V. Andrushkevich, and T. B. Dneprovskaya, Kinet. Katal., 12, 371(1971).

114. Bacon, R., Chem. Phys. Carbon, (P. L. Walker, Jr., and P. A. Thrower, eds.) 9, 1(1973).

115. Reynolds, W. N., ibid., 11, 1(1973).

116. Goodhew, P. J., A. J. Clarke and J. E. Bailey, Mater. Sci. Eng., 17, 3(1975).

117. Larsen, J. V., Ph.D. Thesis, University of Maryland, College Pk., MD.

118. Harris, B., Carbon Fibres Eng., 1(1973).

119. Fourdeax, A., R. Perret and W. Ruland, Plast. Polym., Conf. Suppl., No. 5, 57(1971).

120. Perret, R. and W. Ruland, J. Appl. Cryst., 3, 525(1970).

121. Barnet, F. R. and M. K. Norr, US NTIS AD Rep. 1974, No. 784415/2 GA.

122. Perret, R. and W. Ruland, J. Appl. Cryst., 1, 308(1968).

123. Moller, P. J. and T. Fort, Coll. Polym. Sci., 253, 98(1975).

124. Rand, B. and R. Robinson, Carbon, 15, 257(1977).

125. Mimeault, V. J. and D. W. McKee, Nature, 224, 793(1969).

126. Drzal, L. T., Carbon, 15, 129(1977).

127. Donnet, J. B. and H. Dauksch, Plast. Polym., Conf. Suppl., No. 5, 49(1971).

128. Lin, R. Y. and J. Economy, Appl. Polym. Symp., No. 21, 143(1973).

129. Arons, G. N., R. N. Macnair and R. L. Erickson, Text. Res. J., 43, 539(1973).

130. Molleyre, F. and M. Bastick, High Temp. - High Pres., 9, 237(1977).

131. Adams, L. B. and E. A. Boucher, Carbon, 16, 75(1978).

132. Ermolenko, I. N., A. A. Morozova, Yu. M. Kobzev and L. I. Fridman, Prepr. - Mezhdunar Simp. Khim. Voloknam, 2nd, 4, 125(1977).

133. Hamada, H., S. Matsumoto and K. Komatsu, Japan. Kokai 75 133, 195 (Cl. C01B, B010), 22 Oct. 1975, Appl. 74, 39, 895, 10 Apr. 1974.

134. Bohra, J. N., J. Sci. Ind. Res., 34, 451(1975).

135. Kuroda, A., H. Aizawa, Y. Masubuchi, G. Ishihara, S. Matsuhisa and S. Taira, Japan. Kokai 75 33, 187 (Cl. 13(a) G02, 13(a) G01), 31 Jul. 1973, Appl. 73 83, 608, 26 Jul. 1973.

136 Olfer' eva, T. G., O. V. Bragin, I. N. Ermolenko and A. M. Safonova, Kinet. Katal., 18, 933(1977).

137. Ermolenko, I. N., A. M. Safonova, R. I. Bel'skaya, G. K. Berezovik and Ya. M. Paushkin, Vesti Akad. Nauk Belorus. SSSR, Ser. Khim. Nauk, 6, 20(1974).

139. Meguerian, G. H., A. L. Hensley, Jr., and E. P. Steigelmans, Fr. 2,072,561 (Cl. Bolj, Colb, Foln), 29 Oct. 1971, US Appl. 880, 850, 28 Nov. 1969.

140. Ninomiga, N., H. Nishino, T. Aibe and K. Itoga, Ger. Offen. 2,433,076, (Cl. B01d), 06 Feb. 1975, Japan Appl. 73, 78,980, 12 Jul. 1973.

141. Fujimoto, K. and T. Kunugi, Proc. Inst. Congr. Catal., 5th, (J.W. Hightower, ed.) North-Holland, Amsterdam, paper no. 28(1973).

142. Clark, R. H., W. E. Graham and A. G. Winter, J. Amer. Chem. Soc., 47, 2748(1925).

143. Hinshelwood, C. N., "The Kinetics of Chemical Change", Oxford University Press, London, 1949.

144. Kokes, R., H. Tobin and P. H. Emmett, J. Amer. Chem. Soc., 77, 5860(1955)

145. Boudart, M., AIChE Journal, 18, 465(1972).

146. Weisz, P. B. and C. D. Prater, Adv. Catal., 6, 143(1954).

147. Schwab, G. -M. and N. Theophilides, J. Phys. Chem., 50, 427(1947).

148. Ettre, L. S. and N. Brenner, J. Chromotog., 3, 524(1960).

149. Damkokler, G., "Der Chemie-Inglnieur" (A. Eucken and M. Jacobs, eds.), 3, 424, Akademische Verlagsgesellschaft. Leipzig, 1937.

150. Menold, R., Chem. Eng. Tech., 34, 769(1962).

151. Lovelock, J. E., Anal. Chem., 33, 162(1961).

152. Orr, C. and J. M. Dallawalle, "Fine Particle Measurement", Macmillan, London, 1960.

153. Brunauer, S., P. H. Emmett and E. Teller, J. Amer. Chem. Soc., 60, 309(1938).

154. Hill, T. L., J. Chem. Phys., 14, 263(1946).

155. Flood, E. A., "The Solid-Gas Interface", Vol. 1, Marcel Dekker, New York, 1967.

156. Gregg, S. J. and K. S. W. Sing, "Adsorption, Surface Area, and Porosity", Academic Press, New York and London, 1967.

157. Rosenberg, A. J., J. Amer. Chem. Soc., 78, 2929(1956).

158. American Society for Testing Materials, Card Index, 1967.

159. Ellis, M., T. Moore and P. W. Selwood, J. Amer. Chem. Soc., 72, 856(1950).

160. Dollimore, D., J. Dollimore and J. Little, J. Chem. Soc. A, 2946(1969).

161. Kadec, O. and V. Danes, Coll. Czech. Chem. Commun., 32, 1871(1967).

162. Vogel, A. I., "A Textbook of Inorganic Analysis", Third edition, Longman's, Green and Co., London, p. 434, 1962.

163. Slin'ko, M. G., Kinet. Katal., 21, 71(1980).

164. Satterfield, C. N., "Mass Transfer in Heterogeneous Catalysis", M.I.T. Press, Cambridge MS, 1970.

165. Zimmerman, J. F., J. Phys. Chem., 53, 562(1949).

166. Riddiford, A. C., J. Phys. Chem., 56, 745(1952).

167. Dowden, D. A. and G. W. Bridger, Adv. Catal., 9, 669(1957).

168. Bond, G. C., "Heterogeneous Catalysis: principles and applications", Oxford University Press, London, 1974.

169. Levenspiel, O., "Chemical Reaction Engineering", Wiley, New York, p. 453, 1962.

170. Chambers, R. P. and M. Boudart, J. Catal., 6, 141(1966).

171. Blue, R. W., V. C. F. Holm, R. B. Regier, E. Fast and L. F. Hechelsberg, Ind. Eng. Chem., 44, 2710(1950).

172. Weiz, P. B. and C. D. Prater, Adv. Catal., 3, 143(1951).

173. McCaffrey, E. F., Ph.D. Thesis, The Queens University of Belfast, 1972.

174. Yang, K. H. and O. A. Hougen, Chem. Eng. Prog., 46, 146(1950).

175. Zdrazil, M., J. Catal., 31, 313(1973).

176. Weller, S. W., AIChE Journal, 2, 59(1956).

177. Sastri, M. V. C., J. C. Ghosh and K. A. Kini, Ind. Eng. Chem., 44, 2463(1952).

178. Sastri, M. V. C. and H. Srikant, Current Sci. (India), 20, 15(1951).

179. Potter, C. and S. Baron, Chem. Eng. Prog., 47, 473(1951).

180. Boudart, M., AIChE Journal, 2, 62(1956).

181. Boudart, M., AIChE Journal, 18, 465(1972).

182. Weller, S. W., "Chemical Reaction Engineering Reviews", (H. M. Hulbert, ed.), Amer. Chem. Soc., Washington D.C., 1975.

183. Beranek, L., Catal. Rev. Sci. Eng., 16, 1(1977).

184. Maatman, R. W., Adv. Catal., 29, 97(1980).

185. Halsey, G., Adv. Catal., 4, 259(1952).

186. Bond, G. C., "Catalysis by Metals", Academic Press, New York and London, 1962.

187. Emmett, P. H. (ed.), "Catalysis Volume V", Reinhold, New York, 1954.

188. Otto, K. and M. Shelef, Proc. Int. Congr. Catal., 5th, (J. W. Hightower, ed.) North-Holland, Amsterdam, paper no. 16, 1973.

189. Otto, K. and M. Shelef, J. Phys. Chem., 74, 2690(1970); 75, 875(1971); 76, 37(1972).

190. Yao, H. C. and M. Shelef, J. Catal., 31, 377(1973).

191. Lorimer, D. and A. T. Bell, J. Catal., 59, 223(1979).

192. Lambert, R. M. and C. M. Comrie, Surf. Sci., 46, 61(1974).

193. Halpern, B. and J. E. Germain, J. Catal., 37, 49(1975).

194. Carver, J. C., G. K. Schwertzer and T. A. Carlson, J. Chem. Phys., 57, 573(1972).

195. Boreskov, G. K., Kinet. Katal., 14, 2(1973).

196. Boreskov, G. K., Dakl. Akad. Nauk SSSR, 213, 926(1973).

197. Krupay, B. W., Ph.D. Thesis, University of Salford, 1977.

198. Boreskov, G. K., Adv. Catal., 15, 285(1964); Kinet. Katal., 8, 879(1967).

199. Boreskov, G. K., V. V. Popovskii and V. A. Sazanov, Kinet. Katal., 9, 307(1968).

200. Winter, E. R. S., J. Catal., 22, 158(1971).

201. McCaffrey, E. F., D. G. Klissurski and R. A. Ross, Proc. Int. Cong. Catal., 5th, (J. W. Hightower, ed.), North-Holland, Amsterdam, paper no. 3, 1973.

202. Greenwood, N. N., "Ionic Crystals, Lattice Defects and Nonstoicheometry" Butterworths, London, (1968).

203. Cremer, E., Adv. Catal., 7, 75(1955).

204. Galwey, A. K., Adv. Catal., 26, 247(1977).

205. Exner, O., Nature, 201, 144(1964); 227, 366(1970).

206. Exner, O., Coll. Czech. Chem. Commun., 29, 1094(1964); 37, 4425(1972); 38, 799(1973).